LATE HOLOCENE CLIMATE FLUCTUATIONS AT CASCADE LAKE, NORTHEASTERN AHKLUN MOUNTAINS, SOUTHWESTERN ALASKA

By Kasey Kathan

A Thesis
Submitted in Partial Fulfillment
of the Requirement for the Degree of
Master of Science
in Geology

Northern Arizona University
December 2006

Approved:

_____
Darrell S. Kaufman, Ph.D., Chair

_____
R. Scott Anderson, Ph.D.

_____
James Sample, Ph.D.

_____
Al Werner, Ph.D.

ABSTRACT

LATE HOLOCENE CLIMATE FLUCTUATIONS AT CASCADE LAKE, NORTHEASTERN AHKLUN MOUNTAINS, SOUTHWESTERN ALASKA

KASEY KATHAN

This study examines the relationships between glacier fluctuations, multiple proxies from lake sediments and late Holocene climate fluctuations in southwestern Alaska. Cascade Lake (3.1 km^2; 60.1°N; 159.4°W; 330 m asl) is glacier-fed with 12% of its drainage basin occupied by modern (1970) glaciers. The primary sediment contributor is Cascade Glacier located 5.4 km up-valley. During the Little Ice Age, cirque and valley glaciers of the Cascade Lake area experienced an average equilibrium-line altitude lowering of 22 ± 12 m (n = 8) relative to 1957. Little Ice Age moraines stabilized ~1860 AD.

Three sediment cores were recovered from the lake and the lake was instrumented with water-temperature loggers and sediment traps from 2004-2006. ^{137}Cs, ^{210}Pb profiles, the Aniakchak tephra (3500 cal yr BP) and the regional tephra (Tephra B; 6100 cal yr BP) provide limited age control and indicate an average late Holocene sedimentation rate of ~0.07 cm/yr. The cores are composed of rhythmically laminated mud, with an average lamination thickness of 0.4 cm; these laminations do not represent annual sedimentation (e.g. varves).

Biogenic silica was analyzed at an average spacing of 0.2 cm (~3 yr) over the last 150 yr and is well correlated with spring temperature ($r = 0.70$, $p = 9.16 \times 10^{-5}$), precipitation (Nuyakuk discharge; $r = 0.73$, $p = 2.2 \times 10^{-6}$) and the Aleutian Low Pacific

Index ($r = 0.68$, $p = 1.37 \times 10^{-7}$). These relationships suggest a link to nutrient input to the lake. High BSi flux can generally been related to mild conditions and low BSi flux to cool conditions. This interpretation and other proxy data indicate mild climates at ~7000 cal yr BP (Holocene thermal maximum) and 1600-1400 cal yr BP (Medieval Warm Period?). Cool conditions persisted between ~3000-2500 cal yr BP (onset of Neoglaciation) and 1400 cal yr BP to 1870 AD (Little Ice Age). The pattern of climate variability in Cascade Lake generally agrees with widely recognized Holocene climate fluctuations, though the ages differ. This may be due to a time-transgressive nature of these climate events or, more likely, a poorly constrained age model.

Based on the interpretation of several periods of climate variability in the Ahklun Mountains during the late Holocene, the climate of the 20th century can be placed in context. Within the Cascade Lake record, no other period has comparable biogenic silica) concentrations to the 20th century. This suggests an unprecedented strengthening of the Aleutian low during this most recent period.

ACKNOWLEDGMENTS

It was through the hard-work and help of many people that this project was completed. My sincere gratitude first goes to Darrell Kaufman, as he has been a remarkable advisor and role-model throughout every step of this project. Without his energy during field-work, excitement over new data and encouragement during the writing process, this thesis would lack the integrity and detail that it now has. I thank him for always having an open office door, even when his schedule was busy, and for asking the questions that kept me motivated.

My thanks also extend to my committee members, Jim Sample, Scott Anderson, and Al Werner. Their comments and observations helped to tie my loose ends together. I've always enjoyed our conversations both within the formal committee meeting setting and informally in the hallway. I appreciate the extensive time and brainpower that you poured into my thesis. I especially appreciate the help of Al Werner, because it was through his encouragement that I choose to continue my education beyond Mount Holyoke College.

There are many additional people who have contributed to this project with their time, and expertise. Tom Daigle, Erin Dopfel, Mike Hamilton, Heidi Roop, Apayo Moore, Al Werner and of course Darrell Kaufman provided much needed assistance and ideas in the field, while Togiak National Wildlife Refuge provided the logistical support. Feng Sheng Hu of University of Illinois and Richard Ku of University of Southern California provided the ^{210}Pb and ^{137}Cs analyses and John Southon of University of California, Irvine for the radiocarbon analysis. Jim Wittke spent a significant amount of

time helping analyze tephra on the electron microprobe and scanning electron microscope. Tom Daigle, Jordan Bright, Caleb Schiff, Nick McKay and Chris Kassel each get thanked for spending time talking over ideas with me and asking the hard questions.

Special thanks go to my family and friends for putting up with me. Sheena Styger, Chloe Bonamici, Christyanne Melendez, and Monica Hansen provided necessary distractions and coffee breaks. My parents have always supported their wandering child and continue to be the most significant role models in my life. Skip Martin has provided me with retreats to cabins in the woods and many hugs from 3000 miles away.

This project was funded by National Science Foundation grants ARC-0455043 and ATM-0318341 awarded to Dr. Darrell Kaufman, and a Geological Society of America graduate student research grant.

TABLE OF CONTENTS

LIST OF TABLES

LIST OF FIGURES

CHAPTER 1:
INTRODUCTION

The high latitudes have been shown to be particularly sensitive to global climate change, with dramatic environmental changes induced by subtle climate variations (Overpeck et al., 1997). Throughout the Quaternary, inter-annual and century-scale climate variation has been the norm; however, the timing, synchronicity and forcing mechanisms of these fluctuations are still poorly understood and necessitate further work. The investigation and interpretation of these past environmental changes provide a context within which to place our understanding of present and future climate fluctuations.

Lake sediment cores have proven particularly successful in providing valuable interpretations of Holocene climate fluctuations (Pienitz et al., 2004). Lake sediments provide continuous records of glacial fluctuations, lake productivity, sediment fluxes and a wide variety of other environmental changes induced by climate variability. Using proxy indicators available in lacustrine sediments, it is possible to determine the range of non-anthropogenic Holocene climate variability. The naturally induced events of the Holocene (e.g., Neoglaciation, Medieval Warm Period, and Little Ice Age) can then be compared with the twentieth-century climate changes that are related to anthropogenic forcing.

Project Objective

The overarching goal of this study is to determine the range of climate variability preserved in the sediments of Cascade Lake, Alaska. This is accomplished by: (1)

establishing an understanding of the modern and historic climate and sedimentation patterns at Cascade Lake, (2) determining the recent glacial fluctuations within the drainage basin of Cascade Lake, (3) identifying the major sedimentation patterns and fluctuations in Cascade Lake sediment cores, and (4) using proxy indicators to interpret Holocene climate variations.

Background

Holocene Climate Variability. Initial paleoclimate reconstructions from the marine and ice cores suggested that the Holocene was a period of relative stability compared to the large-scale climate fluctuations of the Last Glacial Maximum. Modern alpine glaciers were originally assumed to be merely the remnants of maximum Pleistocene ice extent. However, it is now recognized that this 'quiescent' period includes a series of pronounced climate fluctuations (e.g., Mayewski et al., 2004). Multiple cooling events have been identified that punctuate the current interglacial period; perhaps the most well known is the 400-year-long Little Ice Age (LIA). This period of multiple "glacial expansion(s) subsequent to the maximum Hypsithermal shrinkage" has been termed Neoglaciation (Porter and Denton, 1967).

One of the first studies to systematically approach North American climate fluctuations of the late Holocene was by Denton and Karlén (1973). Their study of the expansion and contraction of 51 North American and European alpine glaciers recognized three prominent intervals of glacial expansion: 3300-2400, 1250-1050 cal yr BP (where "BP" = before 1950 AD), and the Little Ice Age (1500-1900 AD). This millennial-scale pattern (~1500 and 2000-2800 year climate periodicity) of widespread

late Holocene cooling events is gaining support as evidence of similar climate variability emerges from other high-resolution records (Bond and Showers, 1997; Campbell et al., 1998; Bianchi and McCave, 1999; Leonard and Reasoner, 1999; Noren et al., 2002; Mayewski et al., 2004). Mayewski et al. (2004) summarized this supporting evidence in a study of ~50 spatially distributed paleoclimate records. They determined that a minimum of six global Holocene cooling events are associated with this pattern occurring at 9000-8000, 6000-5000, 4200-3800, 3500-2500, 1200-1000 and 600-150 cal yr BP (Figure 1).

The millennial-scale climate variability of the Holocene is not only marked by cool periods. Mild, warm and dry periods have also been recognized at 10600-9300, 7900-6300, 2700-1500, 960-610 cal yr BP (Figure 1, O'Brien et al., 1995). The warm period of approximately 1000 cal yr BP (1000-1300 AD) has been termed the Medieval Warm Period (MWP). This period is often cited as being similar to the modern 20th century warming; however, a compilation by Crowley and Lowrey (2000) determined that the MWP was only ~0.20°C warmer than the LIA. The spatial and temporal patterns and the amplitude of this warm period must be resolved before it can be used as a model for 20th century warming.

A forcing mechanism for this millennial-scale climate periodicity has yet to be determined. Some evidence suggests that these cycles are related to Dansgaard-Oeschger like ice-rafting events, and therefore linked to North Atlantic thermohaline circulation and a strongly coupled ocean-atmosphere system (Alley et al., 1997; Bond and Showers, 1997). Other evidence suggests that external factors, such as persistent solar variability,

explain the widespread distribution of these climate events (Denton and Karlén, 1973; Mayewski et al., 1997; Bond et al., 2001).

Neoglaciation in Alaska. The glacial records of past climate variability in Alaska generally concur with the more widely recognized events of the late Holocene. Calkin's (1988) summary of Holocene glaciation in Alaska focused on glacial moraines that indicate four major periods of glacial advance including: an initial advance between 6000-5000 cal yr BP, two distinct advances at 3600-2000, and 1700-1100 cal yr BP and the most recent advance of the Little Ice Age at 750-400 cal yr BP. While these periods of glacial advance have been recognized throughout Alaska, their timing, duration and magnitude vary considerably. For instance, the maximum Holocene ice extent in regions of the Kenai Peninsula was achieved during the 3600-2000 cal yr BP advance whereas many other local areas experienced maximum ice extent during the LIA (Calkin, 1988).

Some of the variation in the timing of Neoglacial advances could be attributed to the difficulty in identifying geomorphic evidence for the extent of early Neoglacial advances, which might have been obliterated by more extensive LIA advances. However, supporting evidence has been derived from proxy records such as pollen, lake-level and tree-ring studies. In southern Alaska these supporting studies indicate that periods of glacial advance identified in glacial geomorphic studies correspond to periods of increased wetness (e.g., Hansen and Engstrom, 1996; Abbott et al., 2000; Calkin et al., 2001).

Pacific Ocean and Alaska Climate. Interdecadal climate variability in the North Pacific region has been well documented throughout the last century and likely influences the

millennial-scale climate fluctuations of the Holocene (Minobe and Mantua, 1999; Schneider and Cornuelle, 2006). Although the mechanism for this interdecadal climate variability is unknown, a basin-wide phenomenon that originates in the tropics and is closely related to the shorter-term oscillations of sea-surface temperature and sea-level pressure has been suggested (D'Arrigo et al., 2005). The primary two short-term oscillations are the El Niño-Southern Oscillation (ENSO) and the Aleutian low-pressure cell (AL). ENSO regimes typically persist for 6-18 months and are responsible for shifts in the locations of warm tropical waters. These shifts in sea-surface temperatures (SST) in turn affect the regional precipitation and mean annual temperatures (Papineau, 2001; Neal et al., 2002). The dominant mode of North Pacific wintertime atmospheric circulation is the Aleutian low. A deepened AL results in a strengthened southerly flow over the eastern Pacific, and warmer temperatures along the western coast of North America (Rodionov et al., 2005). Each of these components contributes to the Pacific Decadal Oscillation (PDO; measured by SST), which is one of the best summaries of North Pacific interdecadal climate variability.

The PDO has its primary signature in the North Pacific Ocean with a secondary imprint in the tropics (where the ENSO fingerprint is primary) and a periodicity of approximately every 20-30 yr. Over the historic period the PDO has had several documented shifts in its primary modes (Kayano et al., 2005). 'Cool' phases (cold waters in the Gulf of Alaska) persisted from 1900-1924 and 1947-1976. Subsequent 'warm' phases occurred from 1925-1946 and 1977 to the mid-1990s. These interdecadal shifts in the PDO have a strong link to interannual variation of the AL. Warm modes of the PDO are associated with a general strengthening of the AL; however, the interannual variance

of the AL during the warm PDO phases is two to three times greater than other periods (Minobe and Mantua, 1999). Though these patterns of variability in the closely coupled ocean-atmosphere system of the North Pacific have only been documented over the last 100 yr, paleoclimate studies suggest that these patterns have persistently influenced southern Alaska climate throughout the Holocene. Generally, the association between increased wetness and periods of glacial advances in northwestern North America implies a strong influence of the AL on Holocene glaciation (Spooner et al., 2003; Anderson et al., 2005).

Previous Work in Ahklun Mountains, Alaska. Although significant paleoclimate research has been completed in Alaska, relatively little attention has focused on the late Holocene in the southwestern portion of the state. Previous work in southwestern Alaska has largely focused on the Ahklun Mountains. The Ahklun Mountains are a 250-km-long mountain belt trending southwest to northeast between Bristol Bay and Kuskokwim Bay lowlands (Figure 2). They form the largest mountain range west of the Alaska Range and harbored a large ice cap during the late Wisconsin that was separate from the Cordilleran Ice Sheet. Most of the paleoclimate research completed in the region has focused on Pleistocene and Younger Dryas glacial advances (Briner and Kaufman, 2000; Kaufman et al., 2001; Manley et al., 2001; Briner et al., 2002; Hu and Shemesh, 2003; Hu et al., 2006).

Studies of the Holocene climate in the Ahklun Mountains remain rather limited. A lacustrine sediment sequence recovered from Arolik Lake in the southwestern Ahklun Mountains produced a 33,000 yr record of climate variability (Kaufman et al., 2003). While high climate variability was observed in the Arolik Lake record, sampling

resolution was too coarse to resolve Holocene fluctuations. A more detailed study (Hu et al., 2003) observed regular oscillations in lake productivity coinciding with solar variability, but this study focused on a portion of the core ranging in age from 12,000 to 2300 cal yr BP and did not address Neoglacial cooling events.

Studies that directly address late Holocene paleoclimate in the Ahklun Mountains include a pollen study by Axford and Kaufman (2004) and a combined lacustrine/glacial-moraine study by Levy et al. (2004). While Little Swift Lake, in the northwestern Ahklun Mountains, does not contain clear evidence of specific Neoglacial cooling events, the pollen record does indicate progressive climatic deterioration (cooling) throughout the late Holocene (Axford and Kaufman, 2004). Levy et al.'s (2004) work on Waskey Lake is the most complete work to date on Ahklun Mountain Neoglaciation. They identified multiple late Holocene glacial advances by the presence of several discrete end moraines in the forefields of the modern glaciers. Both the geomorphic evidence and the lake-sediment record indicate that the peak Neoglacial activity occurred at Waskey Lake between 700 and 200 cal yr BP. The lake sediments indicate an onset of Neoglaciation at 3100 cal yr BP. This age is significantly younger than the ages suggested for major Neoglacial advances across the rest of Alaska (Brooks Range, Kenai Mountains, and Seward Peninsula). This suggests that the Ahklun Mountains may be slightly out of phase with widespread climate events of the late Holocene. Without additional records of Neoglaciation in the Ahklun Mountains, however, it is difficult to determine the full significance of the Waskey Lake record. If the timing of glacial activity at Waskey Lake matches other places across the Ahklun Mountains this would imply that an unknown regional-scale climate forcing exerts a stronger influence than the large-widespread

climate forcing affecting other areas of Alaska and potentially the globe. Cascade Lake is located only 38 km from Waskey Lake providing an opportunity to test the reproducibility of the Waskey Lake Holocene climate record reported by Levy et al. (2004).

Study Area

Presently, over 100 active glaciers are located in the northern portions of the Ahklun Mountains where numerous peaks are over 1500 m a.s.l. The largest of these northern glacial complexes are Chikuminuk Glacier (~5.6 km^2) and an unnamed glacier (hereafter, "Cascade Glacier", ~3.4 km^2) to the west and south respectively (Figure 3). Cascade Lake (60° 8' 11.9''N; 159° 23' 57.3''W) lies 5.4 km downstream from the primary outflow of Cascade Glacier at 335 m elevation.

The drainage basin area of Cascade Lake is 43.7 km^2, 12% of which is occupied by active glaciers. The area is vegetated with stands of alder and willow shrub and upland tundra. Cascade Lake (3.1 km^2) has multiple inflows, both melt-water streams and non-glacial channels, though the primary sediment contributor is Cascade Glacier (Figure 3). Cascade Lake is formed in late Wisconsin drift underlain by Jurassic volcaniclastic sandstones, conglomerates and argillites that are members of the Gemuk group (Box et al., 1993). Two interpreted faults bisect the field area, one crossing the northern portion of the lake and the other crossing mid-way down the melt-water channel of Cascade Glacier (Hoare and Coonrad, 1959).

CHAPTER 2:
MODERN CLIMATE AND SEDIMENTATION AT CASCADE LAKE

In order to make quantitative interpretations of Holocene climate variations preserved in lake sediments, it is necessary to understand the climate factors affecting sediment transfer and deposition. Factors such as temperature, rainfall, and snowmelt intensity, have a direct impact on the sediment characteristics preserved in lakes (Leeman and Niessen, 1994; Hardy et al., 1996; Noon et al., 2001; Francus et al., 2002). A small-scale study of the modern sedimentation and climate at Cascade Lake was undertaken to enable a better understanding of the influence of climate on its sediment record and to evaluate the potential for annual sedimentation patterns.

Methods

Moorings. Instrument moorings were deployed at water depths of 24.2 m (mooring 1) and 52.4 m (mooring 2) at glacial distal and proximal sites, respectively, within Cascade Lake (Figure 3, Table 1). Each mooring consisted of a rock anchor, two sediment traps, two temperature loggers and a buoy. The sediment traps were made from 12.5-cm-diameter funnels that fed rigid lexan tubes with an inner diameter of 1.6 cm (focusing factor = 62 times) (Figure 4). Traps were placed at ~1 m above the lake bottom and ~3 m below the lake surface. Buoys were set at ~2 m below the lake surface to avoid exposure during lower winter lake levels or freezing in winter ice. Each sediment trap was paired with an Onset Water Temp Pro temperature logger that recorded temperature every hour beginning June 28, 2004.

Trapped Sediments. The sediment traps were recovered on August 10 and 11, 2005 and on July 19th, 2006. The sediment was described and sub-sampled into stratigraphically distinct units visible in the receiving tube. The sediment from the 2005 traps at mooring 2 was analyzed for bulk-sediment density, and 2005 sediment from mooring 1 was processed for organic-matter content (OM), grain size, and biogenic silica content (BSi). The 2006 sediment from mooring 2 was analyzed for bulk-sediment density and BSi content.

Sediment grain-size distribution was determined using 0.25 cm^3 samples analyzed by a Coulter LS230 laser diffraction analyzer. Samples were pre-treated with 30% H_2O_2 to remove organics and 1M NaOH to dissolve BSi, and stored in sodium hexametaphosphate (a dispersing agent) to prevent flocculation prior to analysis. Each sample was analyzed four times for 80 seconds and all runs were averaged for the samples final grain-size estimate. OM content was determined by percent loss-on-ignition (LOI) and BSi analysis was completed using the methods of Mortlock and Froelich (1989, see Lake Sediments Methods).

Air Temperature. Onset Hobo temperature loggers were installed on the western shore of Cascade Lake and ~0.6 km from the modern Cascade Glacier front (Figure 3). The lakeshore logger was placed inside a solar radiation shield and mounted at a height of ~3 m on a large willow tree in a stand of alder (Figure 4). The logger recorded air temperature every hour for a period of June 28, 2004 to August 9, 2005, and from August 12, 2005 to July 20, 2006. The glacier front air temperature logger was mounted on stabilized copper poles ~2 m above the ground and recorded temperature every hour from August 13, 2005 to July 21, 2006.

Results and Discussion

Sediment Traps. Mooring 1 was recovered from its deployed location in both 2005 and 2006; mooring 2 was recovered from deeper water than which it was originally deployed in 2005. The mooring likely moved (drifted or was carried by lake ice) during the collection year, but the sediment traps and temperature loggers were all intact and seemingly undisturbed. Upon recovery the top traps were covered in a thick algal mat and had collected limited porous sediments with live organisms. The bottom traps contained significantly more sediment than the top traps (2005 mooring 2 had slightly overflowed into the collection tube) and were sub-sampled into an average of five stratigraphic units (Figure 5). Sediment in the bottom traps was typically gray to gray-green with organic material overlaying dense mud with gradational contacts between units.

Significantly less sediment accumulated during 2005-2006 than in 2004-2005. Unfortunately, a fingerling fish was caught in the receiving tube of 2006 mooring 1 and made field collection of the sediment impossible. However, mooring 2 collected 8.5 cm of sediment in 2006 compared to the 18.1 cm in 2005. The average sediment accumulation in the bottom trap of mooring 2 was 0.10 $g/cm^2/yr$ in 2004-2005, and 0.03 $g/cm^2/yr$ in 2005-2006, a 70% reduction (Tables 1 and 2). Because of possible complications caused by the movement of mooring 2 during the year and the overflowed collection tube, I focused on 2004-2005 mooring 1 for detailed analysis. Each of the stratigraphic units was analyzed for OM, grain size, and BSi content. The 2006 mooring 2 sediments were also analyzed for bulk density and BSi content for comparison (Figure

5). OM, grain size, and BSi content all covaried in the sediment from mooring 1 in 2005, with their lowest values in the middle units (Figure 5). The sediment from mooring 2 in 2006 contained less BSi overall (16% reduction in BSi percentage) and did not show decreased BSi content in the center units. Adjusting BSi values for the dilution caused by the increased sedimentation in the 2004-2005 collection year, results in a 77% reduction in BSi flux during 2005-2006 (Table 2).

The results from the bottom trap of 2004 mooring 1 exhibit a seasonal pattern (Figure 5). Because the traps were not equipped to record the timing of sediment deposition within the collection tubes, the seasonality of each lithologic unit is not known. Nonetheless, the decrease in OM, BSi, and grain size in the central part of the receiving tube of mooring 1 is indicative of winter sediment deposition in a glacial-fed lake. The increase in BSi in the uppermost sediments (units 1 and 2) and the coarse sediments (coarse silt) in unit 1 might indicate higher stream discharge associated with spring melt-out. Mooring 1 was located farther from the glacial melt-water inflows, and therefore was less sensitive to the glacial melt-water influences and may not have captured the seasonal signal as well as the more proximal site might have.

The 70% decrease in sediment flux and the 77% reduction in BSi deposition between the two collection years are indicative of a strong influence of interannual weather differences on sediment transport and accumulation. Spring and summer (May to September) surface-water temperatures (air temperature not available for 2005) were ~1.5 °C colder in 2006 than in 2005, and in July of 2006, significantly more snow remained on the landscape. Additionally, less (no quantitative measurements exist) melt-water occupied the channels of the Cascade Glacier outwash plain than in the previous

year. There is no precipitation data for Dillingham post-1998; however, precipitation data from Bethel over the collection years shows a 7.6 cm decrease in annual precipitation from 2005 to 2006 (62.5 vs. 54.9 cm; WRCC, 2006). Possibly the main pulse of sediment associated with peak melt-water discharge had not occurred by the time the traps were recovered in July 2006. More likely, the cooler spring/early summer temperatures and decreased precipitation retarded melt-water production (i.e. peak discharge) and decreased the sediment flux and associated nutrients for algal growth.

Water Temperature. The four temperature loggers were recovered in August 2005 and July 2006 (Figure 6). The water temperature data indicate that Cascade Lake is dimictic with fall mixing occurring in late October and spring melt-out and mixing occurring in late May to early June. Thermal mixing during the fall lasted 21 days in 2004 and 13 days in 2005 whereas spring mixing took place over 8 days in 2005 and 4 days in 2006. Fall cooling and spring warming leading to or following overturning were gradual at a rate of about 1 °C per 9 days. The lake-surface temperatures are similar at both mooring sites (0.1 °C warmer at the mooring 1 site). During the ice-free months, the lake-surface temperatures track air temperature with a minimal lag time (hours) and average 5 ± 9 °C cooler (based on hourly averages).

Air Temperature. In 2005, the lakeshore temperature logger malfunctioned and stopped recording on December 22, 2004 (after 176 days, Figure 6). A new lakeshore logger and the glacier terminus logger were deployed in August 2005 and downloaded in July 2006. The radiation shield at the glacier terminus was knocked off its mount and the logger

recorded a stable temperature of ~-7 °C from the end of January to the beginning of June 2006, probably because the fallen logger was buried by snow during this interval.

Freezing air temperatures at the lake were first reached in September and generally remained below freezing by November in both 2004-2005 and 2005-2006. Temperatures averaged above freezing starting in early May. For the period successfully recorded by both lakeshore air temperature loggers (August 12-January 22), the average 2004 temperature was 1.2 °C and the average 2005 temperature was –1.4 °C. The coldest recorded temperature in 2004 was –28 °C in early December, and in 2006 it was –40 °C in late January. The onset of freezing air temperatures and the timing of above-freezing temperatures in the spring correspond well to the build-up and melt-out of lake ice, just prior to and after lake overturning. Air temperatures lead lake ice-up and melt-out by about a month.

The glacier logger first recorded freezing temperatures two months earlier than the lake, and minimum temperatures occurred just before it went isothermal (-35°C, Figure 6). During the summer (JJA) the lakeshore air temperature averaged 2 ± 1 °C warmer than the glacier, whereas the lakeshore was 2 ± 4 °C cooler during the winter (DJF). With an elevation difference of 340 m these two temperature stations record an environmental lapse rate of ~6 °C/km during the summer and an inverted profile in the winter.

The air temperature logged at Cascade Lake can be compared with other climate stations in the region. The goal of this comparison was to determine whether the longer-term temperature records of the climate stations could confidently be extrapolated to Cascade Lake. The two closest climate stations are Bethel (~148 km to the northwest)

and Dillingham (~140 km to the southeast), where daily maximum and minimum temperature data are available (PNWPEST, 2006). I compared the daily maximum, minimum, and average daily temperatures from the climate stations (mean of two values) and from the Cascade Lake hourly air-temperature logger (mean of 24 values) and found the strongest correlation between the average daily temperature ($r = 0.97$ and 0.96 for Dillingham and Bethel, respectively). Daily temperature at Cascade Lake averaged 3.5 ± 3.1 °C ($n = 498$) cooler than Dillingham and 1.1 ± 3.4 °C cooler than Bethel (Figure 7). The temperature differences between Cascade Lake shoreline and Dillingham vary by season. During the summer, Cascade Lake was 2 °C cooler than Dillingham and 5 °C colder in the winter (Figure 7). The temperature differences between Dillingham and Cascade Lake indicate a summer environmental lapse rate of 7 °C/km. This is higher than the typical lapse rates of 6 °C/km (Porter, 2001), but similar to that of the lake and glacier temperature loggers. The somewhat higher lapse rate may be due to the more southerly and coastal location of Dillingham. Although temperature at both Dillingham and Bethel are strongly correlated with Cascade Lake, I chose to focus on the climate record at Dillingham because the temperature record there extends back to 1919, (compared with 1949 at Bethel).

CHAPTER 3:
GLACIAL GEOLOGY

Glaciers are sensitive to climate variations and are known to have fluctuated during the late Holocene in mountains across Alaska (Calkin, 1988; Calkin et al., 2001). The study of glacial deposits can provide information on the timing and magnitude of climate change that caused their deposition. By combining a glacial-geologic and a lake-sediment study from the same drainage, the two complimentary records of climate variability can be compared.

Background

Lichenometry. Lichenometry is a useful dating method applied to late Holocene landforms (Locke et al., 1979). In many cases, the historic record is too fragmented, carbonaceous material is absent or the landforms are too young (<500 yr) for reliable radiocarbon dating, or the tree-ring record is too short. Lichenometry is based on the premise that lichens grow at a predictable rate once they colonize a surface. *Rhizocarpon geographicum* and *R. alpicola* are the two most commonly used species because they have slow growth rates (0.02-2.0 mm/yr; Innes, 1985). These two species have slightly different growth rates and they are impossible to distinguish in the field (Werner, 1990). Most authors report data as *Rhizocarpon geographicum* senso lato (s.l.) and assume that this includes measurements of both *R. geographicum* and *R. alpicola* thalli.

The growth rate of *Rhizocarpon* is dependent on a variety of factors including, but not limited to: substrate lithology, moisture availability, temperature, altitude, and

snowcover (Innes, 1985). Each of these factors can vary significantly from one location to another, therefore, it is important to use a growth curve developed either from the region of interest, or from a similar environment. Lichen ages reflect the timing of landform stabilization and because moraines take some time to stabilize following the retreat of abutting glacial ice, they provide minimum ages for moraine deposition. Additionally, actively eroding landforms can not produce reliable lichenometric ages and should not be used (O'Neal, 2006).

Equilibrium-Line Altitude. The equilibrium-line altitude (ELA) serves as one of the most useful parameters to quantify the effect of climate on a glacier. The ELA separates the areas of accumulation and ablation and is controlled by a variety of factors including glacier hypsometry, glacier aspect, and other local climate conditions (Torsnes et al., 1993). Changes in ELA over time are generally most sensitive to winter precipitation and summer temperature, thereby enabling effective paleoclimate reconstructions (Dahl and Nesje, 1992).

A variety of methods have been developed to reconstruct former ELAs. Torsnes et al. (1993) compared various methodologies and determined that the accumulation area ratio (AAR) method resulted in the least error when calculating the ELA of modern glaciers with ELAs known through mass-balance measurements. The accumulation area ratio is defined as the ratio of the accumulation area to the total glacier area and is used to determine steady-state ELA. Meier and Post (1962) demonstrated that the AAR for steady-state glaciers in northwestern North America ranged from 0.5 to 0.8. The average of these values (0.65) is often used in ELA reconstructions (Porter, 2001).

Methods

Lichenometry. Glacial and fluvial deposits believed to be Holocene in age were identified on aerial photos and then studied in the field, or in some cases deposits were first recognized in the field. These deposits included moraines of the most accessible glaciers in the study area, fluvial terraces in the outwash plains of these glaciers, and stable surfaces that were formed during glacier retreat. The long and short axes of large *Rhizocarpon geographicum* s.l. thalli were measured using digital calipers. Landform surfaces were searched until no larger thalli could be found. This involved searching the entire landform surface and measuring approximately 15 lichen thalli. Generally, the largest lichens were found on stable slopes (crests of moraines) and in protected depressions on landform surfaces. Lichens with a long axis that measured over 20% larger than the short axis were rejected because of this non-regular growth pattern (Calkin and Ellis, 1980).

Because a lichen growth curve has not been developed for the Ahklun Mountains, the lichen sizes were compared to the growth rates at five other Alaska locales including: the Brooks Range, Seward Peninsula, central Alaska Range, Wrangell-St. Elias Mountains, and southern Kenai Mountains (Figure 2). Solomina and Calkin (2003) recently revised the growth curves for each of these areas based on additional control points, newly calibrated ^{14}C ages, and standardized fitting routines. These growth curves either used the single largest thallus diameter or the averages of the five largest diameters. Both of these values were calculated for the Cascade River valley data and compared with the corresponding growth curves. Uncertainty in the derived ages results

from the variety of climates represented by the five growth rates and their dissimilarities from the Cascade River valley and measurement errors. Of the five areas for which Solomina and Calkin (2003) developed growth curves, the mean annual and summer temperature (and likely the precipitation) of the Cascade Lake area are most similar to Seward Peninsula and therefore was used for age assignments (Table 3).

Equilibrium-Line Altitudes. Eight glaciers were chosen for ELA analysis, including those visited during the 2005 field season, and those associated with laterally extensive and prominent moraines on the 1957 aerial photographs. These eight glaciers include the Cascade and Chikuminuk valley glaciers and six cirque glaciers (Hungry Joe Cirque, Divided Cirque, East Inflow Cirque, Cirque 1, Cirque 2, Cirque 3, Figure 8). Four of the glaciers are within the Cascade Lake drainage basin and all are located within 9 km of the lake.

I used the AAR method for ELA reconstructions with an AAR value of 0.6 to facilitate direct comparison with the Waskey Lake area (Levy et al., 2004). The extent of ice in the 1957 aerial photographs and the reconstructed LIA ice limits (based on field glacial-geomorphic evidence and aerial photograph interpretation) were plotted on a 1:63,360-scale topographic map (1973) in ArcGIS v. 9 (i.e., 'modern' = 1957). This assumes that the 1973 contours were a reasonably accurate representation of the 1957 glacier surface. The area of each glacier was measured at ~100-ft-altitude intervals for both the modern and reconstructed LIA ice limits. A multi-order polynomial was fit to the data and used to determine the altitude corresponding to an AAR of 0.6 (40% of the total area lies within the zone of ablation; Figure 9).

Results and Discussion

Lichenometry. A total of 160 lichens with circular thalli were measured on 13 deposits in the forefield of five extant glaciers (Figure 8, Table 4). The outer moraines represent the largest Neoglacial advance while other deposits further up-valley represent smaller subsequent readvances, delays in retreat, or are deposits of a non-glacial origin (debris-flow deposits, river terraces, etc.). Of the five forefields, only two contained stable late Holocene moraines with measurable lichens, the other deposits were either unstable (slumped) over this period, or could not be clearly associated with the maximum ice advance . Lichens were measured on two distinct moraine deposits on both the left and right lateral sides of Cascade River valley and the terminal moraine of the East Inflow cirque (Figures 8, 10). The age estimates for these five moraines derived from the range of growth rates span from 860 cal yr BP based on the slow growth curve (Brooks Range) to 20 cal yr BP using the fast growth curve (Kenai Peninsula, Figure 11). The moderate growth curve from the Seward Peninsula (with a ~30-yr colonization time, see below) yields an average age of 90 cal yr BP (~1860 AD) for these LIA maximum moraines. Although the control points from the Seward Peninsula growth curve are not well-constrained around this time period, the Alaska Range growth curve yields a similar age for this lichen size. Because lichens date the stabilization rather than the initial deposition of a moraine, this age is a minimum estimate of the LIA maximum in the Cascade River valley.

Two of the lichen stations (12, 13) are up-valley of the LIA terminal moraine of the Cascade Glacier and were used to calculate a retreat rate. Lichens were measured on stable boulders overlying bedrock that were deposited upon ice retreat from the site.

Station 12 is located 990 m from the 2004 ice margin and was dated to 1945 AD using the Seward Peninsula growth curve (with the 17-yr colonization time of Solomina and Calkin (2003); Table 4). Station 13 is 540 m from the terminal moraine with an age of 1965 AD, but this age is too young as the site lies ~30 m beyond the 1957 ice front. This implies that the 17-yr colonization time built into the Seward Peninsula growth curve may be too short for the Cascade Lake area. A longer colonization time of about 30-yr is also indicated by the lack of lichens on surfaces exposed after 1984 and by only the earliest stages (<1 mm) of lichen colonization on the surfaces exposed between 1957 and 1984. The lichen ages reported in this thesis are therefore adjusted to be ten years younger than the ages derived from the Seward Peninsula growth curve.

The rate of retreat at Cascade Glacier was reconstructed by constraining the ice margin of Cascade Glacier at five points, using lichen ages and aerial photographs, namely: the 2004 observed ice front, 1984 and 1957 aerial photographs, lichen station 12 with an age of 1935, and the maximum LIA moraine dated to ~1860 AD based on lichenometry. These points indicate that Cascade Glacier retreated at the following average rates: 1860-1935 = 5 m/yr; 1935-1957 = 21 m/yr; 1957-1984 = 8 m/yr; 1984-2004 = 16 m/yr (Figure 12). The overall retreat rate for Cascade Glacier since the LIA maximum was 11 m/yr.

The retreat rate of Cascade Glacier from its maximum LIA extent was not steady over the last 140 yr, reflecting climatic variations and topographic constraints. The lowest retreat rate was documented between 1860 and 1935 (5 m/yr). This time period includes the climate recovery following the termination of the LIA. The shift to a rapid retreat between 1935 and 1957 (21 m/yr) is more difficult to explain. The period of

1947-1976 coincides with a 'cool' PDO and weakened AL, which would have produced cooler conditions in southwest Alaska (Papineau, 2001). These conditions should have inhibited glacier retreat, whereas the warmer temperatures associated with the preceding 'warm' PDO (strengthened AL) period of 1925-1946 should have promoted glacier retreat. Glaciers respond more rapidly to the affects of summer ablation on the glacier toe than they do to winter accumulation during positive mass-balance years. Because the response time of mountain glaciers averages 10-15 yr (Porter, 1986), the retreat rate of Cascade Glacier between 1946 and 1957 may be out-of-phase with the PDO and AL and may not have yet responded to the positive mass-balance years of 1947-1976. The 1957 and 1984 aerial photographs show the terminus of Cascade Glacier at nearly the same location in a bedrock-constrained, narrow section of the valley, which explains the lower retreat rate (8 m/yr) during this period. The most recent shift (post-1984) in retreat rates to 16 m/yr is likely the glacier response to 'warm' PDO shift from 1977 to 1995 with some lag in response time.

The multiple late Holocene advances recognized by Levy et al. (2004) at Waskey Lake (~30 km south of Cascade Lake) contrast with the single LIA moraines recognized in Cascade Lake study area. Both this study and Levy et al.'s (2004) used the same lichenometric methods, yet Levy et al. (2004) identified three periods of ice advance at 900-1800, 350-1050, and 200-650 cal yr BP, none of which are represented in this study area. Conversely, the most extensive advance in my study area took place at 90 cal yr BP, but is not represented in Waskey Lake valley. This discrepancy in Neoglacial ice advance is difficult to understand. The glaciers of both study areas are similar in size and occupy mountains with similar physiography and climate regime. None of the glaciers

overlie unconsolidated sediment that may lead to variations in sliding velocities; rather, they directly overlie bedrock. The Waskey Glacier is underlain by granodiorite, whereas the Cascade River valley glaciers overlie meta-sedimentary rocks with significant regional faulting. It is a possibility that differences in sub-glacial hydrology (bedrock permeability) may cause some of the variations in ice extent between the Cascade River valley glaciers and Waskey Glacier.

The late 19th century age for the LIA moraines in Cascade River valley corresponds to LIA moraine ages elsewhere in Alaska. In the northeastern Brooks Range, for example, LIA retreat occurred around 1890 AD (Evinson et al., 1996). Late 19th century moraine stabilization has also been recognized in the southeastern coastal glaciers, and the Kenai Mountains (Wiles and Calkin, 1994; Calkin et al., 2001). Taken together, these ages suggest that the second half of the 19th century was marked by widespread moraine formation across Alaska.

Equilibrium-Line Altitude. The modern glaciers (1957) in the area of Cascade Lake have an average size of 1.6 km^2 (n = 8) and an average ELA of 980 m ± 90 m (Table 5). The glaciers in the study area extended 0.2 to 1.7 km farther down-valley during the LIA, an average of 0.6 km (65%) larger than their 1957 counterparts. Chikuminuk Glacier experienced the largest down-valley expansion of 1.7 km. Cascade Glacier's ELA of 980 m coincides with the mean of the average ELA and its 1.4 km down-valley expansion during the LIA is the second largest.

The average ΔELA (lowering of ELA from LIA maximum to 1957) for the Cascade Lake area was 23 ± 13 m (Table 5). ΔELA ranges from 45 m (Cirque 2) to 5 m

(Cirque 1). The difference in ΔELA between these two cirque glaciers is unexpected because they have similar southerly aspects, are within 1 km of one another, and have similar modern ELAs (1010 and 1050 m respectively), but Cirque 1 contains the most exposed glacier with an extensive, low-relief forefield, which may explain its limited expansion during the LIA. ΔELA does not appear to covary with glacier area, head altitude, or aspect (Table 5).

The modern ELA of 980 ± 90 m determined in this study is similar to a GIS assessment of 106 cirque glaciers in the Ahklun Mountains completed by Manley (1999). Manley estimated a regional ELA of 929 ± 127 m, with 73% of the variance in ELA accounted for by microclimate variables (winter precipitation, summer temperature, aspect, etc.). Manley (1999) also demonstrated that the Ahklun Mountains cirque glaciers are sensitive to climate changes that affect accumulation and ablation. For example, a 50 m rise in the ELA would result in a 40% decrease in the total glacier area. The only other ELA analysis from southwestern Alaska is that of Levy et al. (2004) for Waskey Lake. Their ΔELA estimate for the LIA (35 ± 22 m) overlaps with the Cascade Lake study area. Additionally, Skiorski (2004) and Daigle and Kaufman (2006) determined ΔELA's of 25 ± 17 m in the Brooks Range and 50 ± 20 m on the Kenai Peninsula, respectively. In contrast, ΔELA values reported for the LIA in Alaska by Calkin et al. (1985) range from 100-200 m. Their calculation of 'modern' ELA was based on mass-balance data from 1976-1982, whereas Levy et al. (2004) Skiorski (2004), Daigle and Kaufman (2006), and my study used topographic maps and aerial photographs to derive modern ELA values. The location of the 'modern' ice front is a cumulative product of the previous decade's (post-LIA) climate, whereas the mass-balance studies

reflect the ELA of the limited study period. Therefore the higher ΔELA values of Calkin et al. (1985) may be attributed to the high ELA values of the 20th century.

The estimated ΔELA in the Cascade Lake study area (23 ± 13 m) can be used to estimate temperature lowering during the LIA. Using a typical environmental lapse rate of 6°/km (Porter, 2001) and assuming no change in precipitation, results in a cooling of 0.13 ± 0.07 °C during the LIA. This lapse rate is only slightly lower than the regional environmental lapse rate (7°/km) calculated from the summer temperature data in this study. This amount of cooling is significantly less than the LIA cooling of 2-3°C reported for the Brooks Range (Calkin et al., 1985), ≤ 1 °C temperature depression for the Wrangell Saint Elias Mountains (Davi et al., 2003), ~1.7 °C cooling in the Alaska Range (Hu et al., 2001), and the average 0.5-1.5 °C reported for the Northern Hemisphere (Grove, 2003; Maasch et al., 2005). The significantly cooler temperatures of Calkin et al. (1985) derive from their large ΔELA values. The calculation of temperature cooling from lapse rates and ΔELA values is dependent on the assumption that no change in moisture affected glacial expansion. However, if the northeastern Ahklun Mountains were drier during the LIA, this would have limited glacier expansion despite cooler temperatures. This scenario of a cold and dry LIA maximum in the study area may explain the discrepancy in LIA temperature cooling calculated from lapse rate values.

CHAPTER 4:
CASCADE LAKE SEDIMENTS

Background

Cascade Lake was targeted for a lake sediment study because it has a high sediment load and is hydraulically connected to up-valley glaciers that show evidence of late Holocene fluctuations. Additionally, Waskey Lake (Levy et al., 2004) to the south, and Arolik Lake (Kaufman et al., 2003) to the west have been used successfully to reconstruct paleoclimates in the region. Cascade Lake sediments were analyzed for a variety of proxy indicators including their geochronology, magnetic susceptibility (MS), organic-matter content (OM), biogenic silica (BSi), and lamination stratigraphy.

In lake sediments, MS is affected by organic content, density, grain size and mineralogy (Dearing, 1999), and it is not always possible to discern which property is forcing the MS signal. For this reason, MS is used to identify shifts in sedimentation patterns that can be correlated between cores and in some cases attributed to climate variability when used in combination with other proxy records. Variations in OM reflect a number of factors, including lake productivity, minerogenic flux, the input of terrestrial vegetation to the lake and diagenetic preservation. Because climate fluctuations can directly affect each of these factors, OM is a valuable indicator of climate (e.g., Willemse and Tornqvist, 1999; Kaufman et al., 2003; Bakke et al., 2005). BSi reflects the abundance of diatoms in lacustrine sediments. Diatoms are single-celled algae that typically dominate internal productivity in a lake and are sensitive to environmental changes, making them good climate proxies (e.g., Willemse and Tornqvist, 1999; Anderson, 2000). The deposition of laminations in a lacustrine setting can be driven by a

variety of hydrologic and meteorological controls (Leeman and Niessan, 1994; Lamoureux, 1999). This relationship between climate and lamination thickness has been used to produce quantitative and qualitative estimates of climate variability on annual to seasonal scales (Hughen et al., 2000; Moore et al., 2001; Loso et al., 2006). Each of these parameters were analyzed in Cascade Lake and interpreted for patterns that may be indicative of climate variability.

Methods

Bathymetry, Acoustic Profiling, and Core-Site Selection. Core site selection was based on bathymetric data and acoustic profiles. Bathymetric data were acquired with a Lowrance sonar unit and subsequently plotted in GIS with the shoreline based on 1973 maps. The sub-bottom stratigraphy was surveyed using an EdgeTech GeoStar acoustic profiler operating between 4 and 24 kHz. This profiling identified regions of continuous and condensed stratigraphy (avoiding slumps, methane, etc.). Three sites (distal-shallow, proximal-shallow, and proximal-deep) were targeted for percussion coring (Figure 13). Cores up to 6 m in length (7.5 cm diameter), were successfully recovered from these sites (Table 6). Coring was completed from an anchored floating platform and was continued until the core tubes were filled or an impenetrable layer was encountered. Because the uppermost sediments in the long cores are often disturbed, surface cores were also recovered from each site. These preserve the sediment-water interface and allow for an evaluation of the stratigraphic completeness in the long cores. Surface cores were either sub-sampled in the field into 0.5-cm increments or dewatered and packed. All cores were shipped to Northern Arizona University and placed in cold storage.

Lithostratigraphy. Cores were split and photographed at ~10-cm intervals to document sediment color prior to oxidation. General sediment descriptions (color, layers, bedding thickness, texture, etc.) were logged. Unique features, such as tephra beds (described below), were sub-sampled and viewed under a binocular microscope.

Additionally, a test pit was dug on the northern shoreline of Cascade Lake (Figures 13). The stratigraphy of the test pit was described and sub-samples were taken for radiocarbon analysis and visual comparison to the lake core stratigraphy.

Geochronology. A variety of methods were employed to determine the ages of the lacustrine sediments, each with well-established practices. These included: radiometric ^{210}Pb and ^{137}Cs dating, tephrochronology, and radiocarbon dating. ^{210}Pb analysis was completed on surface core 02A at the University of Illinois by alpha counting and on Core 02 at University of Southern California by gamma spectrometry in conjunction with ^{137}Cs analysis. Contiguous 0.5-cm-thick (~1 cm^3) samples were submitted for analysis. Both ^{210}Pb profiles were modeled using a constant rate of supply (CRS) model because this model copes with variable sedimentation rates, which probably fluctuated significantly (Appleby, 2004).

Tephras were located by their coarser grain size and their volcanic glass shards and pumice. MS peaks were also targeted due to the association of volcanic glass and magnetite. Each tephra was described under a binocular microscope to compare with other tephras known from the region. I analyzed the major-element geochemistry of the most prominent (visible and thickest) tephra in the Cascade Lake cores to correlate it with

tephra of a known age. The tephra was sampled from the center of the unit in Core 02 at a depth of 2.85 m. It was cleaned with 2% NaOCl and dried. Glass grains were hand picked under a binocular scope, epoxied onto a glass slide, polished with 1000 µm grit, then carbon coated for analysis on a Cameca MBX electron microprobe at Northern Arizona University. A single point on each of 31 glass grains was analyzed along with a standard of basaltic glass (USM 11349811) used to calibrate the microprobe prior to use. Total oxide percents of 10 elements were normalized to 100%. Similarity coefficients (Borchardt et al., 1972) were determined by comparison with published values for the 3500 cal yr BP Aniakchak tephra (Riehle et al., 1987; Béget et al., 1992; Levy, 2002).

Lake sediment samples were sieved every ~5 cm down the core profile in search of macrofossils, but no sample contained sufficient material for radiocarbon analysis. A single radiocarbon age was obtained from a buried soil in the test pit on the north shoreline of Cascade Lake. A sub-sample of the buried soil was wet-sieved and handpicked for vegetation macrofossils. Clean and dry macrofossils were analyzed by AMS at the University of California, Irvine. The radiocarbon age was calibrated using CALIB v. 5.0 (Stuvier et al., 1998) and the reported age is the median probability age of the 1σ calibrated age range.

Magnetic Susceptibility. MS was measured on the split core face using a Bartington MS2 meter, a hand-held MS2E1 detector, and Multisus computer software to correct for measurement drift. Refrigerated cores were brought to room temperature before analysis. Measurements were taken every 0.5 cm with drift correction every five readings. MS values are reported in Systéme International (SI) units and were taken at a 0.1 sensitivity

range setting. Sediments with anomalously high MS values were examined under a binocular microscope to confirm the presence of tephra shards, or unique mineralogy.

Organic-Matter Content. OM and bulk density were measured on two of the three cores. Contiguous 1 cm^3 samples were taken every 1 cm down to a depth of 198 cm in Core 01, and over the entire length of Core 02. In a few places sample resolution was reduced over coarse-grained, dense tephra units. Samples were processed using the procedure described by Dean (1974). They were dried at 90°C for 12 hr, and then weighed to measure dry bulk density. OM was approximated by LOI after combusting samples at 500°C for 5 hr. Because inorganic carbon content is negligible in the sediments, it was not measured.

Lamination Stratigraphy. Although laminations were faintly visible on much of the surface of the cores they were too diffuse for accurate measurement of thickness based on visual inspection. Therefore, the core face was sub-sampled to a depth of 140 cm and imaged by X-radiography. Slabs were 15 x 0.4 cm and were taken from the core axis with ~1 cm of overlap between the slabs. These uniform-thickness slabs were X-rayed at the NAU health center on detail film (3/20 sec, 50 mA, 50 kVp). Laminations were visible on the X-rays as discrete zones of millimeter-scale, alternating high and low density. Images were digitally spliced and lamination couplets were counted (four times) and the thickness of both the high- and low-density layers and the total couplet was measured (Figure 14).

Biogenic Silica. Biogenic silica (BSi) analysis was performed using the methods described by Mortlock and Froelich (1989). Contiguous 2-mm-thick samples were taken from Core 02 between 0 and 0.15 m, and from 0.15 to 1.50 m at a 5 mm sample interval. The rest of the core was sampled in 5-mm-thick sections at 5-cm intervals. Hydrogen peroxide (H_2O_2) and hydrochloric acid (HCl) were added to ~100 mg of dried and powdered sample to remove organic material and carbonate. BSi was then extracted with 10% sodium carbonate solution (Na_2CO_3). The supernate containing dissolved silica was then treated for molybdate-blue spectrophotometry through the reduction of the silicomolybdate complex. BSi concentration was determined with a HACH DR/2000 spectrophotometer set to 812 μm wavelength and zeroed against a blank standard of Na_2CO_3. Absorbance values were converted to BSi content using a standard curve created by NAU lab technician Caleb Schiff (Fall 2005).

Samples were run in groups of 40 and experienced some batch effects predominantly caused by slight variations in the mixing of the siliciomolybdate reduction solutions. In order to adjust for these batch effects, three samples from the initial batch were treated as standards and processed with every subsequent batch. Batches were then calibrated to the original batch by adjusting BSi values by the average difference of the three sample standards. Although the reported BSi content depends on these adjustments, the relative difference among sampled is reproducible to ± 0.3% (1σ) based on multiple runs of the standard samples.

Results and Discussion

Bathymetry, Acoustic Profiling, and Core Sites. Cascade Lake contains a deep trough (>50 m) running from the main inflow on the south end of the lake to the outlet on the north. Broad, sloping deltas extend from the main and eastern inflows (Figure 13). Acoustic profiling revealed generally continuous stratigraphy with localized zones of gas disruption (Figure 15). The recovered cores did not penetrate the full stratigraphic sequence visible in the acoustic profiles, with about 3 m of sediment remaining below the base Core 01; however, there was little acoustic stratigraphy visible beneath the base of Core 02. This could be because the stratigraphic sequence of this core is more complete or because the acoustic signal was degraded.

Lithostratigraphy. Core 01, from the north distal core site, consists of five main stratigraphic units with gradational contacts (Figure 16). (1) The basal unit (4.7 to 4.2 m) is composed of sand interbedded with gray (5B 5/1) mud. The fine-grained layers are separated by sharp contacts from the sandy mud. Unit 2 (4.2 to 3.6 m) is well-laminated with laminations apparently defined by grain size (silt rich vs. clay rich). The laminations range between ~0.25 and 1.0 cm thick. Unit 3 (3.6 to 2.8 m) consists of brown (2.5Y 5/4, 106 5/6) clay-rich mud. Unit 4 (2.8 to 1.1 m) is blue-gray clay-rich mud with three coarse-grained tephras layers. Unit 5 (1.1 to 0 m) is light-brown (2.5Y 5/4, 5Y 5/1) mud with very faint laminations in the uppermost ~30 cm.

The lithostratigraphy of Core 02 is very similar to Core 01 (Figure 16). It comprises five fine-grained units defined by color differences and separated by gradational contacts. (1) The basal unit (4.4 to 3.8 m) consists of sand interbedded with

gray, clay-rich mud. The sand layers are better defined than those of Core 01. Unit 2 (3.8 to 3.7 m) contains well-defined laminations > 1 cm thick, separated by sharp contacts. Unit 3 (3.7 to 3.1 m) is composed of clay-rich, light-yellow-brown (10YR 5/6) sediment with coarser-grained (not tephra) beds averaging 2 cm thick. Unit 4 (3.1 to 1.6 m) consists of blue and olive gray, fine-grained sediment (5B 5/1, 5Y 5/2) with five coarse-grained tephras. Unit 5 (1.6 to 0 m) is olive to yellow-brown (2.5Y 4/4, 10YR 5/6, 2.5Y 6/2) mud with faint laminations throughout. These laminations are a centimeter to millimeter thick.

Core 03 (deep, main basin core) is markedly different than Cores 01 and 02 (Figure 16). It contains well-defined, thick (0.5-3.0 cm) beds of alternating silt- to clay-rich mud and disturbed and deformed sediments that interrupt the bedded stratigraphy. Unit 1 (6.0 to 4.4 m) is composed of deformed sediments, coarse-grained beds and > 1-cm-thick laminations. Unit 2 (4.4 to 3.2 m) consists of coarse-grained layers interbedded with massive mud. Unit 3 (3.2 to 0.9 m) is predominantly deformed sediments with some discrete units of mud. Unit 4 (0.9 to 0 m) is composed of well-defined laminations that are discontinuous and separated by deformed sediments. Overall, Core 03 contains four zones of well-formed, grain-size-defined laminations. No tephras were observed in the Core 03.

The tops of Cores 01 and 02 were correlated with their sister surface cores using a distinct fine-grained marker bed that grades upward from dark brown to red-brown. In Core 01 this marker bed is at 8.0-8.5 cm depth, and at 8.5-9.0 cm in the surface core. In Core 02 the bed is thicker and at a depth of 13.5-15.0 cm compared to 14.0-15.0 cm in the surface core (Figure 17). Using these correlations, ~0.5 cm is missing from the

surface of each of the long cores and core-tube depths were adjusted accordingly so that all reported depths are relative to the lake floor.

The lithostratigraphy of Cores 01 and 02 can be roughly correlated (Figure 16). Both contain a thick (~15 cm) tephra (at 2.12 m in Core 01 and 2.85 m in Core 02), and the basal sediments are similar in both cores. Laminations are better preserved in Core 02, though they are subtly visible on the surface of Core 01.

Because discrete horizontal beds are preserved in sections of Core 03, the disturbance and deformation probably was not caused by the coring process. Instead, the sediment deformation is likely caused by underflow currents or slumps within the deep trough where the core was recovered. The thick tephra unit visible in Cores 01 and 02 at 2.12 and 2.85 m, respectively, was not found in Core 03. This, in combination with the thick laminations of Core 03 (> 1 cm), indicates that sedimentation rate at the Core 03 site is significantly higher than that of Cores 01 and 02. For these reasons little further work was completed on Core 03.

I focused most of my work on Core 02 because the laminations were better preserved than in Core 01, likely due to its closer proximity to the main inflow, and it has a longer sedimentary sequence and is less disturbed than that of Core 03. The proximal-shallow water location of Core 02 also might be more sensitive to climate variability due to the greater influence of the main inflow compared to the distal site of Core 01.

The test pit dug on the northern shoreline of Cascade Lake was 25 cm deep and was subdivided into five units (Figure 18). (1) The base of the soil pit ended in a poorly sorted, sub-angular to sub-rounded cobble gravel. This is overlain by Unit 2 (24.5-10.0 cm) a beige-orange to brown-orange tephra that grades from coarse to fine sand and

contains pumice shards visible with a hand lens. Unit (3) (10.0 to 4.3 cm) is a buried A-horizon that is dark-brown to black. Unit 4 (4.3 to 2.6 cm) contains a discontinuous gray tephra, with pumice lapilli, forming discrete lenses and mixed with organic material from the buried soil below. Unit 5 (0-2.6 cm) is organic matter of living tundra.

^{210}Pb and ^{137}Cs. The two ^{210}Pb profiles analyzed from cores 02 and 02A are quite similar (Figure 19, Table A-1). In the core 02A, excess ^{210}Pb activity levels off at 1.0 dpm/g at ~13 cm depth, resulting in an age of 1856 AD at 12.25 cm (CRS model) and an average sediment flux of 0.08 g/cm^2/yr. The profile indicates a shift in sediment accumulation rate at ~8.25 cm (1948 AD). Below this point the sedimentation rate averages 0.48 mm/yr, compared with 1.76 mm/yr above it. This sedimentation-rate shift is only constrained by four points at the base of the profile. The ^{210}Pb profile from Core 02 results in an age of 1851 AD at a depth of 12.5 cm (Figure 19) similar to Core 02A. The ^{210}Pb activity of Core 02 exhibits a shift in sedimentation rate from 0.40 mm/yr below 8.25 cm to 1.48 mm/yr above this point. This shift occurred a 1952 AD according to the ^{210}Pb age model from Core 02, but is constrained by only two points. The ^{210}Pb profile of Core 02 was supplemented with ^{137}Cs analyses from the same sediments. ^{137}Cs peaked with atmospheric nuclear testing in 1963, and therefore can be used as an independent measure of sediment age. The activity of ^{137}Cs shows a prominent peak from 8-6 cm with a maximum at 6.25 cm (Figure 19). According to the ^{210}Pb profile, a depth of 6.25 corresponds to an age of 1971, not 1963.

The two ^{210}Pb models for core 02A and Core 02 differ slightly, especially in the youngest sediments, but are similar in sediments older than the 1800's. Both cores

exhibit a major shift in sedimentation rate at 1950 AD. Because the ^{210}Pb profile produce by gamma spectrometry was analyzed on sediments directly from Core 02, which was also analyzed for other parameters, I focused on this profile and incorporated it into the age model. The offset between the ^{210}Pb and ^{137}Cs ages determined from the same sediments might suggest an age error in the ^{210}Pb ages. However, ^{137}Cs was only analyzed every 0.5 cm, and the age of 1963 lies between the two points that define the ^{137}Cs peak in this profile. Assuming that the ^{137}Cs peak occurs at ~6 cm, then the ^{210}Pb ages are within ~4 yr.

Radiocarbon. A single ^{14}C age was obtained from the top 1 cm of the buried soil in the test pit on the lakeshore. The sample consisted of a mixture of detrital wood and leaf fragments (UCI AMS# 23856). The sample yielded a radiocarbon age of 435 ± 15 cal yr BP, which calibrates to 505 ± 20 cal yr BP. This is a maximum age for the tephra that overlies this buried soil.

Tephrochronology. Five prominent tephras were recognized in Core 02 at 3.41, 3.33, 3.24, 2.85, and 2.59 m (Table 7, Figure 16). All of these tephras were also recognized in Core 01 (except the uppermost tephra). In addition, two tephras were described from the test pit dug on the northern lakeshore (Table 7, Figure 13).

Two distinct populations were recognized in the geochemical data from the 2.85 m tephra in Core 02 (Figure 20, Table A-2), one with 74 ± 3% SiO_2 (n = 16) and one with 59 ± 4% SiO_2 (n = 15). This bimodal composition could derive from either zonation within the magma chamber or from the mixing of multiple eruptions into this single

layer. Similarity coefficients between these average data and published geochemical data for the Aniakchak tephra are as follows: 0.75 with Riehle et al. (1987, for the high SiO_2 group); 0.76 with Béget et al. (1992, for the high SiO_2 group); and 0.75 with Levy (2002, both SiO_2 groups). However, four of the individual point analyses showed a significant (>0.95 similarity coefficient) correlation with the Riehle et al. (1987) samples.

The geochemistry of the 2.85 m tephra correlates poorly with the reference samples of the 3500 cal yr BP Aniakchak tephra. On the other hand, the bimodal composition of this tephra is indicative of the Aniakchak tephra. Of the four tephras located in Ahklun Mountain lakes and analyzed for geochemistry by Levy (2002), only the Aniakchak tephra exhibits this bimodal composition. The Aniakchak tephra is also the thickest and coarsest-grained tephra in the region (Kaufman et al., 2003; Levy et al., 2004), as is the 2.85 m tephra in Cascade Lake. Scanning electron microscope images of the 2.85 m ash from Cascade Lake and a sample of known Aniakchak tephra also show similar shard morphologies (Figure 21). Both samples have fibrous pumice, blocky clasts, and bubble-walled platelets, all of which were also identified by Riehle et al. (1987) in their distal Aniakchak samples. For these reasons, I believe that the 2.85 m tephra in Core 02 is the Aniakchak tephra (= 3500 cal yr BP).

The stratigraphic position of the Aniakchak tephra helps to correlate other tephras. Assuming the Aniakchak tephra is correctly identified in the Core 02, then the base of the core is ~11,000 cal yr BP based on the extrapolation of sedimentation rates. Waskey Lake cores contain four other tephras, only one of which is younger than 11,000 cal yr BP (Levy et al., 2004) and therefore young enough to be in the Cascade Lake cores. This tephra, Tephra B, is a "pure, 1-cm-thick, dark tephra…dominantly fine sand

to coarse silt…the glass shards are platy, brown, phenocrystic and microlitic…bubble-wall junctions are present". In both Waskey Lake and Arolik Lake (Kaufman et al., 2003), Tephra B dates to ~6100 cal yr BP, and is the next recognized tephra below the Aniakchak tephra. In the Cascade Lake cores, the 3.24 m tephra is the next lower and a likely candidate for Tephra B. However, the tephras at 3.33 and 3.41 m also fit the description of Tephra B and are possible correlatives, although none were analyzed for major-element geochemistry.

Overall, more Holocene tephras are observed in the Cascade Lake cores than in any other lake core from the Ahklun Mountains; however, the record is complicated. The 505 cal yr BP gray tephra in the test pit could not be located in the cores despite an intensive search. Additionally, the tephra at 2.59 m is located only in Core 02, and was not found in the test pit or in Core 01. Of the other lakes cored in the Ahklun Mountains, only Little Swift Lake (Axford and Kaufman, 2004) contains two tephras older than the Aniakchak tephra and younger than 12,000 cal yr BP. Both Arolik Lake (Kaufman et al., 2003) and Waskey Lake (Levy et al., 2004) contain a single tephra over this interval. This is inconsistent with the three tephras in Cascade Lake below the Aniakchak tephra. The inconsistencies among these tephra records are difficult to explain. The deposition of tephra onto a snow-covered landscape and ice-covered lake may retard deposition of the tephra in an individual lake. Additionally, spatial patchiness has been documented in the physical parameters of lake sediments (e.g., water content, organic-matter, pigment, and phosphorus; Downing and Rath, 1988). Similar spatial heterogeneity might apply to the deposition of tephra in lake sediments. The presence of the 2.59 m tephra in Core 02 but not in Core 01 indicates that tephras are not deposited uniformly within large lakes.

Age Model. An age model was constructed for Core 02 based on the ^{210}Pb CRS model and the correlated ages of the Aniakchak tephra and Tephra B. Because Tephra B was not definitively located in Core 02 and could be any of the three tephras between the 3.24 or 3.41 m, two age models were created to bracket the range of these possible correlations (Figure 22). The age model was subdivided into three segments. The basal section is an assumed linear sedimentation between Tephra B and the base of the Aniakchak tephra. The average of the Tephra B alternatives results in a sedimentation rate of 0.2 mm/yr. The deposition of the Aniakchak tephra between 2.85 and 2.70 m was interpreted as being instantaneous. The next segment between the Aniakchak tephra and the ^{210}Pb age at 12 cm was assumed to be linear, with a sedimentation rate of 0.8 mm/yr. For the upper segment, the CRS ^{210}Pb model was approximated by a 3rd-order polynomial fit with increasing sedimentation rates upwards (from 0.4 mm/yr at the bottom to 1.5 mm/yr at the top).

The pronounced shifts in sedimentation rates can be reconciled with other evidence. The factor-of-four lower sedimentation rate below the Aniakchak tephra agrees with the sedimentation-rate shift that Levy (2002) documented in Waskey Lake. The striking increase in sedimentation rate at the top of the core (post-1950) corresponds to the high (21 m/yr) retreat rate of Cascade Glacier from 1935-1957 and a period of accelerated warming across the arctic (Overpeck et al., 1997).

If the low sedimentation rate between the Aniakchak tephra and Tephra B is assumed to continue to the base of the core, then the basal sediments are approximately 11,000 cal yr BP using an average linear sedimentation rate of 0.2 mm/yr. This continuation of a linear, low sedimentation rate below Tephra B is similar to that

determined by Levy et al. (2004) for Waskey Lake and the basal age corresponds with the a northwestern Ahklun Mountain deglaciation age of ~12,000 cal yr BP (Manley et al., 2001).

Magnetic Susceptibility. The average background MS value in all three cores is ~30 x 10^{-6} SI (Figure 23, Table A-3). Both Core 01 and 02 show elevated MS levels in the basal 1 m and discrete zones of high MS (> 50 x 10^{-6} SI). In Core 01, the peaks in MS occur at: 3.29 m (75.5 x 10^{-6} SI), 2.73 m (175 x 10^{-6} SI), 2.27 m (58 x 10^{-6} SI), and 2.1 m (412 x 10^{-6} SI). The sediment at 2.1 and 2.73 m contains tephra. There was no visible change in sediment composition at the 2.27 m MS peak, but the MS peak at 3.29 m contains >80% diatoms (primarily *Cyclotella*). MS peaks in Core 02 occur at: 3.35 m (105 x 10^{-6} SI), 2.84 m (343 x 10^{-6} SI), and 2.59 m (114 x 10^{-6} SI). The peaks at 2.59 m and 2.84 m correspond with tephras (see Tephrochronology). The sediments at 3.35 m (6250 cal yr BP) are similar to those at 3.29 m in Core 01; both contain a high percentage of *Cyclotella* diatoms. MS peaks in Core 03 are all less than 50 x 10^{-6} SI, and values vary between 7 and 47 x 10^{-6} SI.

Most of the MS peaks in the Cascade Lake cores coincide with tephras. The presence of multi-domain magnetite in coarse-grained tephras yields an elevated MS value when compared to the ambient lake sediments. The only MS peaks that do not coincide with tephra are the ~1-cm-thick layers containing >80% diatoms at 3.29 m in Core 01 and 3.35 m in Core 02. The association of elevated MS values with high diatom concentrations is unexpected because diatoms are pure opaline silica and should not have high MS. Possibly, the algal bloom responsible for the high concentration of diatoms

was also associated with increased growth of magnetobacteria. Magnetobacteria have been shown to respond directly to the same environmental factors that affect general lake productivity (Kim et al., 2005). Additionally, the draw-down of oxygen by a large algae bloom could produce anoxic conditions favorable for magnetobacteria growth (Kim et al., 2005). The general rise in background MS at the base of Cores 01 and 02 is related to the lithologic variability of sandy mud interbedded with fine-grained beds. This rise could reflect the mafic-rich sandy beds or the increased density of the fine-grained beds.

Organic-Matter Content. OM in Core 01 ranges from 3.1 to 5.0%, whereas in Core 02 it varies between 1.4 and 4.7% (Figure 24, Table A-4). Bulk density ranges between 0.7 to 2.2, and 0.5 to 2.1 g/cm^3, respectively, in the two cores. The OM profile for Core 02 has relatively low OM values at the base of the core that rise rapidly to a broad peak at ~3.55 m (7250 cal yr BP); then OM values gradually decrease to the top of the core. Bulk density shows little overall change in this core. OM and bulk density generally decrease towards the core top in Core 01. The highest OM values are at 1.54 m (4.9%) and 0.9 m (4.8%). Each of these peaks is constrained by multiple samples.

Bulk density and OM in Core 02 are weakly correlated ($r = -0.42$; $p = 1.3 \times 10^{-18}$). The overall low OM values reflect the pervasive minerogenic input from the glacial inflows and the relatively low lake productivity and vegetation growth on the surrounding landscape. The inverse relationship between OM and bulk density probably is due to increased sediment accumulation (high bulk density) diluting the organic matter. The decrease in OM in Core 02 at 3.55 m occurs over the prominent lithologic change from gray mud to yellow-brown mud with well-developed, thick laminations. The lowest OM

values at the base of Core 02 and at 2.85 m correlate with the coarsest sediments related to a tephra and sandy mud in these intervals.

Laminations. A total of 316 lamination couplets were counted between 0.05 (core top) and 1.45 m. These couplets averaged 4.2 mm in thickness, with the dense layers averaging 1.8 mm and the less-dense layers 2.4 mm thick (Figure 25). Based on observations from the core face, the dense (light) layers are associated with an increased proportion of fine-grained (clay) sediment relative to the less-dense (dark) layers. Total couplet thickness is more strongly related to the thickness of the less-dense layers ($r = 0.88$) than to the dense layers ($r = 0.73$). The thickness of the dense and less-dense layers show no relationship to one another ($r = 0.32$). Lamination thickness is highly variable ranging from 1 to 15 mm.

The discernable seasonal signal in the sediment-trap material suggests that Cascade Lake laminations are annual (varves). However, their relatively large average thickness and the geochronology suggest that this is not the case. The high variability in lamination thickness, with the lack of a systematic down-core pattern of fluctuation (i.e., no section contains laminations persistently above or below average thickness), indicate that lamination thickness is not a reliable proxy for climate fluctuation in this lake.

Applying the age model to the lamination counts indicates that the average lamination encompasses ~6 yr. This is on the scale of the sub-decadal climate-regime shifts that affect southwestern Alaska (AL, ENSO; Papineau, 2001). Changes in North Pacific climate regimes have been shown to influence fluvial dynamics and likely lacustrine sedimentation. For example, in southeastern Alaska, Neal et al. (2002)

demonstrated that ‘warm’ PDO regimes correlated with higher-discharge winters (more precipitation falling as rain as opposed to snow) and ‘cool’ PDO’s were related to higher summer discharge (precipitation stored as snow and released during the peak of the melt season). This type of multi-annual shift in runoff may drive shifts in sediment storage and therefore the formation of laminations in Cascade Lake. Hodgkins et al. (2003) showed that proglacial outwash plains can serve as either net sinks or net sources of sediment with the shifts in sediment storage driven by the runoff regime. This variation in sediment storage (potentially caused by North Pacific climate regime shifts) may explain the variations in sediment flux responsible for lamination thicknesses.

The deposition and preservation of laminations can also be caused by processes within the lake. The occurrence of large magnitude underflows or short-lived environmental events (e.g., storms) can dominate the sediment record of some lakes and result in the deposition of non-annual laminations (Lamoureux and Gilbert, 2004). These processes are often associated with sedimentary structures that can be related to turbidity flows or slumps, none of which were observed in Cascade Lake. Rhythmic laminations were also recognized by Lemmen et al. (1988) in a glacial-fed lake on Baffin Island. They interpreted the laminations as being caused by changes in the rate of sediment input to the lake and/or changes within the circulation of the lake. They also attributed the lack of varves to low total sediment input to the lake and the extremely fine nature of the sediment entering the lake. Cascade Lake has relatively high levels of summer suspended load, though concentrations were never measured, but the particle size is small (avg. 4 μm) and may result in a long sediment residence time in the water column and the non-deposition of varves.

Biogenic Silica. BSi in Core 02 averages 2% (i.e. 20 mg/g) and ranges from 0.6 to 6%, and shows significant variability including three prominent peaks (Figure 26, Table A-5). BSi values are the lowest at the base of the core and rise sharply at 3.35 m (6.0%; 6275 cal yr BP). Between 3.35 and 2.65 m, BSi values decrease again (3.0%) before rising to form a broad peak at 2.65 m (5.4%; 3500 cal yr BP). BSi values return to an average 1.6% and then peak between 1.18 and 1.03 m at 2.5%. The average BSi value towards the top of the core (1.03 to 0.0 m) is 1.9%.

The sharp peak in BSi at 3.35 m encompasses the ~1-cm-thick layer of diatoms. The deposition of these diatoms was probably short-lived (perhaps within a single season) and not caused by a long-term climate fluctuation. The BSi peak at 2.65 m occurs above the thick Aniakchak tephra deposited at 3500 cal yr BP. The deposition of tephra within a lake can encourage algal blooms, especially in environments where Si is a limiting factor (Telford et al., 2004). Although BSi was increasing just prior to the deposition of the 2.85 m tephra, the peak is significantly higher than the extrapolation of this rise, and the BSi recovers to a lower level within 0.4 m of the tephra, suggesting that this spike in BSi was caused by the tephra deposition.

CHAPTER 5:
BIOGENIC SILICA AND CLIMATE INTERPRETATIONS

Diatoms are excellent climate indicators because they have a short life span and respond directly and sensitively to physical, chemical and biological changes to their environment. Because the translation of climate fluctuations to diatom productivity is indirect, several assumptions must be made in order to use BSi as a proxy for climate, among these is the assumption that BSi concentrations are directly related to the productivity of diatoms.

The diversity and abundance of a diatom community in a lake is dependent on a variety of factors, including: temperature, nutrient load, length of ice cover, turbidity, thermal stratification, and duration of spring and fall turnover (Lotter et al., 1999; Anderson, 2000; Smol and Cumming, 2000; Douglas et al., 2004). Each of these environmental factors is directly linked to meteorological forcing (temperature, wind, precipitation, etc.), and, in turn, to climate processes. The relationship between diatom productivity and the physical/chemical characteristics of lakes is not always straight forward. For example, Bradbury et al. (2002) described the relationship between spring temperature and diatom concentration for Elk Lake, Minnesota. They discovered that cold springs could result in either a small diatom population through late ice-out and rapid over-turning or a large diatom population as a result of a slow transition to summer and a long over-turning period.

Nutrient load is perhaps the most complex factor affecting diatom growth. Silicon, nitrogen, and phosphorous are the dominant nutrients affecting the growth of diatom communities and can be derived from a variety of sources. In arctic and alpine

environments, silicon is primarily derived from groundwater and the dissolution of diatoms at the sediment/water interface, nitrogen (N) enters a lake from soils and vegetation, and phosphorous is regenerated from the lake sediment during the winter and transported to the photic zone during spring circulation, but is ultimately supplied from bedrock and eolian dust (Bradbury et al., 2002). The establishment and concentration of alder (*Alnus*) within the catchment following deglaciation, strongly controls N concentrations in southern Alaska lakes (Hu et al., 2001; Engstrom and Fritz, 2006). The development of soil and vegetation therefore is a primary influence on diatom growth.

The connection between lake productivity and climate is further complicated by the methods used to determine lake productivity. The use of BSi as a measure of lake productivity is dependent on the assumptions that: (1) The BSi preserved in the lake sediment is from algal growth rather than phytoliths, (2) there is little recycling of silica (dissolution of diatoms at the sediment/water interface), (3) there is minimal grazing of diatoms by higher trophic levels, (4) all algal species contributing to primary productivity are preserved in the lake sediment, and (5) there is no significant change in the size and silica concentration of the diatom species (Bradbury et al., 2002; Colman and Bratton, 2003). The validity of these assumptions is difficult to assess from the sediment record. In studies of lake productivity from Lake Baikal some have proven to be inadequate. For example, Qui et al. (1993) and Swann and Mackay (2006) both measured low BSi content in sediment with high diatom concentrations based on point counts and other techniques. This discrepancy was attributed to dissolution of the diatoms at the sediment/water interface during periods of low sedimentation.

Variations in BSi content in Cascade Lake are believed to reflect fluctuations in lake productivity. The lake is ice-free for approximately five months of the year, and likely has a significant nutrient load entering the lake, enabling a seasonal diatom bloom. The rather high sediment load of the lake may limit the area of the photic zone available for diatom growth, but surface area of the lake is large enough to support a significant diatom population. Diatom dissolution is dependent on the pH, temperature, salinity and ionic composition of the water and sediments (Ryves et al., 2001). Temperature was the only one of these parameters measured in the Cascade Lake; however, it is unlikely that extreme values of pH, salinity or ionic composition would be maintained in the lake for a significant period of time, and diatom dissolution is considered to be in the lake. The pronounced difference in BSi content in the trapped Cascade Lake sediments between 2004-2005 and 2005-2006 indicates that BSi is sensitive to interannual differences in weather conditions and therefore to longer term climate relationships. Because the laminations in Cascade Lake were determined to not be annual, I focused on fluctuations in BSi as the primary indicator of paleoclimate variability.

Methods

In order to determine which climate parameter is most strongly correlated with BSi in Cascade Lake sediments, I compared the BSi flux with meteorological records. The 3rd-order polynomial fit to the CRS age model was used to infer the ages of the high-resolution BSi samples analyzed from the top (0-14 cm) of Core 02 and to interpolate the sedimentation rates of each 0.2-cm-thick BSi sample. The average temporal resolution of the samples was determined to be 3 yr. BSi values were converted to BSi flux (BSi % x bulk density x sedimentation rate) using bulk density values that were linearly

interpolated between the 1-cm-thick samples analyzed for OM. This conversion to flux accounts for the effects of variable sediment dilution. These flux values were then correlated with meteorological parameters (e.g., mean annual temperature, June-July-August average temperature) from the instrumental records at Dillingham (NCDC, 2005; WRCC, 2006), discharge data from Nuyakuk River (70 km to the southeast; NWIS, 2006), and climate indexes from the North Pacific Ocean (e.g., North Pacific Index, Aleutian Low Pacific Index; Ebbesmeyer et al., 1995; Mantua et al., 1997; Beamish et al., 1997; NCAR, 2006). Correlations were made using both unsmoothed data and five-year running averages of the climate data. The five-year running average was to account for possible error in the ^{210}Pb age model, smoothing in the sedimentary record (bioturbation), and the prolonged influence of sub-decadal climate variability leading to 'memory effects' (e.g., a rise in the groundwater table that sensitizes a landscape to runoff in the years following). Temperature and precipitation data are discontinuous from the Dillingham station with significant gaps in the 1970's and 1930-1940's. Temperature averages were not used if more than three days were missing during a month and annual precipitation values were acceptable only for years with no missing values (n-values in Table 8).

Results

Correlations with BSi flux were made with 33 meteorological and North Pacific climate parameters. Of these correlations, 11 were deemed of interpretive value (Table 8). BSi flux showed the highest correlation with Nuyakuk River discharge ($r = 0.73$, $p = 2.2 \times 10^{-6}$); the five-yr running average of mean May temperature ($r = 0.70$, $p = 9.16 \times 10^{-}$

^{5}); and the five-yr running average of the Aleutian Low Pacific Index (ALPI, r = 0.68, p = 1.37 x 10^{-7}). BSi flux also correlated with the Pacific Decadal Oscillation Index (PDO, r = 0.42, p =0.003), and the Pacific Northwest Index (PNI, r = 0.41, p = 0.003), but not with the North Pacific Index (NPI, r = 0.17, p = 0.229).

Discussion

Controls on BSi in Cascade Lake. I attribute the relatively strong correlations between BSi, Nuyakuk River discharge, and May temperatures to the hydroclimate and landscape processes that control nutrient input to the lake. Because Cascade Lake does not support an anadromous fish population, all nutrients must enter the lake from terrestrial sources (fluvial, eolian, through-flow, groundwater, etc.). The majority of fluvial input to Cascade Lake traverses the glacial outwash plain of Cascade Glacier with the exception of the small western inflow (Figure 13). Glacial runoff is typically low in nutrient content (Qui et al., 1993), especially during periods of glacier retreat when the rock-water (ice) contact time is decreased (Lanfreniere and Sharp, 2005). Because of this, nutrient input to Cascade Lake (and algal growth) is probably more strongly related to precipitation than to glacier melt. Summer precipitation and spring snow-melt (winter precipitation) infiltrate the soil and flow over the landscape carrying nutrients to the lake. The gage on the Nuyakuk River measures the outflow of Nuyakuk and Tikchik Lakes (70 km southeast of Cascade Lake). Because less than 0.01% of the drainage basin is occupied by modern glaciers, summer ablation has little influence on Nuyakuk River discharge. There is no precipitation data from Cascade Lake, and Dillingham is more coastal than Cascade Lake, therefore Nuyakuk River discharge is the best approximation

of precipitation at Cascade Lake. The influence of runoff on algal growth in a nutrient-limited system has also been inferred for Grandfather Lake (Hu and Shemesh, 2003) and Arolik Lake (Hu et al., 2003) in the Ahklun Mountains. While this terrestrial input (related to precipitation) is likely the dominant source of Cascade Lake nutrients, some nutrients are probably re-circulated within the lake and along the lake shoreline, driven by wind mixing of sediments and erosion of the shoreline (e.g. Verschuren, 1999).

The relationship between May temperature and terrestrial runoff is more complex. In 2004-2006, Cascade Lake experienced melt-out in the last week of May or the beginning of June. Warmer May temperatures may result in earlier melt-out, rapid spring overturning, and an extended spring growing season. Additionally, earlier melt-out may result in increased overland-flow and near-surface through-flow entering the lake early in the season. If the ground is still frozen and lacks vegetation cover, precipitation may take a more direct, near-surface route to the lake.

In southwest Alaska, spring temperature and regional precipitation are directly influenced by the AL, dominant feature of winter atmospheric and oceanic circulation in the north Pacific Ocean. A strengthened AL tends to be associated with warmer and wetter winters along the Bering Sea due to the increased tendency for storm systems to pump warm air poleward (Rodionov et al., 2005). Additionally, of the climate modes defined by Mock et al. (1998), the northeast Pacific negative type and the northcentral Pacific negative type are the only two that result in positive winter temperature and precipitation anomalies in southwestern Alaska, and these two modes feature a strengthened AL.

The annual NPI is also a measure of AL strength, yet it shows no correlation with the BSi content of Cascade Lake ($r = 0.17$, $p = 0.229$). Although the ALPI and NPI are both measures of AL strength, they are negatively correlated ($r = -0.48$, $p = 3.46 \times 10^{-7}$) because they relate to AL variations differently. The ALPI is a measure of the average ocean area affected by low pressures (<100.5 kPa) from December-March, whereas the annual NPI is the area-weighted sea-level pressure (Beamish, 1997; Tenberth and Hurrell, 1994). Because the NPI is based on annual statistics, not only winter, the index is also influenced by the ENSO cycles of the South Pacific and therefore is less directly related to the climate regimes that affect algal growth at Cascade Lake. However, if the NPI index is calculated over the same months as the ALPI (DJFM), then the two indices are more strongly correlated ($r = -0.73$, $p = 1.41 \times 10^{-18}$) and the correlation between BSi flux and the DJFM NPI five-year running average becomes significant ($r = -0.42$, $p = 0.002$). The ALPI shows moderately strong correlations with the Dillingham winter precipitation and May temperatures ($r = 0.33$, $p = 0.056$, and $r = 0.31$, $p = 0.011$, respectively).

Paleoclimate Interpretations. The AL is likely the dominant factor in the regional climate that affects BSi at Cascade Lake, both in the last century and throughout the late Holocene. If so, then BSi fluctuations in the sediment cores can be used to characterize variations in the AL over the late Holocene with high BSi values being interpreted as 'mild' climates (moist and warm, with a strengthen AL). This interpretation of BSi flux was completed at a sub-decadal resolution back to ~2000 cal yr BP based on the high-resolution sampling interval (Figure 27). BSi flux shows three major fluctuations over

this period. Lake productivity was generally low from 2000 to 1450 cal yr BP (BSi flux = 1.4 $mg \cdot cm^{-2} \cdot yr^{-1}$) and rose from 1450 to 1150 cal yr BP (2.6 $mg \cdot cm^{-2} \cdot yr^{-1}$). BSi flux decreased from 1150 cal yr BP to 1850 AD (1.9 $mg \cdot cm^{-2} \cdot yr^{-1}$) and subsequently increased to its highest value in 1995 (4.4 $mg \cdot cm^{-2} \cdot yr^{-1}$). The pattern of these fluctuations (not the absolute timing) corresponds to the general climate patterns of the late Holocene, primarily the Medieval Warm Period (MWP), the Little Ice Age, and 20th century warming. Additionally, the climate patterns of the LIA interpreted from BSi flux are supported by the geomorphic evidence for glacial fluctuations. Low BSi flux in the 1800's corresponds to ice advance in the study area, followed by subsequent ice retreat and moraine stabilization in ~1860, and a return to increased BSi flux (Figure 27). The high productivity during the mid-1990's in Cascade Lake was unequalled at any time in the last 2000 yr and may indicate that the modern strengthening of the AL is significantly greater than during the past.

Few high-resolution records of climate continuously span the last few millennia in Alaska. The most complete and comparable records are that of Hu et al. (2001) and Loso et al. (2006) in southern Alaska (Figure 2), and Anderson et al. (2005) in the southern Yukon territory. Hu et al.'s (2001) record of oxygen isotopes from Farewell Lake (western Alaska Range) indicates a relatively warm climate from 850 to 1200 AD (1150-750 cal yr BP). This agrees with the general varve thickening in Iceberg Lake (Loso et al., 2006) from 1000 to 1250 AD (1000-800 cal yr BP) and the AL strengthening interpreted at Jellybean Lake (Anderson et al., 2005) between 1200 and 900 cal yr BP. This warm period is also indicated by the general lack of glacial advances across the Northern Hemisphere (Porter, 1986). If the rise in BSi flux between 1450 and 1150 cal

yr BP in Cascade Lake is related to the mild climate of the MWP, then the timing of MWP initiation is not synchronous and shows progressively later initiation eastward across southern Alaska over a 450 yr period. Cascade Lake is ~900 km west of Iceberg Lake and 600 km southwest of Farewell Lake (Figure 2). Warming at Cascade Lake was initiated 200 yr prior to that at Farewell Lake, 400 yr prior to that of Iceberg Lake, and 250 yr prior to Jellybean Lake (Figure 28).

The time transgression of MWP initiation may be explained by three possible causes, or some combination thereof. (1) Each of the climate records discussed above derive from different proxy records (varve thickness in Iceberg Lake, isotopes in Farewell Lake and Jellybean Lake, and BSi in Cascade Lake). While each of these proxies record climate variations, they may each respond to different combinations of temperature and precipitation. Depending on the climate thresholds necessary to produce a measurable change, each proxy may record the initiation of different 'stages' of the climate event. (2) The age model for Cascade Lake over this time period is based on a linear extrapolation of sedimentation rates to the Aniakchak tephra deposited at 3500 cal yr BP. Sedimentation rates likely vary with varying climate regimes, and the assumption of a linear sedimentation rate over this extended period inserts some uncertainty in the Cascade Lake age model. (3) The average position of the AL migrated westward during the MWP.

Extending the climate interpretations beyond the last 2000 yr in Cascade Lake suggests other general late Holocene climate trends (Figure 28). BSi flux prior to ~6000 cal yr BP is low and shows little variation. This may, reflect, the flux calculation using the low sedimentation rate below Tephra B, or might indicate limited nutrient input to the

lake. Following deglaciation, the lack of vegetation (specifically the lack of nitrogen-fixing alder) would limit nutrient levels in the drainage basin. OM values increase between 11,000 and 7000 cal yr BP, indicating a milder climate following deglaciation and the cool period between 13,000-12,000 cal yr BP that has been inferred from lowered productivity in Arolik Lake during that time (Kaufman et al., 2001). Both Waskey Lake (Levy et al., 2004) and Cascade Lake record the highest OM preservation between 6500 and 7500 cal yr BP. Waskey Lake also experience limited glacial input during this time, making this period a likely candidate for the regional Holocene thermal maximum. This is significantly younger than the average 10,000 cal yr BP age of the Holocene thermal maximum across central and eastern Beringia (Kaufman et al., 2004).

Both Waskey Lake and Cascade Lake also record cooler climates between 3000 and 2500 cal yr BP, after the deposition of the Aniakchak tephra, marking the regional initiation of Neoglaciation. This age is younger than initial Neoglacial advances elsewhere in Alaska (4000-3500 cal yr BP in the Brooks Range, Ellis and Calkin, 1984; 4000-3000 cal yr BP on the Seward Peninsula, Calkin et al., 1998) and indicates a time-transgressive climate shift potentially similar to that of the Medieval Warm Period. Following the initiation of Neoglaciation, the glacial records at Waskey Lake and Cascade Lake areas diverge, with multiple Neoglacial moraines in the headwaters of Waskey Lake and only a single moraine formed late during the LIA around Cascade Lake. As discussed previously, the cause of this discrepancy is uncertain, though it may be related to variations in glacier flow mechanics caused by different subglacial bedrock lithologies.

CHAPTER 6:
CONCLUSIONS

This study combines a moraine record of glacial fluctuations with an interpretation of the sediments of Cascade Lake to determine the variability of Holocene climate in the Ahklun Mountains. The glaciers of the Cascade Lake area reached their maximum Neoglacial extent during the LIA. Lichenometric ages of five moraines deposited by glaciers draining into Cascade Lake were derived using the Seward Peninsula growth curve adapted from Solomina and Calkin (2003) with an increased colonization time (~30 years). These ages place the stabilization of maximum LIA moraines at ~1860 AD. Following moraine stabilization, Cascade Glacier retreated at a variable rate, averaging 11 m/yr, to its current location 1.4 km up-valley.

During the LIA, cirque and valley glaciers of the Cascade Lake area experienced an average ELA lowering of ~22 ± 12 m (n = 8) relative to 1957 AD. The ΔELA values of this study agree with other studies (Levy et al., 2004; Skiorski, 2004; Daigle and Kaufman, 2006) that used similar methodologies to derive the 'modern' ELA. This minimal ΔELA in the Cascade Lake area probably reflects limited winter precipitation during the LIA in southwestern Alaska.

The study of modern sedimentation patterns and temperatures of Cascade Lake provides a context for interpreting late Holocene lake sediment. The contrast in sediment accumulation and BSi flux between the two collection years (70% and 77% less, respectively, in the cooler 2006 spring/summer) indicates the strong control of spring/summer conditions on sediment and BSi accumulation in the lake. No precipitation data are available for Cascade Lake or Dillingham, making it difficult to

determine whether this difference is related to temperature or to precipitation. Precipitation has a more direct impact on discharge and terrestrial input of nutrients to the lake, but both of these factors likely affect sediment and BSi accumulation to varying degrees.

Annual fluctuations in the BSi, OM, and grain size analyzed in the trapped 2004-2006 sediments indicate a seasonal signal is preserved in the sediments. Sediment with low (high) BSi values correspond to elevated (decreased) bulk densities, and decreased (increased) OM and grain size, and was probably deposited during the fall/winter (spring/summer).

Of the three sediment cores recovered from Cascade Lake, I focused on Core 02 due to its longer record (compared to Core 03) and the occurrence of laminations. ^{210}Pb, ^{137}Cs, and the provisional identifications of the Aniakchak tephra and Tephra B provide the age control for the core. The chronology below Tephra B is extrapolated using a linear sedimentation rate. Overall, the chronologic control is limited and uncertain. MS and OM values show relatively little variation down core compared to the flux of BSi, and laminations are multi-annular (not varved). Therefore, I focused on BSi flux for the purpose of paleoclimate reconstruction due to its apparent sensitivity to climate variability and the ability to measure BSi at a high resolution (sub-decadal).

BSi flux (avg. 3 yr sampling resolution) was analyzed over the last 150 yr and correlated with a variety of instrumental climate parameters. The climatological parameters most strongly correlated with algal production in Cascade Lake are river discharge at a nearby gaging station, spring temperature, and the strength of the AL, with algal production favored during moist and warm conditions (strengthened AL). High BSi

flux indicates a mild climate from 1450-1150 cal yr BP (MWP?), a cool climate from 1150 cal yr BP to 1850 AD (LIA?), and a 20th century climate that was milder than that of even the MWP.

If the interpretation of climate variation is extended to the full Holocene sequence of lake sediments, other long-term trends can be inferred. The core did not extend into ice-proximal sediments, so conditions immediately following deglaciation are not known. Eventually the deglacial climate warmed and reached a period of maximum warmth ~7000 cal yr BP. Neoglacial cooling was initiated ~3000 cal yr BP, and glaciers reached their maximum LIA extent during the late 19th century.

Interpretations of sediments from Cascade Lake and the glaciers in the surrounding area indicate several periods of climate variability in the Ahklun Mountains during the late Holocene. This variability is closely related to the dynamics of the North Pacific Ocean and provides an important context for interpreting current and potential future climate change. No other interval of the Cascade Lake sediment record is comparable to the most recent period of warm and wet conditions, suggesting an unprecedented strengthening of the AL during the 20th century.

References Cited

Abbott, M.B., Finney, B.P., Edwards, M.E., Kelts, K.R., 2000. Lake-level reconstructions and paleohydrology of Birch Lake, central Alaska, based on seismic reflection profiles and core transects. Quaternary Research 53, 154-166.

Alley, R.B., Mayewski, P.A., Sowers, T., Stuiver, M., Taylor, K.C., Clark, P.U., 1997. Holocene climatic instability: A prominent, widespread event 8200 yr ago. Geology 25, 483-486.

Anderson, N.J., 2000. Diatoms, temperature and climate change. European Journal of Phycology 35, 307-314.

Anderson, L., Abbott, M.B., Finney, B.P., Burns, S.J., 2005. Regional atmospheric circulation change in the North Pacific during the Holocene inferred from lacustrine carbonate oxygen isotopes, Yukon Territory, Canda. Quaternary Research 64, 21-35.

Appleby, P.G., 2004. Chronostratigraphic techniques in recent sediments, in Last, W.M., Smol, J.P. (eds), *Tracking Environmental Change Using Lake sediments: Volume 1. Basin Analysis, Coring and Chronological Techniques*, 171-203 (Dordrecht: Kluwer).

Axford, Y., Kaufman, D.S., 2004. Late glacial and Holocene glacier and vegetation fluctuations at Little Swift Lake, southwestern Alaska, U.S.A. Arctic, Antarctic, and Alpine Research 36, 139-146.

Bakke, J., Lie, O., Nesje, A., Dahl, S.O., Paasche, O., 2005. Utilizing physical sediment variability in glacier-fed lakes for continuous glacier reconstructions during the Holocene, northern Folgefonna, western Norway. The Holocene 15, 161-176.

Béget, J., Mason, O., Anderson, P., 1992. Age, extent and climatic significance of the c. 3400 BP Aniakchak tephra, western Alaska, USA. The Holocene 2, 51-56.

Beamish, R.J., Neville, C.E., Cass, A.J., 1997. Production of Fraser River sockeye salmon (*Oncorhynchus nerka*) in relation to decadal-scale changes in the climate and the ocean. Canadian Journal of Fisheries and Aquatic Science 54, 543-554. Digital data at: http://www.pac.dfo-mpo.gc.ca/sci/sa-mfpd/downloads/indices/alpi.txt.

Bianchi, G.G., McCave, I.N., 1999. Holocene periodicity in North Atlantic climate and deep-ocean flow south of Iceland. Nature 397, 515-517.

Bond, G., Kromer, B., Beer, J., Muscheler, R., Evans, M., Showers, W., Hoffmann, S., Lotti-Bond, R., Hajdas, I., Bonani, G., 2001. Persistent solar influence on North Atlantic climate during the Holocene. Science 294, 2130-2136.

Bond, G., Showers, W., 1997. A pervasive millennial-scale cycle in North Atlantic Holocene and glacial climates. Science 278, 1257-1266.

Borchardt, G.A., Aruscavage P.J., Millard, H.T., 1972. Correlation of the Bishop ash, a Pleistocene marker bed, using instrumental neutron activation analysis. Journal of Sedimentary Petrology 42, 301-306.

Box, S.E., Moll-Stalcup, E.J., Frost, T.P., Murphy, J.M., 1993. Preliminary geologic map of the Bethel and southern Russian Mission quadrangles, Southwestern Alaska. U.S. Geologic Survey Report: MF-2226-A, 20 pp.

Bradbury, P., Cumming, B., Laird, K., 2002. A 1500-year record of climatic and environmental change in Elk Lake, Minnesota III: measures of past primary productivity. Journal of Paleolimnology 27, 321-340.

Briner, J.P., Kaufman, D.S., Werner, A., Caffee, M., Levy, L., Kaplan, M.R., and Finkel, R.C., 2002. Glacier readvance during the late glacial (Younger Dryas?) in the Ahklun Mountains, southwestern Alaska. Geology 30, 679-682.

Briner, J.P., Kaufman, D.S., 2000. Late Pleistocene glaciation of the southwestern Ahklun Mountains, Alaska. Quaternary Research 53, 13-22.

Calkin, P.E., Wiles, G.C., Barclay, D.J., 2001. Holocene coastal glaciation of Alaska. Quaternary Science Reviews 20, 449-461.

Calkin, P.E., 1988. Holocene glaciation of Alaska (and adjoining Yukon Territory, Canada). Quaternary Science Reviews 7, 159-184.

Calkin, P.E., Haworth, L.A., Burns, P.E., 1985. Cirque glacier regime and Neoglaciation, Brooks Range, Alaska. Zeitschrift fur Gletscherkude und Glazialgeologie 21, 371-378.

Calkin, P.E., Ellis, J.M., 1980. A lichenometric dating curve and its application to Holocene glacier studies in the central Brooks Range, Alaska. Arctic and Alpine Research 12, 245-264.

Campbell, I.D., Campbell, C., Apps, M.J., Rutter, N.W., Bush, A.B.G., 1998. Late Holocene ~1500 yr climatic periodicities and their implications. Geology 26, 471-473.

Colman, S.M., Bratton, J.F., 2003. Anthropogenically induced changes in sediment and biogenic silica fluxes in Chesapeake Bay. Geology 31, 71-74.

Crowley, T.J., Lowery, T.S., 2000. How warm was the Medieval Warm Period? Ambio 29, 51-54.

Dahl, S.O., Nesje, A., 1992. Paleoclimatic implications based on equilibrium-line altitude depressions of reconstructed Younger Dryas and Holocene cirque glaciers in inner Nordfjord, western Norway. Palaeogeography, Palaeoclimatology, Palaeoecology 94, 87-97.

Daigle, T.A., Kaufman, D.S., 2007. Late Holocene climate change at Goat Lake, Kenai Mountains, south-central Alaska. American Geophysical Union, Programme with Abstracts, in press.

D'Arrigo, R., Wilson, R., Deser, C., Wiles, G., Cook, E., Villalba, R., Tudhope, A., Cole, J., Linsley, B., 2005. Tropical-North Pacific climate linkages over the past four centuries. Journal of Climate 18, 5253-5265.

Davi, N.K., Jacoby, G.C., Wiles, G.C., 2003. Boreal temperature variability inferred from maximum latewood density and tree-ring width data, Wrangell Mountain region, Alaska. Quaternary Research 60, 252-262.

Dean, W.E., 1974. Determination of carbonate and organic matter in calcareous sediments and sedimentary rocks by loss on ignition: comparison with other methods. Journal of Sedimentary Petrology 44, 242-248.

Dearing, J., 1999. Environmental magnetic susceptibility: Using the Bartington MS2 system. Chi Publishing, Kenilworth, England.

Denton, G.H., Karlén, W., 1973. Holocene climatic variations—Their pattern and possible cause. Quaternary Research 3, 155-205.

Douglas, M.S.V., Hamilton, P.B., Pienitz, R., Smol, J.P., 2004. Algal indicators of environmental change in arctic and Antarctic lakes and ponds, in Pienitz, R. Douglas, M.S.V., Smol, J.P. (eds), *Long-term Environmental Change in Arctic and Antarctic Lakes*, 117-158 (Springer: Dordrecht)

Downing, J.A., Rath, L.C., 1988. Spatial patchiness in the lacustrine sedimentary environment. Limnology and Oceanography 33, 447-458.

Ebbesmeyer, C.C., Strickland, R.M., 1995. Oyster condition and climate: Evidence from Willapa Bay. Publication WSG-MR 95-02, Washington Sea Grant Program, University of Washington, 11 p. Digital data at: www.cqs.washington.edu/data.

Ellis, J.M., Calkin, P.E., 1984. Chronology of Holocene glaciation, central Brooks Range, Alaska. Geological Society of America Bulletin 95, 897-912.

Engstrom, D.R., Fritz, S.C., 2006. Coupling between primary terrestrial succession and the tropic development of lakes at Glacier Bay, Alaska. Journal of Paleolimnology 35, 873-880.

Evison, L.H., Calkin, P.E., Ellis, J.M., 1996. Late-Holocene glaciation and twentieth-century retreat, northeastern Brooks Range, Alaska. The Holocene 6, 17-24.

Francus, P., Bradley, R.S., Abbott, M.B., Patridge, W., Keimig, F., 2002. Paleoclimate studies of minerogenic sediments using annually resolved textural parameters. Geophysical Research Letters 29, 1-4.

Grove, J.M., 2003. *Little Ice Ages: Ancient and Modern*, pp. 643 (Routledge: Taylor & Francis Group).

Hardy, D.R., Bradley, R.S., Zolitschka, B., 1996. The climatic signal in varved sediments from Lake C2, northern Ellesmere Island, Canada. Journal of Paleolimnology 16, 227-238.

Hansen, B.C.S, Engstrom, D.R., 1996. Vegetation history of Pleasant Island, southeastern Alaska, since 13,000 yr B.P. Quaternary Research 46, 161-175.

Hoare, J.M., Coonrad, W.L., 1959. Geology of the Bethel quadrangle, Alaska. U.S. Geologic Survey Miscellaneous Geological Investigations Map I-285.

Hodgkins, R., Cooper, R., Wadham, J., Tranter, M., 2003. Suspended sediment fluxes in a high-Arctic glacierised catchment: implications for fluvial sediment storage. Sedimentary Geology 162, 105-117.

Hu, F.S., Finney, B.P., Bubaker, L.B., 2001. Effects of Holocene *Alnus* expansion on aquatic productivity, nitrogen cycling, and soil development in southwestern Alaska. Ecosystems 4, 358-368.

Hu, F.S., Ito, E., Brown, T.A., Curry, B.B., Engstrom, D.R., 2001. Pronounced climatic variations in Alaska during the last two millennia. Proceedings of the National Academy of Sciences 19, 10552-10556.

Hu, F.S., Kaufman, D., Yoneji, S., Nelson, D., Shemesh, A., Huang, Y., Tian, J., Bond, G., Clegg, B., Brown, T., 2003. Cyclic variation and solar forcing of Holocene climate in the Alaska subarctic. Science 301, 1890-1894.

Hu, F.S., Shemesh, A., 2003. A biogenic silica $\delta^{18}O$ record of climatic change during the last glacial-interglacial transition in southwestern Alaska. Quaternary Research 59, 379-385.

Hu, F.S., Nelson, D.M., Clarke, G.H., Rühland, K.M., Huang Y., Kaufman, D.S., Smol, J.P., 2006. Abrupt climatic events during the last glacial-interglacial transition in Alaska. Geophysical Research Letters 33, L18708.

Hughen, K.A., Overpeck, J.T., Anderson, R.F., 2000. Recent warming in a 500-year palaeotemperature record from varved sediments, Upper Soper Lake, Baffin Island, Canada. The Holocene 10, 9-19.

Innes, J.L., 1985. Lichenometry. Progress in Physical Geography 9, 187-254.

Kaufman, D.S., Ager, T.A., Anderson, N.J., Anderson, P.M., Andrews, J.T., Bartlein, P.J., Brubaker, L.B., Coats, L.L., Cwynar, L.C., Duvall, M.L., Dyke, A.S., Edwards, M.E., Eisner, W.R., Gajewski, K., Geirsdottir, A., Hu, F.S., Jennings, A.E., Kaplan, M.R., Kerwin, M.W., Lozhkin A.V., MacDonald, G.M., Miller, G.H., Mock, C.J., Oswald, W.W., Otto-Bliesner, B.L., Porinchu, D.F., Ruhland, K., Smol, J.P., Steig, E.J., Wolfe, B.B., 2004. Holocene thermal maximum in the western Artic (0-180°W). Quaternary Science Review 23, 529-560.

Kaufman, D.S., Hu, F.S., Briner, J.P., Werner, A., Finney, B.P., and Gregory-Eave, I., 2003. A ~33,000 year record of environmental change from Arolik Lake, Ahklun Mountains, Alaska. Journal of Paleolimnology 30, 343-362.

Kaufman , D.S., Manley, W.F., Forman, S.L., Layer, P.W., 2001. Pre-Late-Wisconsin glacial history, coastal Ahklun Mountains, southwestern Alaska-new amino acid, thermoluminescence, and $^{40}Ar/^{39}Ar$ results. Quaternary Science Reviews 20, 337-352.

Kayano, M.T., Brahmananda Rao, V., Andreoli, R.V., 2005. A review of short-term climate variability mechanisms. Advances in Space Research 35, 843-851.

Kim, B.Y., Kodama, K.P., Moeller, R.E., 2005. Bacterial magnetite produced in water column dominates lake sediment mineral magnetism: Lake Ely, USA. Geophysical Journal International 163, 26-37.

Lamoureux, S.F., 1999. Catchment and lake controls over the formation of varves in monomictic Nicolay Lake, Cornwall Island, Nunavut. Canadian Journal of Earth Science 36, 1533-1546.

Lamoureux, S.F., Gilbert, R., 2004. Physical and chemical properties and proxies of high latitude lake sediments, in *Long-term Environmental Change in Arctic and Antarctic Lakes*, 53-88 (Springer: Dordrecht).

Lafrenière, M.J., Sharp, M.J., 2005. A comparison of solute fluxes and sources from glacial and non-glacial catchments over contrasting melt seasons. Hydrological Processes 19, 2991-3012.

Leemann, A., Niessen, F., 1994. Varve formation and the climatic record in an alpine proglacial lake: calibrating annually-laminated sediments against hydrological and meteorological data. The Holocene 4, 1-8.

Lemmen, D.S., Gilbert, R., Smol, J.P., Hall, R.I., 1998. Holocene sedimentation in glacial Tasikutaaq Lake, Baffin Island. Canadian Journal of Earth Science 25, 810-823.

Leonard, E.M., Reasoner, M.A., 1999. A continuous Holocene glacial record inferred from proglacial lake sediments in Banff National Park, Alberta, Canada. Quaternary Research 51, 1-13.

Levy, L.B., Kaufman, D.S., Werner, A., 2004. Holocene glacier fluctuations, Waskey Lake, northeastern Ahklun Mountains, southwestern Alaska. The Holocene 14, 185-193.

Levy, L.B., 2002. Late Holocene glacier fluctuations, Northeastern Ahklun Mountains, southwestern Alaska. Master's thesis, Northern Arizona University.

Locke, W.W. II., Andrews, J.T., Webber, P.J., 1979. A manual for lichenometry. British Geomorphological Research Group Technical Bulletin 26, 47 p.

Loso, M.G., Anderson, R.S., Anderson, S.P., Reimer, P.J., 2006. A 1500-year record of temperature and glacial response inferred from varved Iceberg Lake, southcentral Alaska. Quaternary Research 66, 12-24.

Lotter, A.F., Pienitz, R., Schmidt, R., 1999. Diatoms as indicators of environmental change near arctic and alpine treeline, in Stoermer, E.F., Smol, J.P. (eds), *The Diatoms: Applications for the Environmental and Earth Sciences*, 205-226 (Cambridge: Cambridge University Press).

Maasch, K.A., Mayewski, P.A. Rohling, E.J., Stager, J.C., Karlén, W., Meeker, L.D., Meyerson, E.A., 2005. A 2000-year context for modern climate change. Geografiska Annaler 87, 7-15.

Manley, W.F., Kaufman, D.S., Briner, J.P., 2001. Pleistocene glacial history of the southern Ahklun Mountains, southwestern Alaska: Soil-development, morphometric, and radiocarbon constraints. Quaternary Science Reviews 20, 353-370.

Manley, W.F., 1999. GIS assessment of glaciers, equilibrium-line altitudes, and climate sensitivity, an example from southwestern Alaska. Geological Society of America, Abstracts with Programs 31, 366.

Mantua, N.J., Hare, S.R., Zhang, Y., Wallace, J.M., Francis, R.C., 1997. A Pacific interdecadal climate oscillation with impacts on salmon production. Bulletin of

the American Meteorological Society 78, 1069-1079. Digital data at: http://jisao.washington.edu/pdo/PDO.latest.

Mayewski, P.A., Rohling, E.E., Stager, J.C., Karlen, W., Maasch, K.A., Meeker, L.D., Meyerson, E.A., Gasse, F., van Kreveld, S., Holmgren, K., Lee-Thorp, J., Rosqvist, G., Rack, F., Staubwasser, M., Schneider, R.R., Steig, E.J., 2004. Holocene climate variability. Quaternary Research 62, 243-255.

Mayewski, P.A., Meeker, L.D., Twickler, M.S., Whitlow, S., Yang, Q., Lyons, W.B., Prentice, M., 1997. Major features and forcing of high-latitude northern hemisphere atmospheric circulation using a 110,000-year long glaciochemical series. Journal of Geophysical Research 102, 2634-26366.

Meier, M.F., Post, A.S., 1962. Recent variations in mass net budgets of glaciers in western North America. International Association of Scientific Hydrology 58, 63-77.

Minobe, S., Mantua, N., 1999. Interdecadal modulation of interannual atmospheric and oceanic variability over the North Pacific. Progress in Oceanography 43, 163-192.

Mock, C.J., Bartlein, P.J., Anderson, P.M., 1998. Atmospheric circulation patterns and spatial climatic variations in Beringia. International Journal f Climatology 10, 1085-1104.

Moore, J.J., Hughen, K.A., Miller, G.H., Overpeck, J.T., 2001. Little Ice Age recorded in summer temperature reconstruction from varved sediments of Donard Lake, Baffin Island, Canada. Journal of Paleolimnology 25, 503-517.

Mortlock, R.A., Froelich, P.N., 1989. A simple method for the rapid determination of biogenic opal in pelagic marine sediments. Deep-Sea Research 36, 1415-1426.

NCAR, 2006. NP data provided by the Climate Analysis Section, NCAR, Boulder, USA, Trenberth and Hurrell (1994). Digital data at: www.cgd.ucar.edu/cas/jhurrell/npindex.html.

NCDC, 2005. National climatic data center data set for daily surface data, Dillingham, AK. Digital data at: http://www.ncdc.noaa.gov/oa/ncdc.html.

Neal, E.G., Walter, M.T., Coffeen, C., 2002. Linking the pacific decadal oscillation to seasonal stream discharge patterns in southeast Alaska. Journal of Hydrology 263, 188-197.

Noon, P.E., Birks, H.J.B., Jones, V.J., Ellis-Evans, J.C., 2001. Quantitative models for reconstructing catchment ice-extent using physical-chemical characteristics of lake sediments. Journal of Paleolimnology 25, 375-392.

Noren, A.J., Bierman, P.R., Steig, E.J., Lini, A., Southon, J.A., 2002. Millennial-scale storminess variability in the northeastern United States during the Holocene. Nature 419, 821-824.

NWIS, 2006. National Water Information System data set for Nuyakuk River discharge 1949-2004. Digital data at: http://waterdata.usgs.gov/ak/nwis/.

O'Brien, S.R., Mayewski, P.A., Meeker, L.D., Meese, D.A., Twickler, M.S., Whitlow, S.I., 1995. Complexity of Holocene climate as reconstructed from a Greenland ice core. Science 270, 1962-1964.

O'Neal, M.A., 2006. The effects of slope degradation on lichenometric dating of Little Ice Age moraines. Quaternary Geochronology 1, 121-128.

Overpeck, J., Hughen, K., Hardy, D., Bradley, R., Case, R., Douglas, M., Finney, B., Gajewski, K., Jacoby, G., Jennings, A., Lamoureux, S., Lasca, A., MacDonald, G., Moore, J., Retelle, M., Smith, S., Wolfe, A., Zielinski, G., 1997. Arctic environment change of the last four centuries. Science 278, 1251-1257.

Papineau, J.M., 2001. Wintertime temperature anomalies in Alaska orrelated with ENSO and PDO. International Journal of Climatology 21, 1577-1592.

PNWPEST, 2006. Current and historical weather data set 2004-2006, maximum and minimum daily temperature for Dillingham, Alaska and Bethel, Alaska. Integrated Plant Protection Center, Oregon State University. Digital data set: http://pnwpest.org/ak/.

Porter, S.C., 2001. Snowline depression in the tropics during the last glaciation. Quaternary Science Reviews 20, 1067-1091.

Porter, S.C., 1986. Pattern and forcing of Northern Hemisphere glacier variations during the last millennium. Quaternary Research 26, 27-48.

Porter, S.C., Denton, G.H., 1967. Chronology of Neoglaciation in the North American cordillera. American Journal of Science 255, 177-210.

Pienitz, R., Douglas, M.S.V., Smol, J.P., eds., 2004. Long-term Environmental Change in Arctic and Antarctic Lakes, v. 8. Springer, Dorderecht, 509 p.

Qiu, L., Williams, D.F., Gvorzdkov, A., Karabanov, E., Shimaraeva, M., 1993. Biogenic silica accumulation and paleoproductivity in the northern basin of Lake Baikal during the Holocene. Geology 21, 25-28.

Riehle, J.R., Meyer, C.E., Ager, T.A., Kaufman, D.S., Ackerman, R.E., 1987. The Aniakchak tephra deposit, a late Holocene marker horizon in western Alaska. US Geological Survey Circular 998, 9-22.

Rodionov, S.N., Overland, J.E., Bond, N.A., 2005. The Aleutian low and winter climatic conditions in the Bering Sea. Part I: Classification. Journal of Climate 18, 160-177.

Ryves, D.B., Juggins, S., Fritz, S.C., Battarbee, R.W., 2001. Experimental diatom dissolution and the quantification of microfossil preservation in sediments. Palaeogeography, Palaeoclimatology, Palaeoecology 172, 99-113.

SCAS, 2005. PRISM data set 1961-1990, mean monthly precipitation and temperature for Alaska and Yukon Territory, Spatial Climate Analysis Service, Oregon State University. Digital data set: http://www.oc.orst.edu/prism/.

Schneider, N., Cornuelle, B.D., 2006. The forcing of the Pacific Decadal Oscillation. Journal of Climate 18, 4355-4373.

Skiorski, J.J., 2004. Little Ice Age glacier fluctuations and winter precipitation, Brooks Range, Alaska. Master of Science thesis, Northern Arizona University.

Smol, J.P., Cumming, B.F., 2000. Tracking long-term changes in climate using algal indicators in lake sediments. Journal of Phycology 36, 986-1011.

Solomina, O., Calkin, P.E., 2003. Lichenometry as applied to moraines in Alaska, U.S.A., and Kamchatka, Russia. Arctic, Antarctic and Alpine Research 35, 129-143.

Spooner, I.S., Barnes, S., Baltzer, K.B., Raeside, R., Osborn, G.D., Mazzucchi, 2003. The impact of air mass circulation dynamics on late Holocene paleoclimate in northwestern North America. Quaternary International 108, 77-83.

Stuiver, M., Reimer, P.J., Bard, E., Beck, J.W., Burr, G.S., Hughen, K.A. et al., 1998. INTCAL98 Radiocarbon age calibration, 24,000-0 cal BP. Radiocarbon 40, 1041-1082.

Swann, G.E.A., Mackay, A.W., 2006. Potential limitations of biogenic silica as an indicator of abrupt climate change in Lake Baikal, Russia. Journal of Paleolimnology 36, 81-89.

Telford, R.J., Barker, P., Metcalfe, S., Newton, A., 2004. Lacustrine responses to tephra deposition: examples from Mexico. Quaternary Science Reviews 23, 2337-2353.

Trenberth, K.E., Hurrell, J.W., 1994. Decadal atmosphere-ocean variation in the Pacific. Climate Dynamics 9, 303-319.

Torsnes, I., Rye, N., Nesje, A., 1993. Modern and Little Ice Age equilibrium-line altitudes on outlet valley glaciers from Jostedalsbreen, Western Norway: an evaluation of different approaches to their calculation. Arctic and Alpine Research 25, 106-116.

Verschuren, D., 1999. Sedimentation controls on the preservation and time resolution of climate-proxy records from shallow fluctuating lakes. Quaternary Science Reviews 18, 821-837.

Waythomas, C.F., Neal, C.A., 1998. Tsunami generation by pyroclastic flow during the 3500-year B.P. caldera-forming eruption of Aniakchak Volcano, Alaska. Bulletin of Volcanology 60, 110-124

Werner, A., 1990. Lichen growth rates for the northwest coast of Spitsbergen, Svalbard. Arctic and Alpine Research 22, 129-140.

Wiles, G.C., Calkin, P.E., 1994. Late Holocene, high-resolution glacial chronologies and climate, Kenai Mountains, Alaska. Geological Society of America Bulletin 106, 281-303.

Willemse, N.W., Tornqvist, T.E., 1999. Holocene century-scale temperature variability from West Greenland lake records. Geology 27, 580-584.

WRCC, 2006. Western Regional Climate Center data set of historical climate data for Dillingham, AK FAA airport. Digital data at: http://www.wrcc.dri.edu/index.html.

TABLE 1. INSTRUMENTS DEPLOYED AT CASCADE LAKE

Instrument	Location	Latitude Longitude (NAD 27)	Launch date	Recovery date	Comments
Mooring 1					
Sediment trap	Core site 01 ~3 m water depth	60.14231 159.41209	6/28/04	8/10/05	Sediment accumulation =0.11 g/cm^3/yr in 2004-2005
Hobo Water Temp Pro					
Sediment trap	Core site 01 ~23 m water depth		8/12/05	7/19/06	
Hobo Water Temp Pro					
Mooring 2					
Sediment trap	Core site 03 ~3 m water depth	60.13643 159.39917	6/28/04	8/11/05	Sediment accumulation =0.10 g/cm^3/yr in 2004-2005 = 0.03 g/cm^3/yr in 2005-2006
Hobo Water Temp Pro					
Sediment trap	Core site 03 ~51 m water depth		8/12/05	7/19/06	
Hobo Water Temp Pro					
Air temperature					
Hobo Pro	Western lake shore (Fig. 3)	60.14082 159.41236	06/28/4 8/12/05	8/9/05 7/20/06	Temp. logger failed between 12/22/04 and 8/9/05
Hobo Pro	Cascade Glacier ice proximal (Fig. 3)	60.08872 159.34043	8/13/05	7/20/06	

TABLE 2. PHYSICAL AND BIOLOGICAL DATA FROM BOTTOM SEDIMENT TRAPS

Unit	Top depth (cm)	Bottom depth (cm)	BSi (%)	BSi flux ($mg \cdot cm^{-2} \cdot yr^{-1}$)	Median grain size (μm)	Organic matter (%)	Bulk density (g/cm^3)
Mooring 1: 2004-2005							
1	0.0	1.9	2.91	3.20	5.19	5.5	0.29
2	1.9	3.9	2.50	2.75	1.95	6.1	0.18
3	3.9	7.9	1.86	2.05	3.62	4.5	0.34
4	7.9	9.4	1.49	1.64	4.55	3.5	0.86
5	9.4	14.4	2.04	2.25	4.61	4.0	0.60
Mooring 2: 2004-2005							
1	0.0	1.7	N.D.	N.D.	N.D.	N.D.	0.40
2	1.7	8.9	N.D.	N.D.	N.D.	N.D.	0.25
3	8.9	11.9	N.D.	N.D.	N.D.	N.D.	0.44
4	11.9	12.9	N.D.	N.D.	N.D.	N.D.	0.47
5	12.9	15.9	N.D.	N.D.	N.D.	N.D.	0.31
6	15.9	17.7	N.D.	N.D.	N.D.	N.D.	0.48
7	17.7	18.1	N.D.	N.D.	N.D.	N.D.	0.66
Mooring 2: 2005-2006							
1	0.0	1.6	1.27	0.38	N.D.	N.D.	0.22
2	1.6	2.3	1.60	0.48	N.D.	N.D.	0.37
3	2.3	2.5	1.59	0.48	N.D.	N.D.	0.56
4	2.5	5.9	1.67	0.50	N.D.	N.D.	0.11
5	5.9	8.1	1.30	0.39	N.D.	N.D.	0.18
6	8.1	8.5	1.60	0.48		N.D.	0.66

Note: N.D. = no data collected on these samples.

TABLE 3. CLIMATE DATA FROM PREVIOUSLY PUBLISHED LICHEN GROWTH-CURVE SITES OF SOLOMINA AND CALKIN (2003), CASCADE LAKE, AND OTHER LONG-TERM WEATHER STATIONS IN SOUTHWEST ALASKA (DILLINGHAM AND BETHEL)

	Elevation (m)	Mean annual temp. (°C)	June, July, August (JJA) average temp. (°C)	Mean annual precipitation (mm)
Lichen growth-curve sites				
Brooks Range	350	-5.5	12.5	267
Seward Peninsula	4	-3.2	9.4	342
Wrangell-St. Elias	522	-5.7	13.3	201
Alaska Range	479	-2.9	12.6	239
Kenai (Homer)	27	3.0	11.1	518
Other climate stations				
Bethel	36	1.4	12.0	430
Dillingham	20	1.0	11.7	647
Cascade Lake*	334	-4.0	8.7	

Note: Climate data from the Spatial Climate Analysis Service (SCAS, 2005).
*Based on daily averages at Cascade Lake from 2004-2006. Considered most similar to Seward Peninsula.

TABLE 4. SUMMARY OF LICHEN SIZES ON MORAINES AND OTHER DEPOSITS

Glacier	Site # (Fig. 8)	Latitude (°N)	Longitude (°W)	Deposit type	Five largest (mm) Mean	Five largest (mm) ±S.D.	All measured (mm) Mean	All measured (mm) ±S.D.	n	Single largest (mm)	Lichen year (based on Seward Pen. growth-curve with ~30 yr colonization time)
Cascade	1	60.1018	159.3493	left lateral*	39	2	33	4	23	42	71
Cascade	2	60.1009	159.3485	left lateral*	29	1	25	4	20	30	115
Cascade	3	60.1020	159.3446	right lateral	32	4	26	6	13	39	129
Cascade	4	60.1019	159.3460	right lateral	34	4	29	4	18	40	140
E. Inflow	5	60.1314	159.3603	moraine crest†	36	3	33	3	14	39	152
E. Inflow	6	60.1339	159.3653	debris flow†	26	1	23	4	8	28	10
E. Inflow	7	60.1343	159.3734	debris flow†	27	4	23	4	19	32	106
E. Inflow	8	60.1344	159.3647	debris flow†	28	4	25	4	12	32	111
Hungry Joe	9	60.1066	159.3235	stable outwash	23	4	23	4	3	33	91
Divided	10	60.1189	159.3215	slump	26	3	23	4	6	29	102
Chikuminuk	11	60.1495	159.3127	river terrace	33	9	27	9	10	49	135
Cascade	12	60.0942	159.3414	stable outwash lichen/no lichen contact	N.A.	N.A.	6	1	4	6	49
Cascade	13	60.0956	159.3426	stable outwash	16	6	13	5	10	27	70

*Shown in Figure 10A.
†Shown in Figure 10B.

TABLE 5. EQUILIBRIUM-LINE ALTITUDE (ELA) FOR GLACIERS IN THE CASCADE LAKE AREA

Glacier	Latitude	Longitude	1957 length	1957 area	Head altitude	Toe altitude	Aspect	1957 ELA	Neoglacial ELA	ELA lowering
(see Fig. 8)	(°N)	(°W)	(km)	(km^2)	(m)	(m)		(m)	(m)	(m)
Cascade Glacier	60.0917	159.3380	3.8	3.76	1250	550	N	980	945	35
Divided Cirque	60.0951	159.3119	1.7	1.24	1190	730	NW	900	890	10
Hungry Joe Cirque	60.1066	159.3196	0.4	3.17	1190	980	SW	1045	1030	15
East Inflow Cirque	60.1311	159.3574	0.5	3.08	1070	820	NW	1085	1060	25
Chikuminuk Glacier	60.1300	159.2973	3.5	5.98	1280	610	NW	965	945	20
Cirque 1	60.0816	159.2999	0.6	1.69	1190	1010	NE	1045	1040	5
Cirque 2	60.0826	159.2843	0.5	2.78	1100	940	SE	1010	965	45
Cirque 3	60.1398	159.3378	1.0	4.08	1160	670	S	820	795	25
Average								980	960	23
Std. deviation								90	80	13

TABLE 6. LOCATION AND OTHER INFORMATION FOR LAKE CORES RECOVERED FROM CASCADE LAKE

Core	Latitude (°N)	Longitude (°W)	Water depth (m)	Length (m)	Notes
04CA-01	60.1432	159.4167	24.2	4.68	
04CA-01A	60.1432	159.4167	24	0.20	Sub-sampled in field
04CA-01B	60.1432	159.4167	24	0.46	
05CA-01A	60.1435	159.4166	23	0.20	Sub-sampled in field
05CA-01B	60.1435	159.4166	23	0.46	
05CA-01C	60.1435	159.4166	23	0.35	
04CA-02	60.1327	159.3988	34.5	4.37	Some material lost from base during core recovery
04CA-02A	60.1327	159.3988	34	0.20	sub-sampled in field
04CA-02B	60.1327	159.3988	34	0.38	
05CA-02D	60.1333	159.3995	34	0.20	Sub-sampled in field
05CA-02E	60.1333	159.3995	34	0.38	
05CA-02F	60.1333	159.3995	34	0.31	
04CA-03	60.1371	159.4039	52.4	6.03	
04CA-03B	60.1371	159.4039	52	0.30	

Note: Surface cores indicated by letter designations.

TABLE 7. TEPHRA DESCRIPTIONS FROM CORE 02 AND THE LAKESHORE TEST PIT

Basal depth (cm)	Thickness (cm)	Glass type and color	Bedding	Contacts	Notes
Core 02					
2.59	1.1	Pink to cream bubble-walled shards	N.A.	Sharp upper and lower	Not located in Core 01
2.85	15.0	Fine gray bubble-walled shards, coarse white pumice, significant microlitic glass shards	Reversely graded at base	Gradational upper and lower	Inferred to be the Aniakchak tephra (3500 cal yr BP)
3.24	3.0	Rounded with bubble wall junctions, clear to brown	N.A.	Sharp upper and lower	Diatoms present
3.33	2.5	Brown glass shards	N.A.	Gradational upper, sharp lower	
3.41	2.5	Brown glass shards	N.A.	Gradational upper, sharp lower	
Test pit					
4.30	2.0	Gray to white bubble wall shards	Preserved in pods	N.A.	Overlies buried soil with a ^{14}C age of 505 ± 20 cal yr BP
15.40	5.4	Orange/beige bubble wall shards with white pumice	Reversely graded at base	Gradational top, sharp bottom	
Note: test pit illustrated in Figure 14.					

TABLE 8. CORRELATIONS BETWEEN BSi FLUX AND METEOROLOGICAL AND PACIFIC OCEAN CLIMATE INDICES

Correlated parameter*	Unsmoothed			5-year running avg.			Source†
	n-years	R	p-value	n-years	R	p-values	
Annual precipitation	19	0.35	0.144	18	0.44	0.437	1
May precipitation	19	0.03	0.892	14	-0.10	0.733	1
Mean annual temp	32	0.14	0.447	26	0.11	0.576	1
Mean DJF temp	26	-0.04	0.828	21	-0.35	0.120	1
Mean JJA temp	21	0.26	0.260	17	0.36	0.159	1
Mean may temp	31	0.54	0.002	25	0.70	9.16×10^{-5}	1
Nuyakuk River discharge	26	0.73	2.22×10^{-5}	23	0.71	1.27×10^{-4}	2
PDOI	51	0.31	0.028	49	0.42	0.003	3
NPI	52	0.04	0.760	50	0.17	0.229	4
DJFM NPI	52	-0.42	0.002	50	-0.42	0.002	4
ALPI	51	0.40	0.004	50	0.68	1.37×10^{-7}	5
PNI	53	0.32	0.022	52	0.41	0.003	6

*DJF = December, January, February; JJA = June, July, August; PDOI = Pacific Decadal Oscillation Index; NPI = North Pacific Index; DJFM = December, January, February, March; ALPI = Aleutian Low Pacific Index; PNI = Pacific Northwest Index.

†(1) WRCC, 2006 and NCDC, 2005; (2) NWIS, 2006; (3) Mantua et al., 1997; (4) NCAR, 2006; (5) Beamish et al., 1997; (6) Ebbesmeyer et al., 1995.

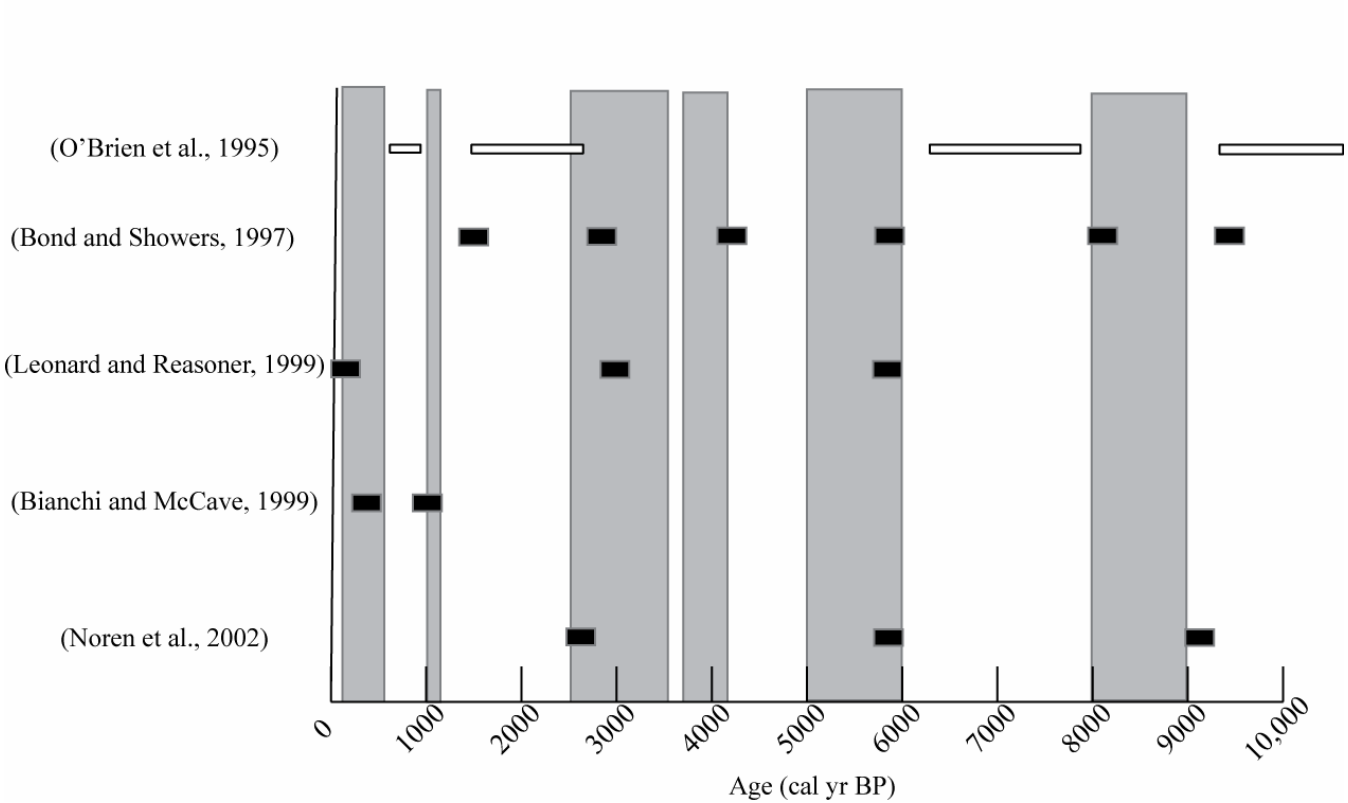

Figure 1: Periods of Holocene climate change. Columns denote the six periods of rapid climate change (polar cooling, tropical aridity) proposed by Mayewski et al. (2004). Black boxes are centered over periods of climate cooling determined by various authors (left column), and white boxes indicate mild, warm periods recognized by O'Brien et al. (1995).

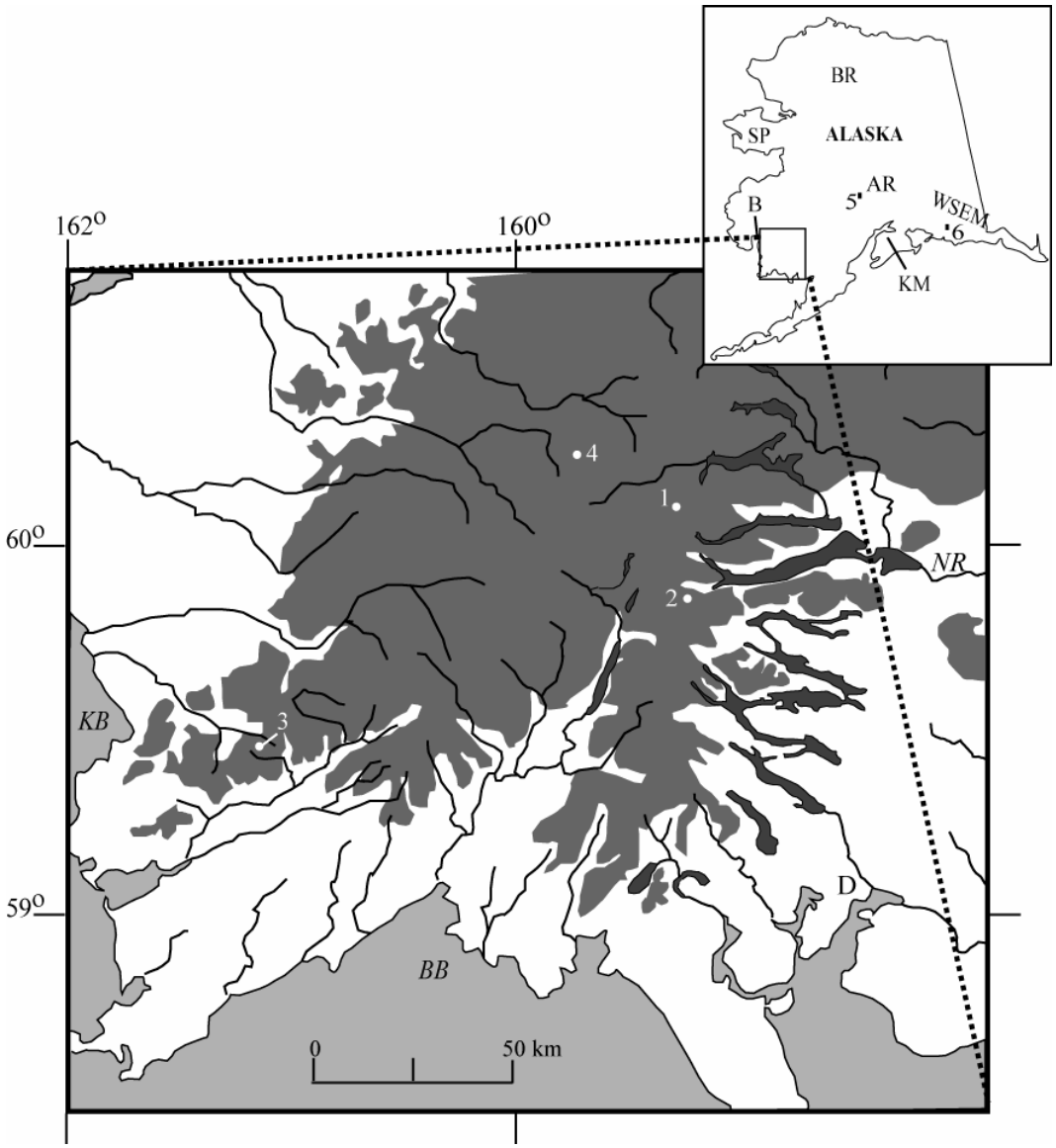

Figure 2: Location of the Ahklun Mountains and features discussed in this thesis (medium shading indicates elevations above 200 m). Lakes are indicated by numbers: (1) = Cascade Lake; (2) = Waskey Lake; (3) = Arolik Lake; (4) = Little Swift Lake; (5) = Farewell Lake; (6) = Iceberg Lake. Other locations indicated by letter designations: (AR) = Alaska Range; (B) = Bethel; (BR) = Brooks Range; (BB) = Bristol Bay; (D) = Dillingham; (KM) = Kenai Mountains; (KB) = Kuskokwim Bay; (NR) = Nuyakuk River; (SP) = Seward Peninsula; (WSEM) = Wrangell-St. Elias Mountains.

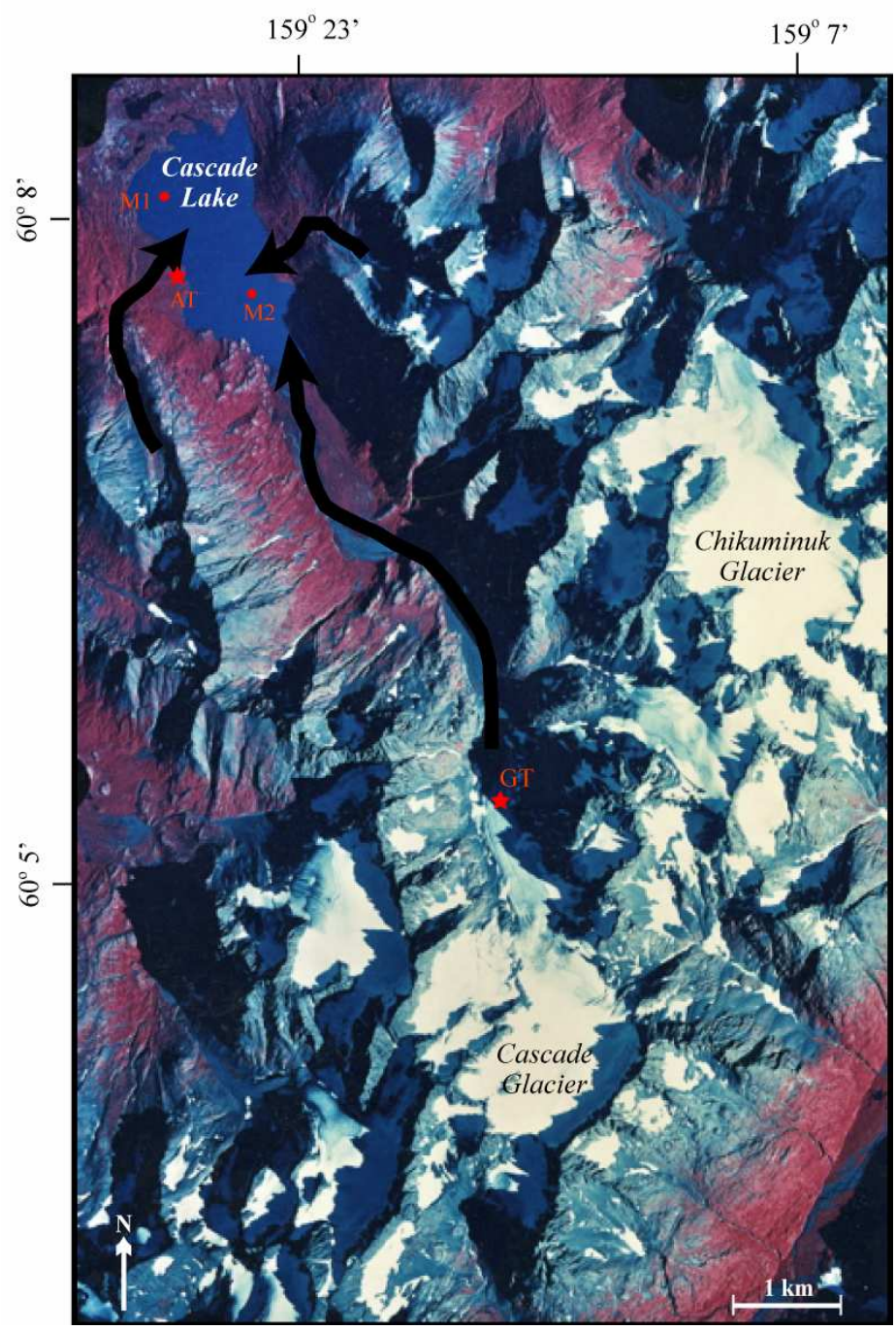

Figure 3: Cascade Lake area. 1983 aerial photograph with arrows denoting inflows to Cascade Lake; the western inflow is not glacier-fed. M1=Mooring 1, M2=Mooring 2, AT=Air temperature station, GT=Glacier temperature station.

A B

Figure 4: Instrumentation deployed at Cascade Lake. (A) Sediment trap and water-temperature logger mounted on mooring line. (B) Installing air-temperature logger housed in a solar-radiation shield in a stand of willow along the shoreline of Cascade Lake.

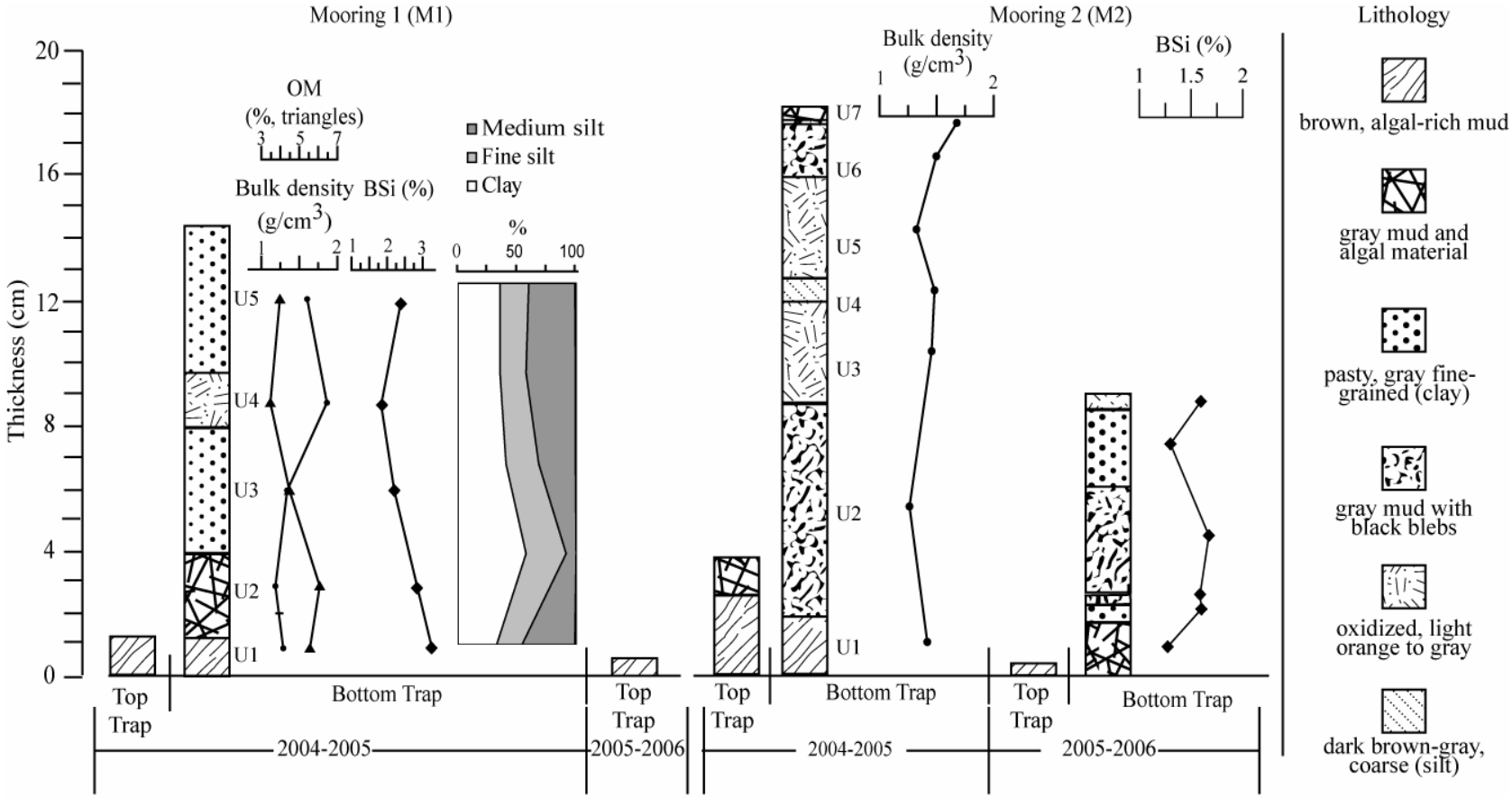

Figure 5: Lithologic descriptions of the sediments collected in traps from Cascade Lake on August 10, 2005 and July 19, 2006. Lithostratigraphy of bottom sediment traps from both mooring sites with physical and biological data (listed in Table 2).

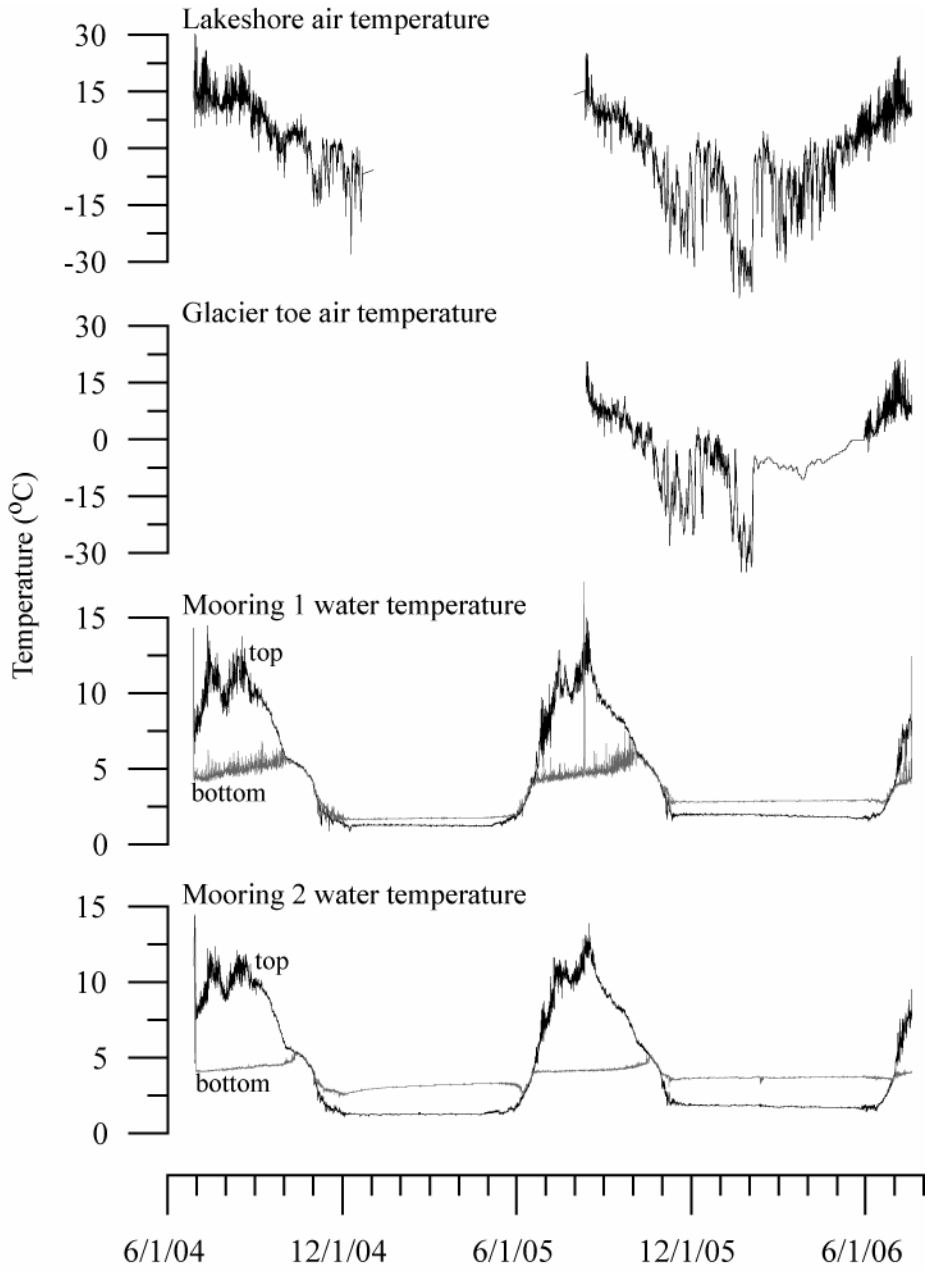

Figure 6: Daily average water temperature in Cascade Lake 2004-2006. Bottom loggers were positioned ~1 m above the lake bottom; top loggers were ~3 m below the water surface.

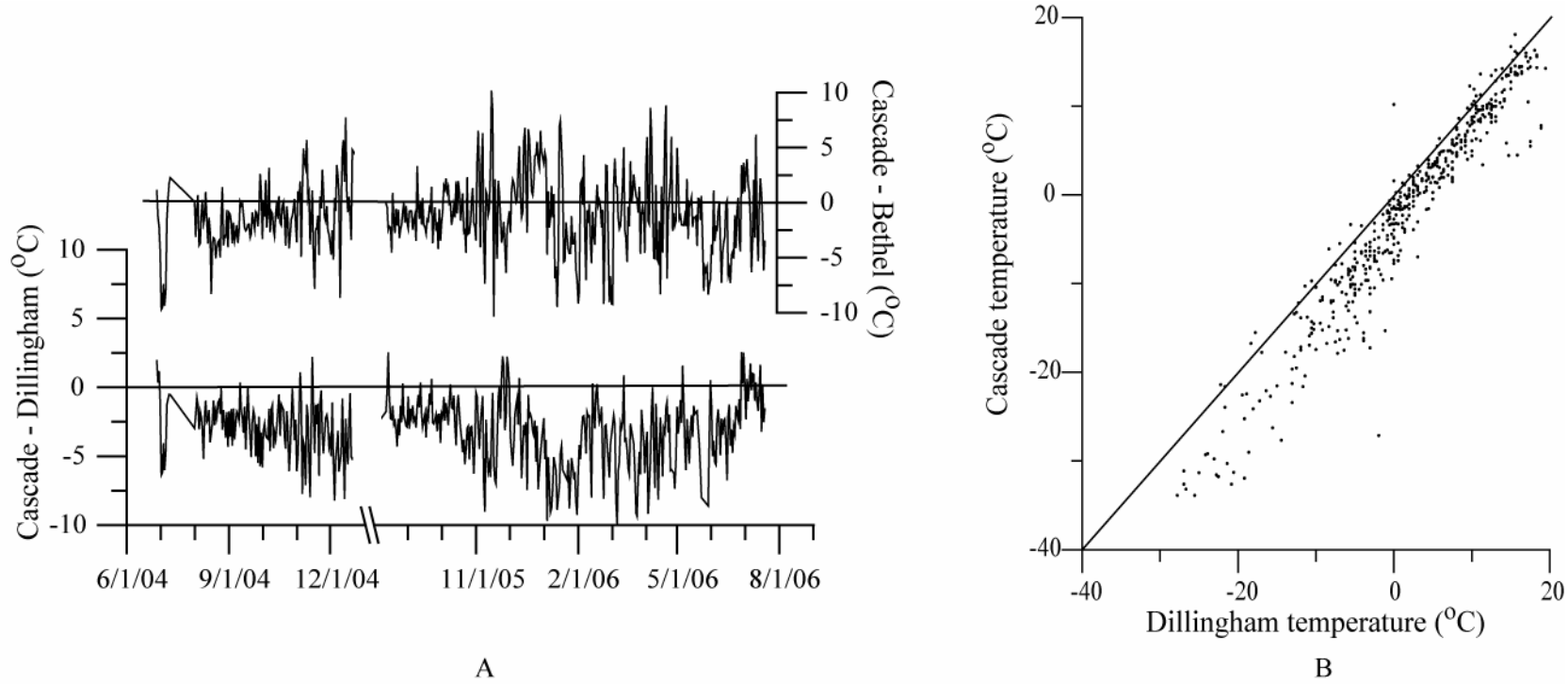

Figure 7: Comparisons between average daily temperature at Cascade Lake, Dillingham, and Bethel, AK. (A) Differences between sites. (B) Relationship between sites; note the slight seasonality effect shown by the increased offset from the 1:1 line for the coldest winter temperatures.

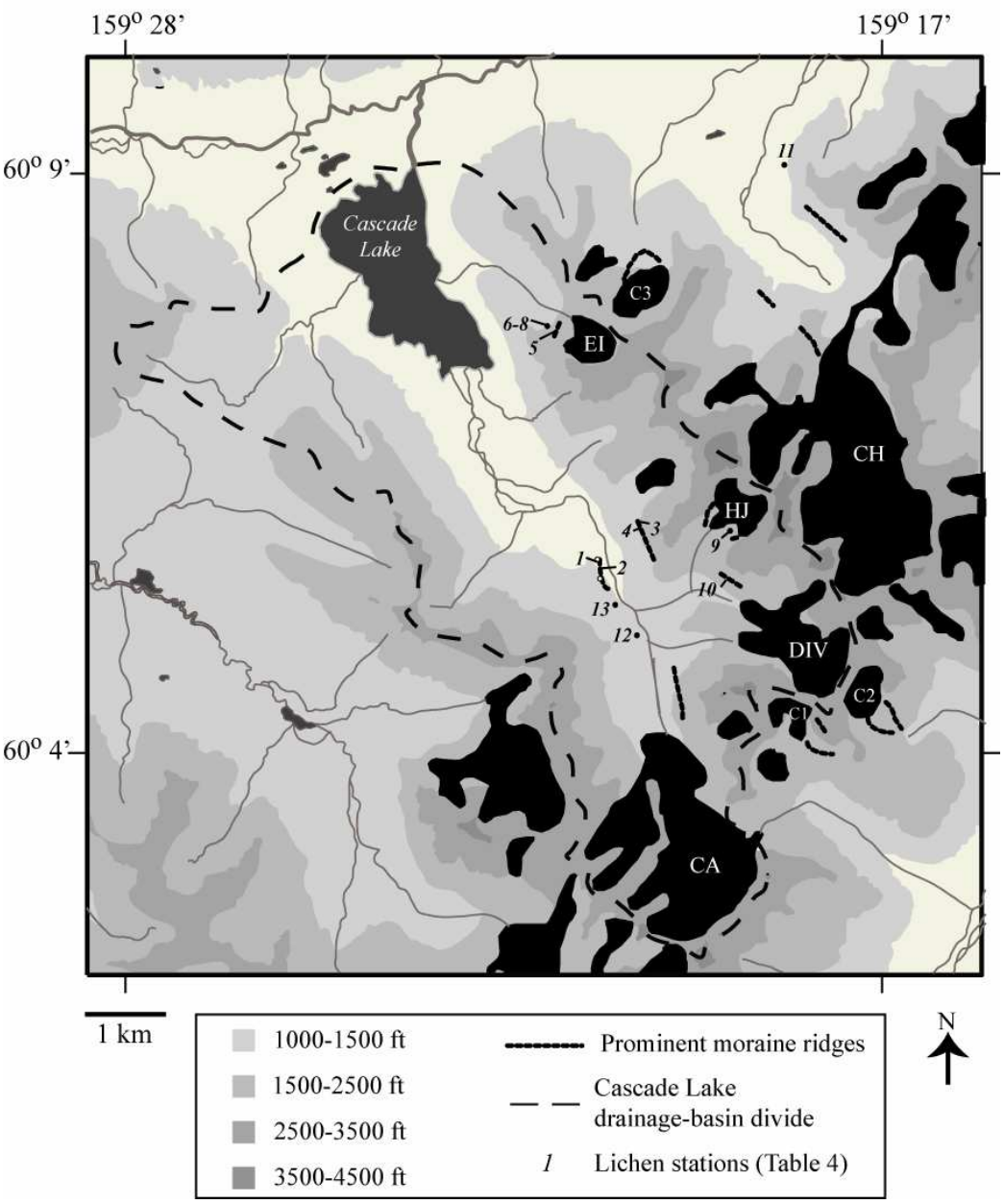

Figure 8: Cascade Lake area showing glaciers referenced by informal names (CA=Cascade Glacier, C1=Cirque 1, C2=Cirque 2, DIV=Divided Glacier, HJ=Hungry Joe, CH=Chikuminuk Glacier, EI=East Inflow Cirque, C3=Cirque 3). Based on 1:63,360 Bethel 1979 topographic map with corrections for ice extent based on 1957 aerial photographs.

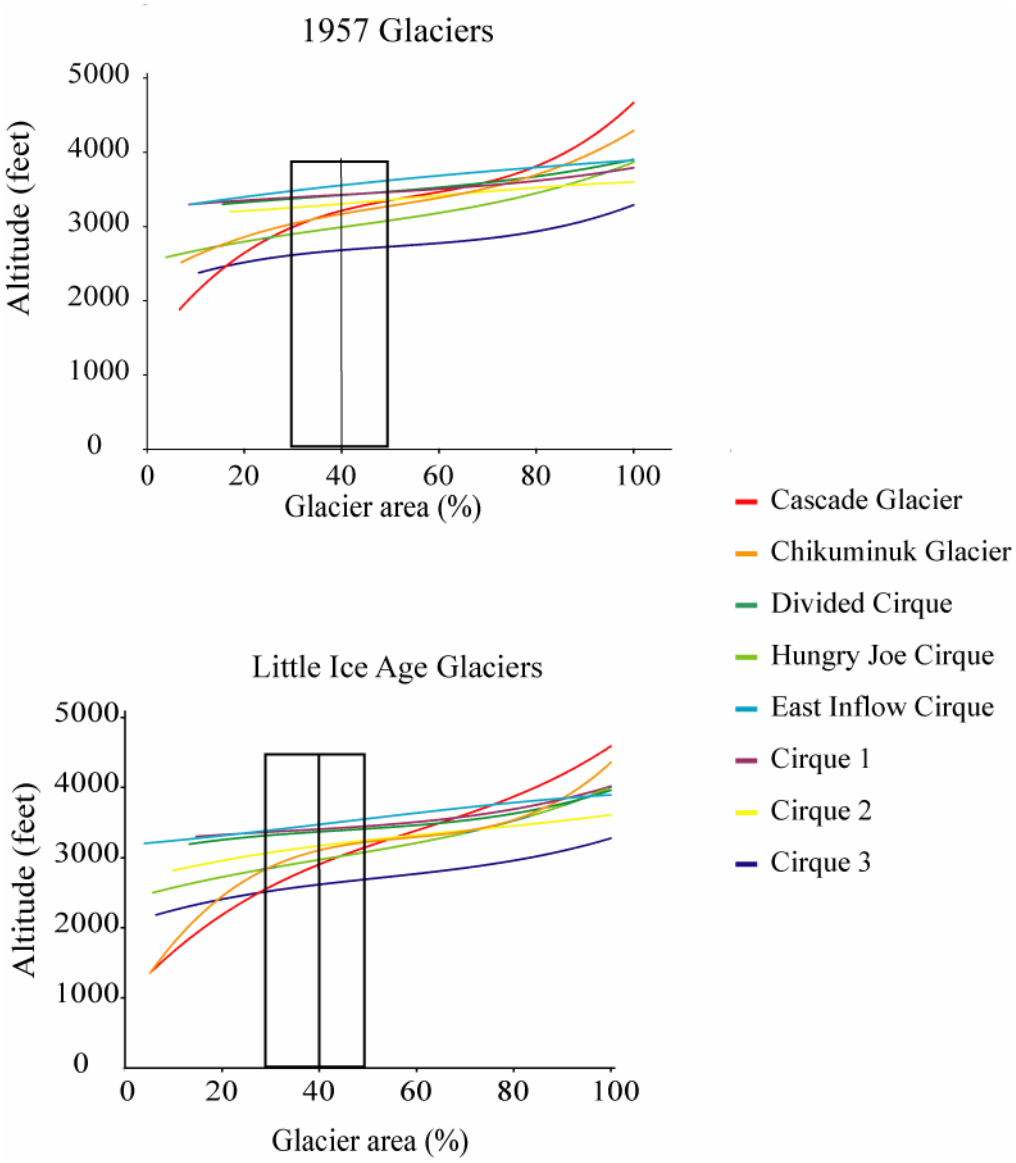

Figure 9: Hypsometric curves used in the calculation of equilibrium-line altitudes (ELA) for eight glaciers in the study area. An accumulation-area ratio (AAR) of 0.6 (60% of the glacier in the accumulation zone, shown by the line at 40% of the glacier area) was used for ELA calculations. ELA calculations (and especially ΔELA) are insensitive to AAR changes as shown by the relatively flat slopes between AAR values of 0.5-0.7 (shown by the box).

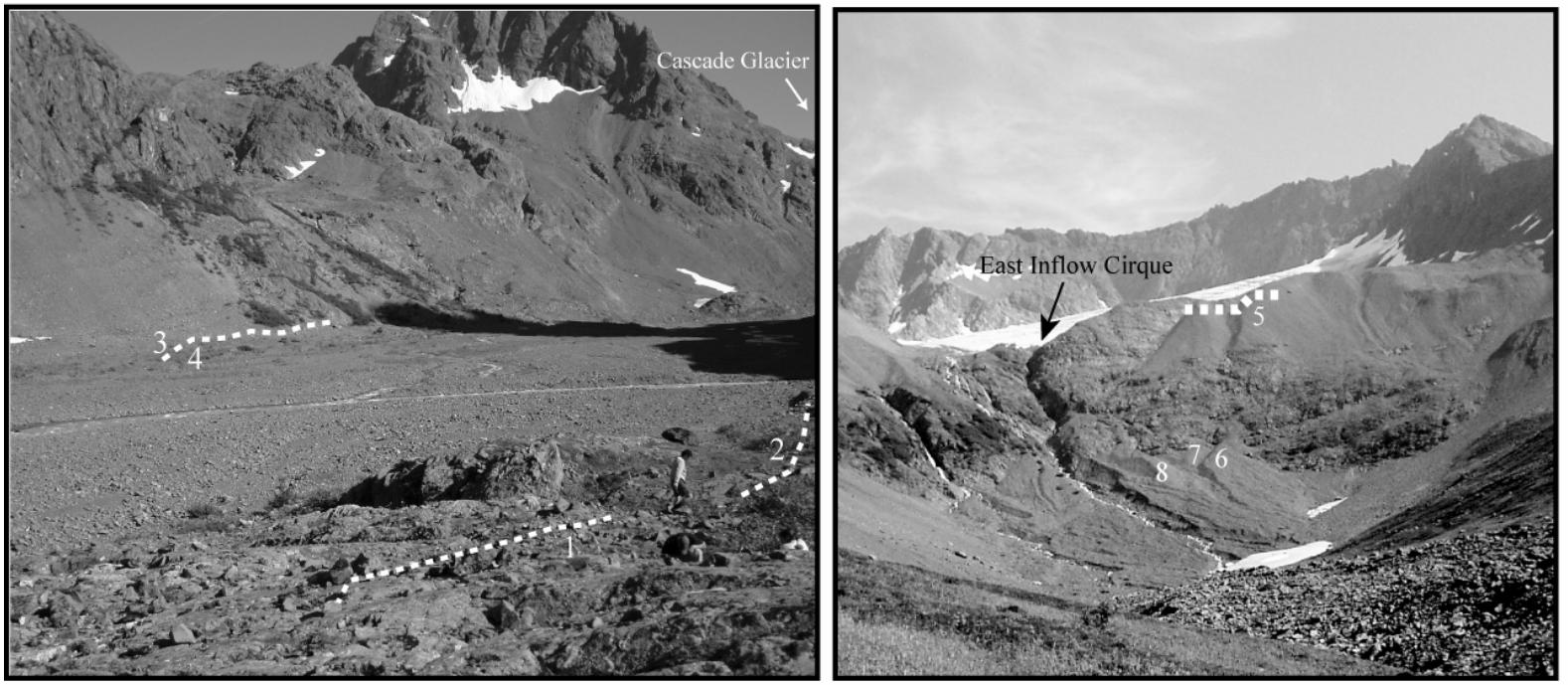

Figure 10: Little Ice Age (LIA) moraines in the Cascade Lake drainage. Dotted lines highlight moraine crests and trim lines. (A) Left and right lateral LIA moraines of Cascade Glacier. Deposits in the foreground are higher than those in the distance. (B) The East Inflow cirque valley. The ridge crest closest to the cirque (dotted line) is the LIA moraine; the fan-shaped feature marked by ridges below are likely debris-flow deposits. Numbers in white denote lichen stations. Photos taken in August 2005.

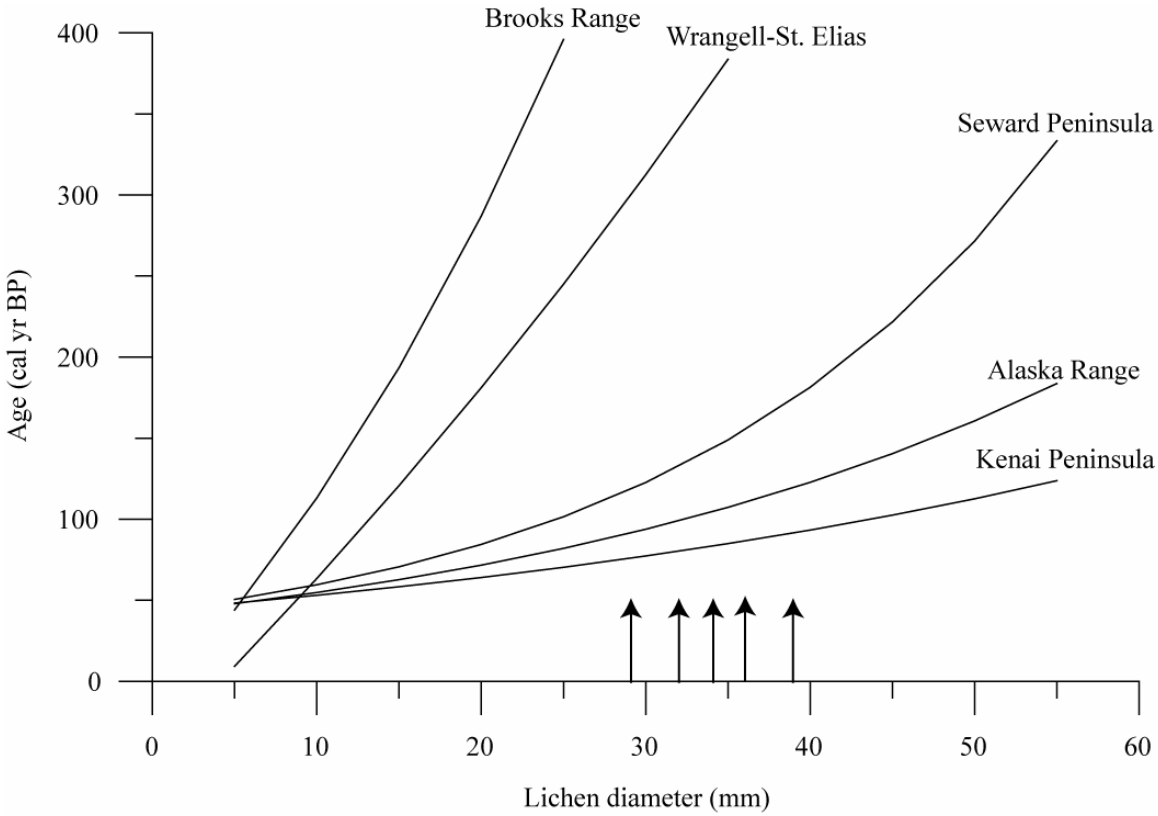

Figure 11: Growth curves used to derive the ages of measured lichens in the Cascade Lake region (from Solomina and Calkin, 2003). The arrows show the average of the five larges lichen diameters on moraines in the Cascade Lake area. Based on Seward Peninsula curve, their ages average ~1860 AD assuming a ~30-yr colonization time.

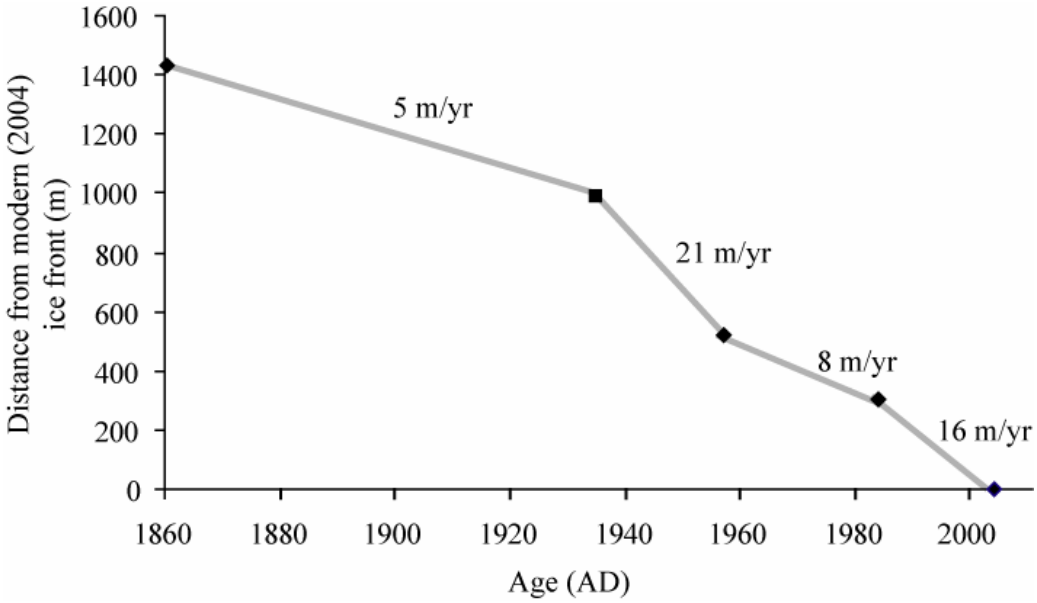

Figure 12: Retreat rates for Cascade Glacier since the Little Ice Age based on aerial photography (1984 and 1957) and lichen stations (1935 and 1860; see text).

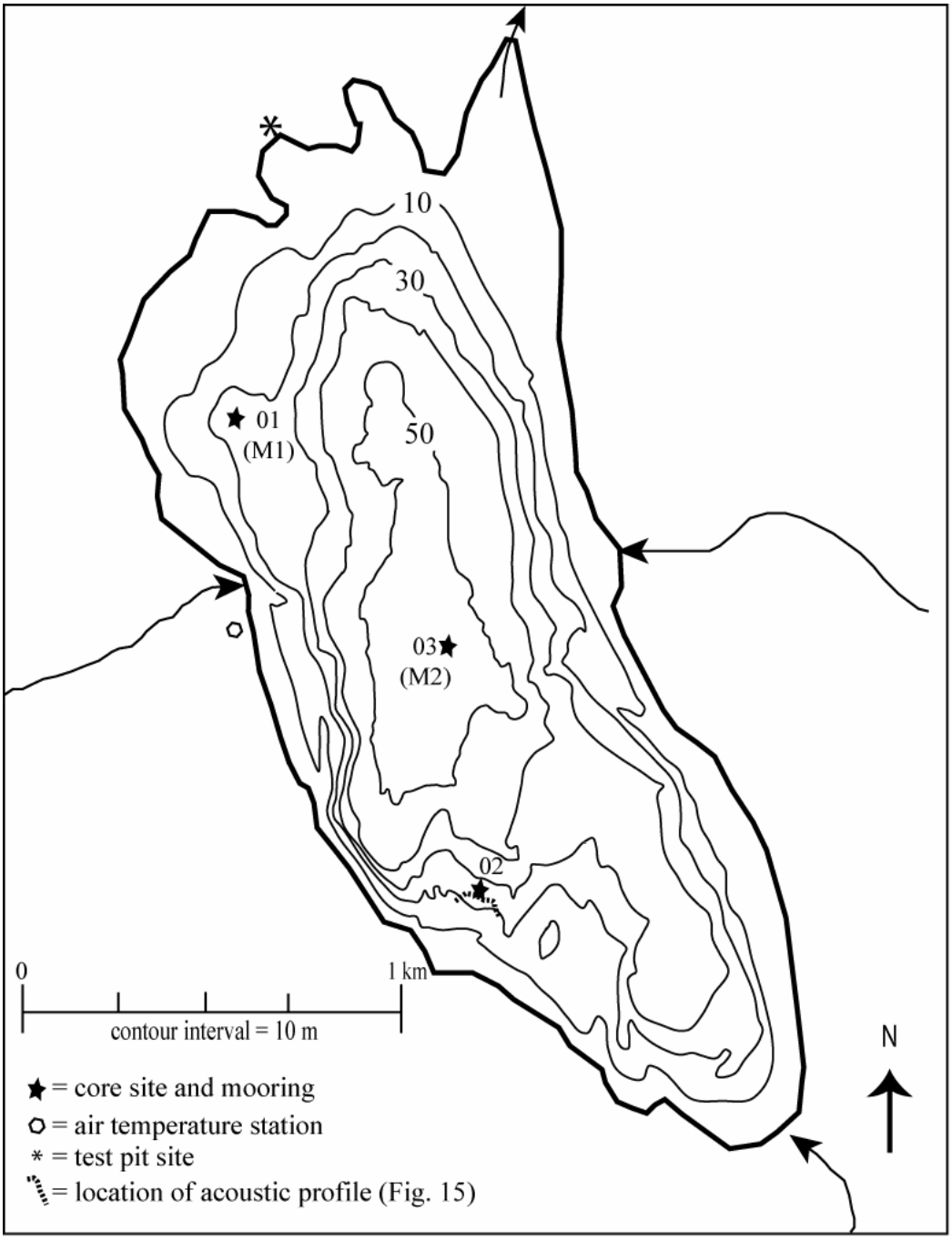

Figure 13: Bathymetry of Cascade Lake with locations of coring sites. The main inflow is in the south and the outflow is to the north.

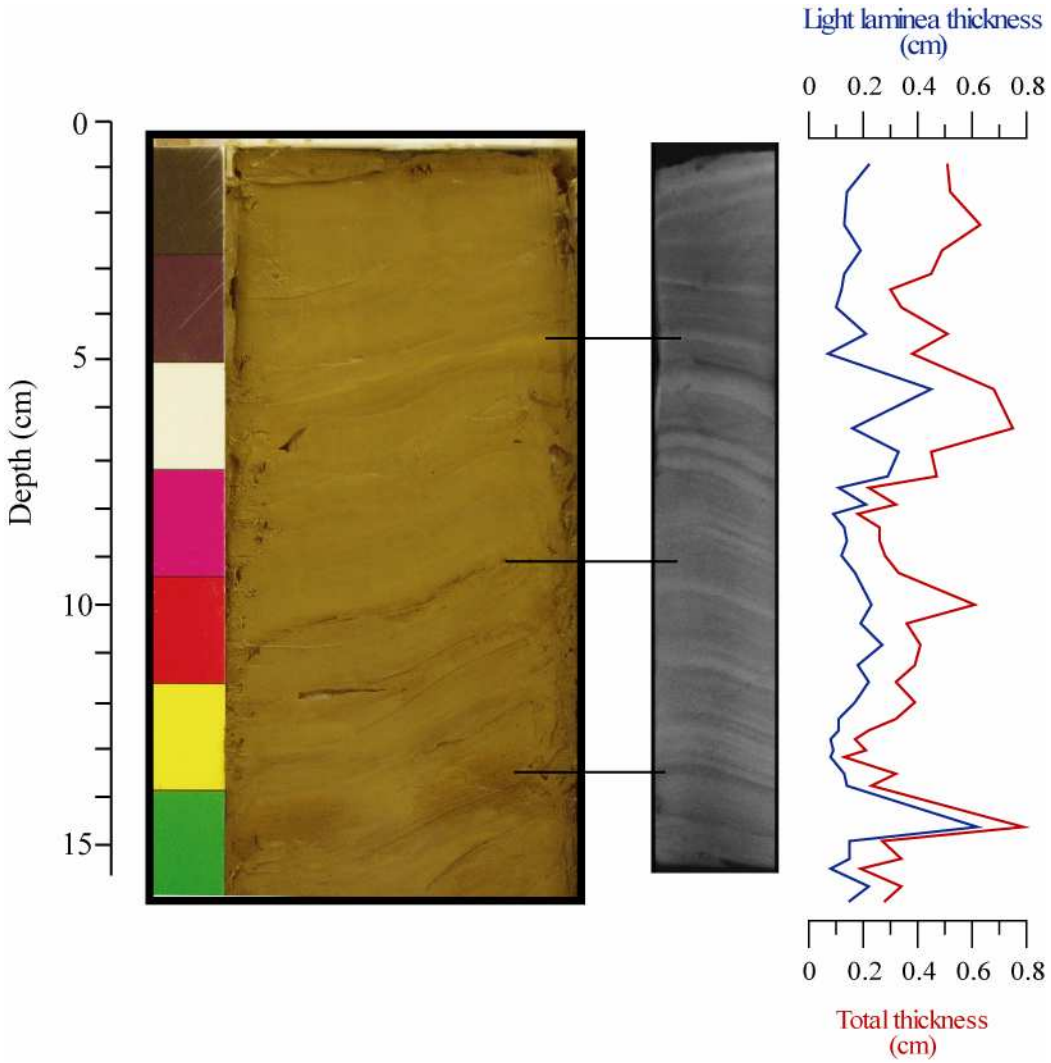

Figure 14: Top 15 cm of Core 02 showing the relationship between the core surface stratigraphy, X-radiograph stratigraphy, and the measurement of lamination thicknesses. Lines connect points identified as being the same on the core face and X-radiograph stratigraphy.

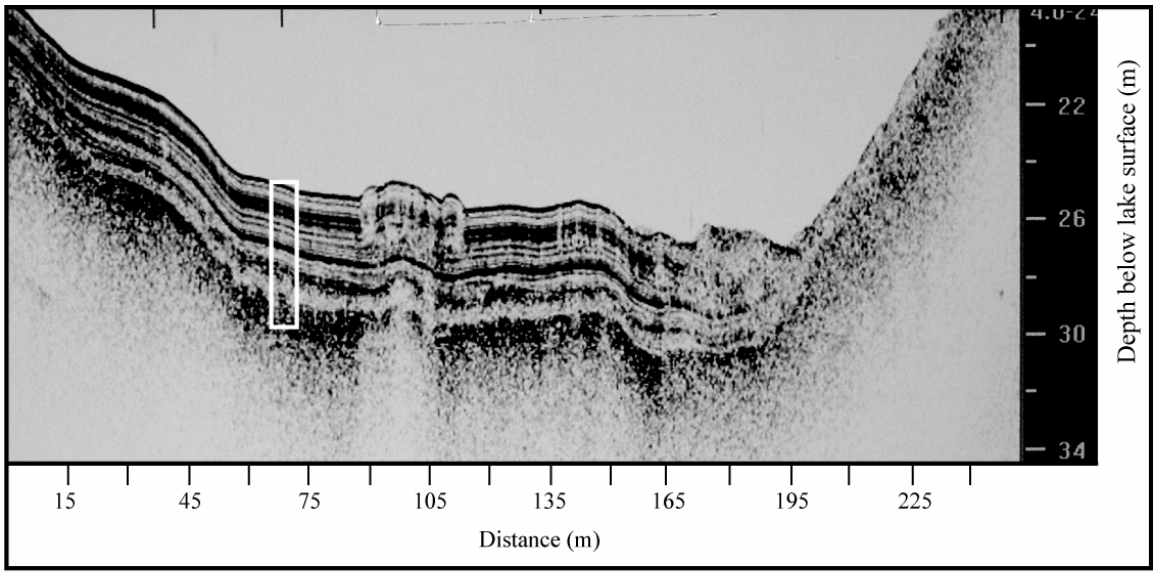

Figure 15: Acoustic profile image in the vicinity of core site 02. The white box denotes the approximate location and length of Core 02. The acoustic signal is degraded at the approximate base of Core 02, but stratigraphy deeper than this was observed in other profiles and below Core 01.

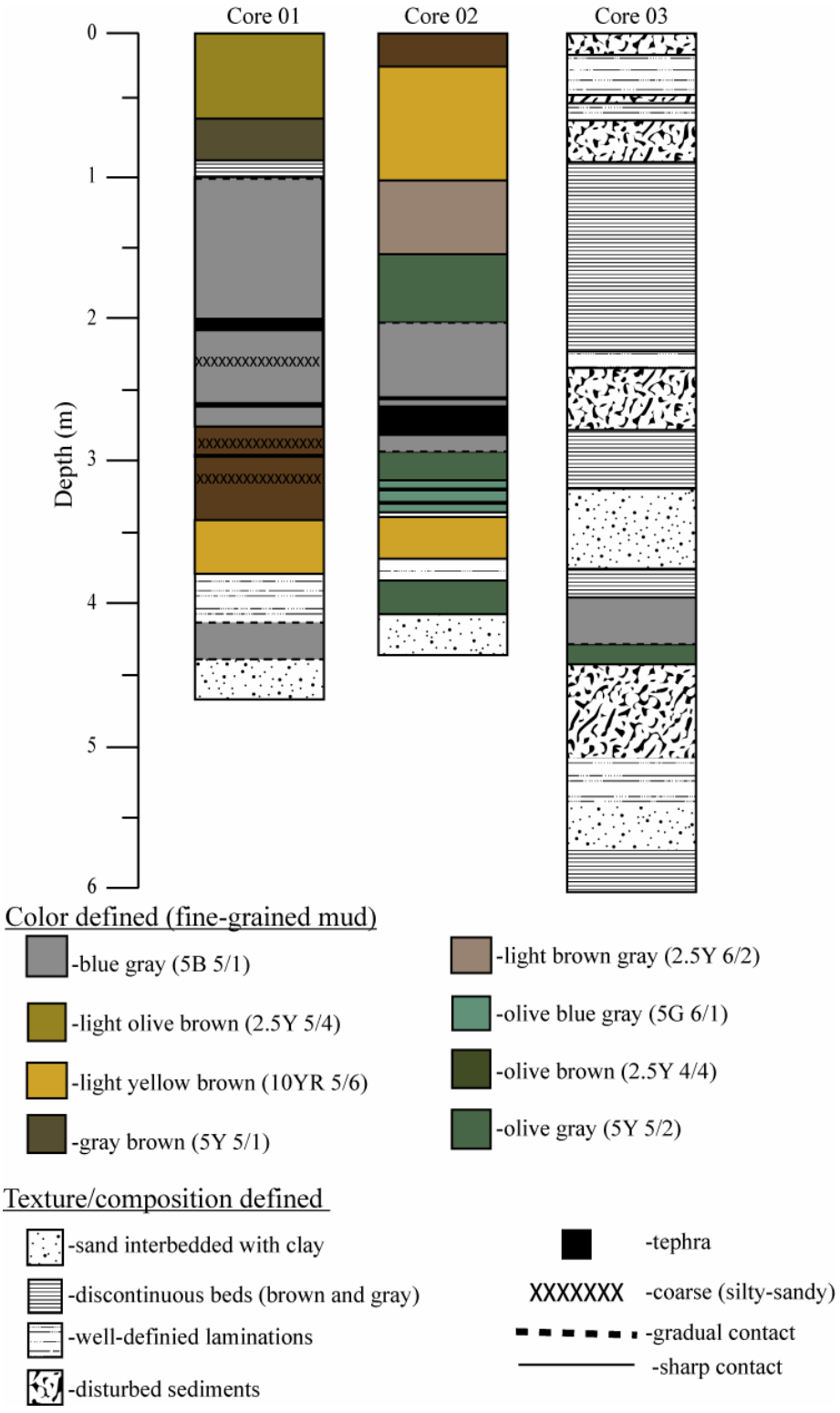

Figure 16: Lithologic logs of three cores recovered from Cascade Lake.

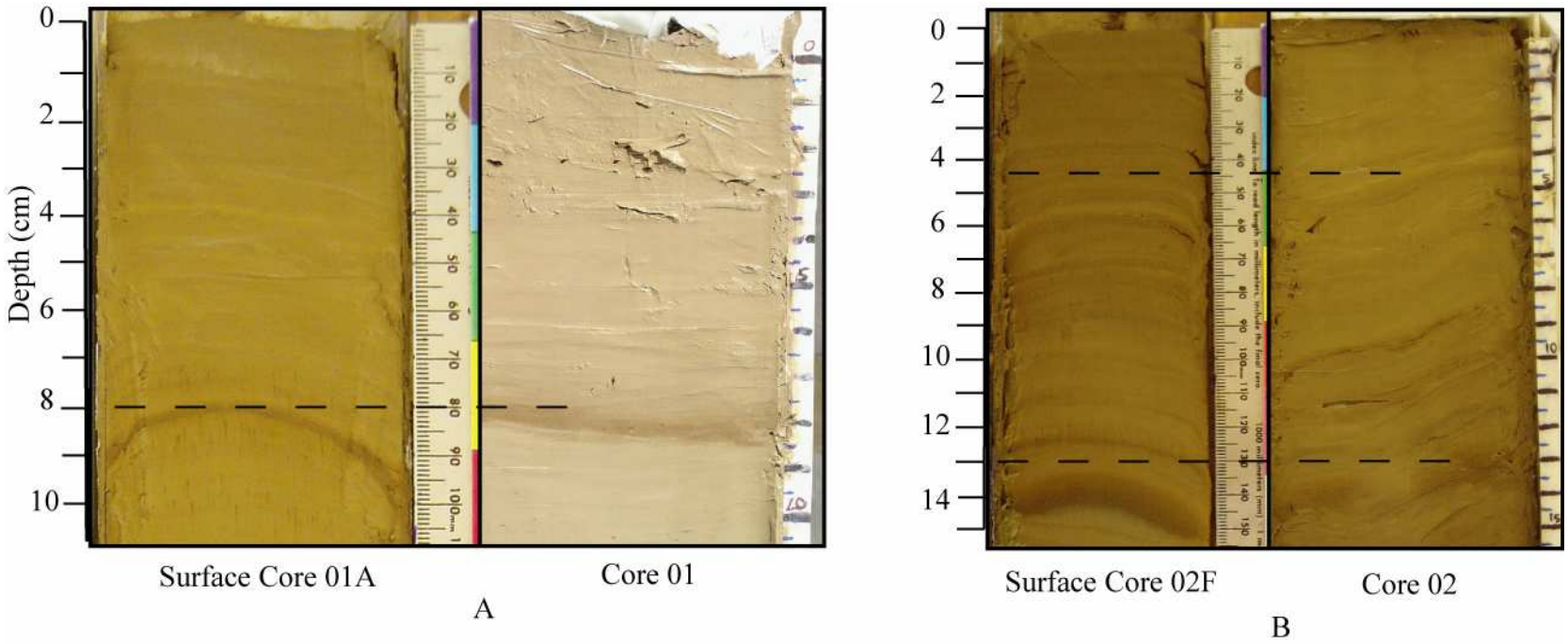

Figure 17: Correlations between surface and long cores based on marker beds (dashed lines) in (A) Core 01 and (B) Core 02. Depths for surface core refer to the sediment-water interface (lake bottom), and are within 0.5 cm of correlative depths in long cores.

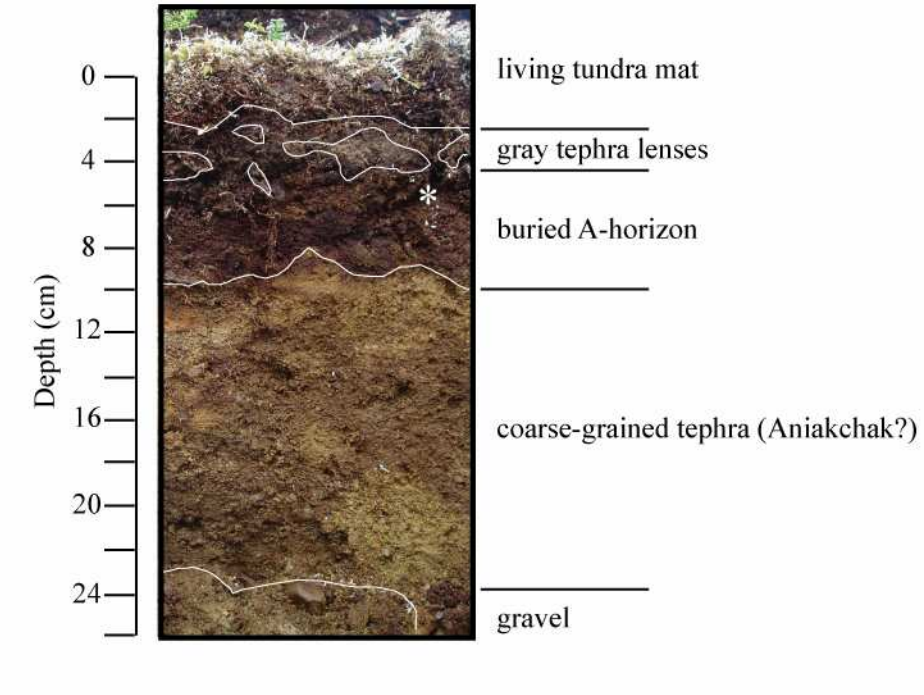

Figure 18: Test-pit wall on the northern shore of Cascade Lake (Figure 13). * denotes location of ^{14}C sample dated at 505 cal yr BP.

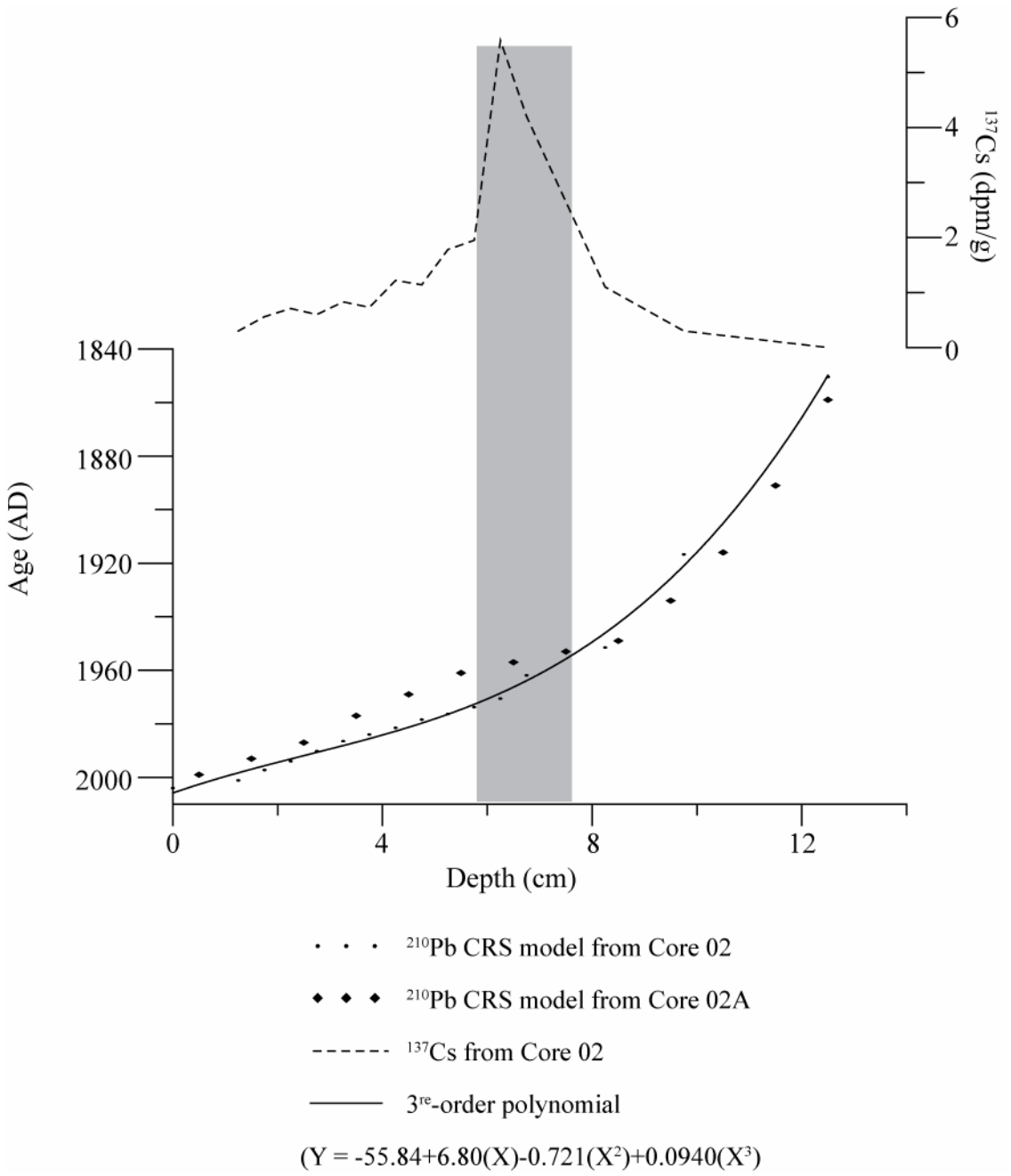

Figure 19: ^{210}Pb and ^{137}Cs profiles from Core 02A and Core 02. The 3rd-order polynomial was used to assign ages to the upper 12 cm of Core 02. Gray box shows the intersection of ^{137}Cs peak with ages derived from the ^{210}Pb profile.

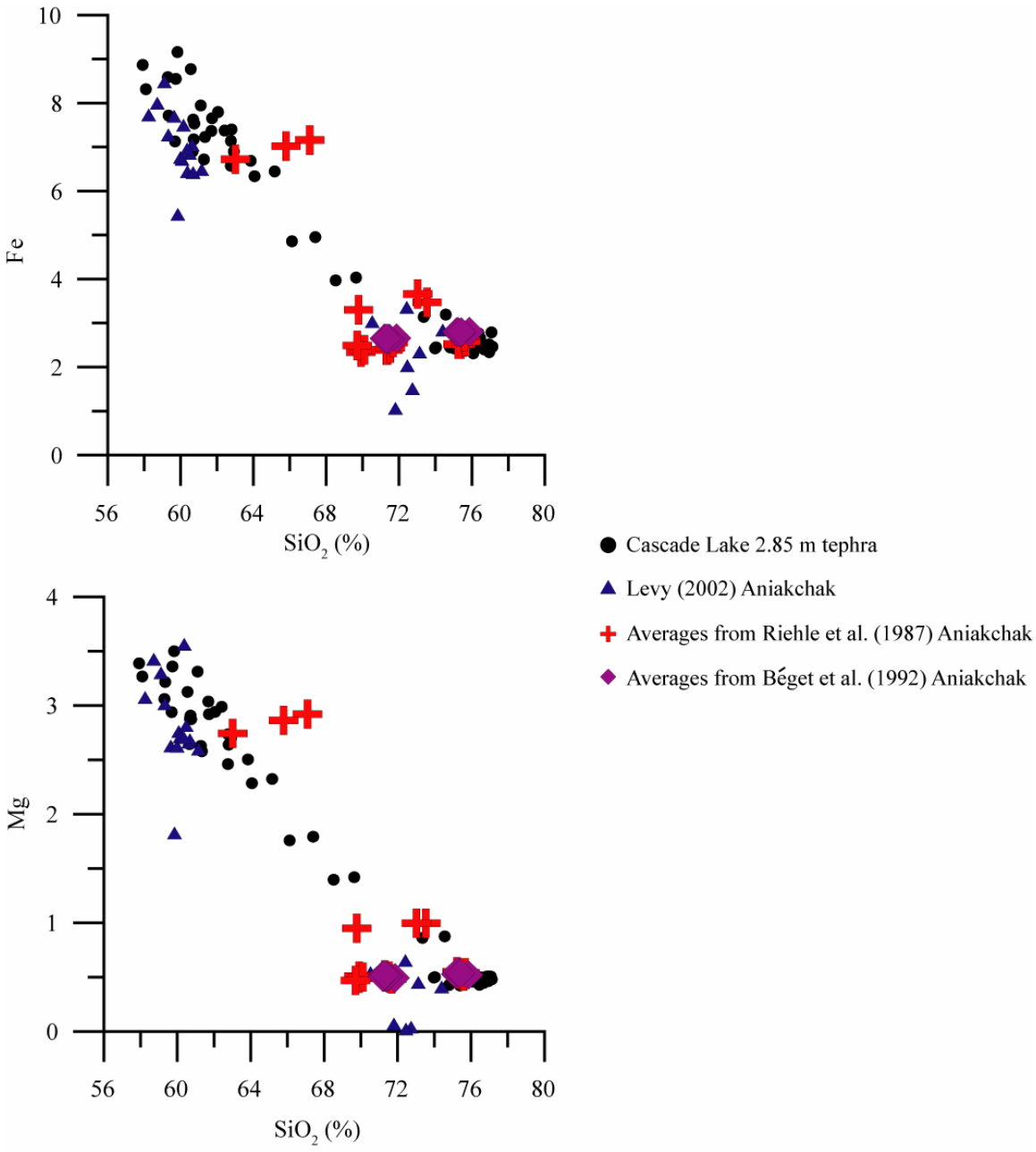

Figure 20: Geochemistry data from the 2.85 m ash in Core 02 and published data sets of known Aniakchak tephras. Data listed in appendix A-2.

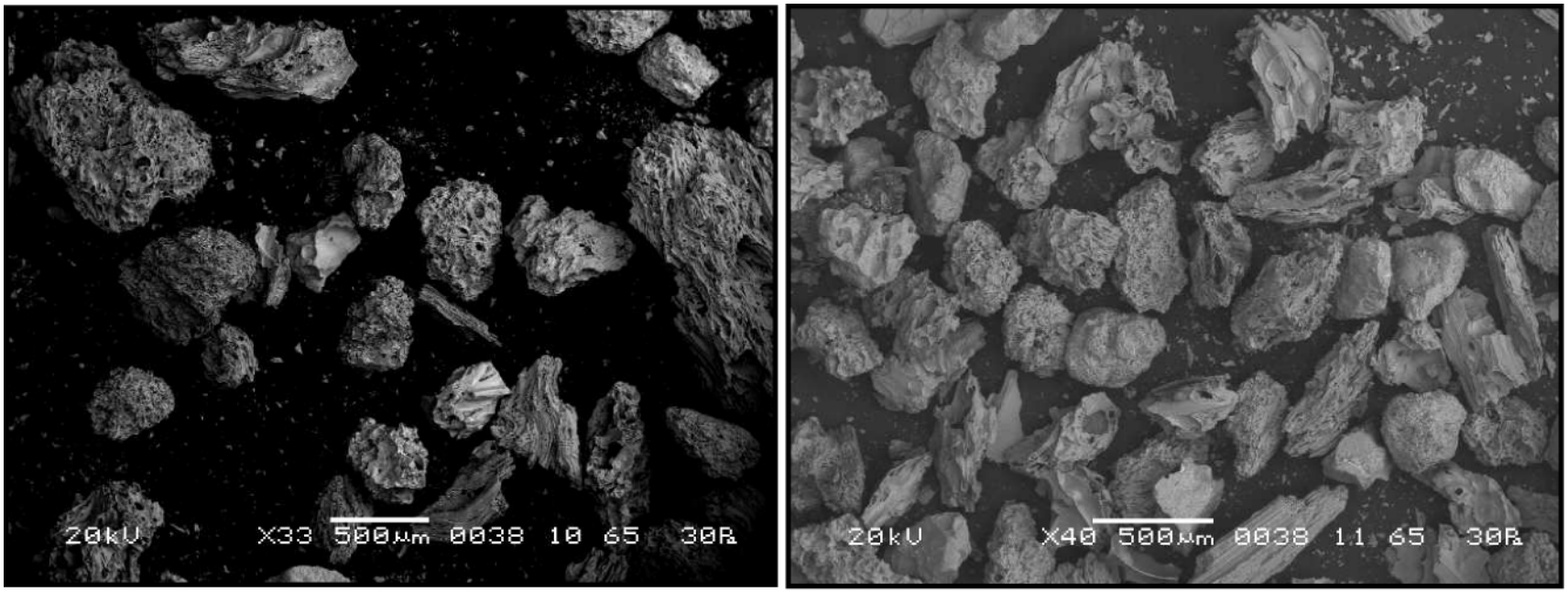

Figure 21: Scanning electron microscope images of tephra shards from (A) the 2.85 m tephra in Core 02 and (B) a known Aniakchak tephra from Arolik Lake.

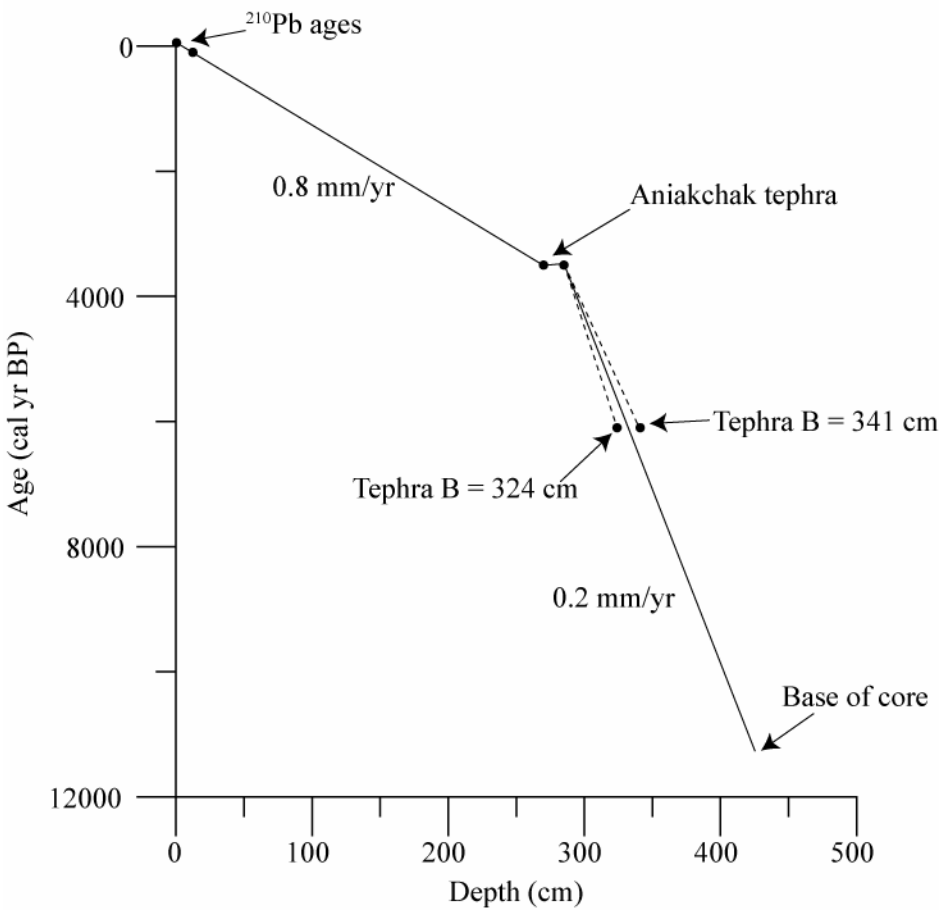

Figure 22: Age model for Core 02. The two models are based on the maximum depth range of Tephra B candidates in Core 02 (see text for explanation).

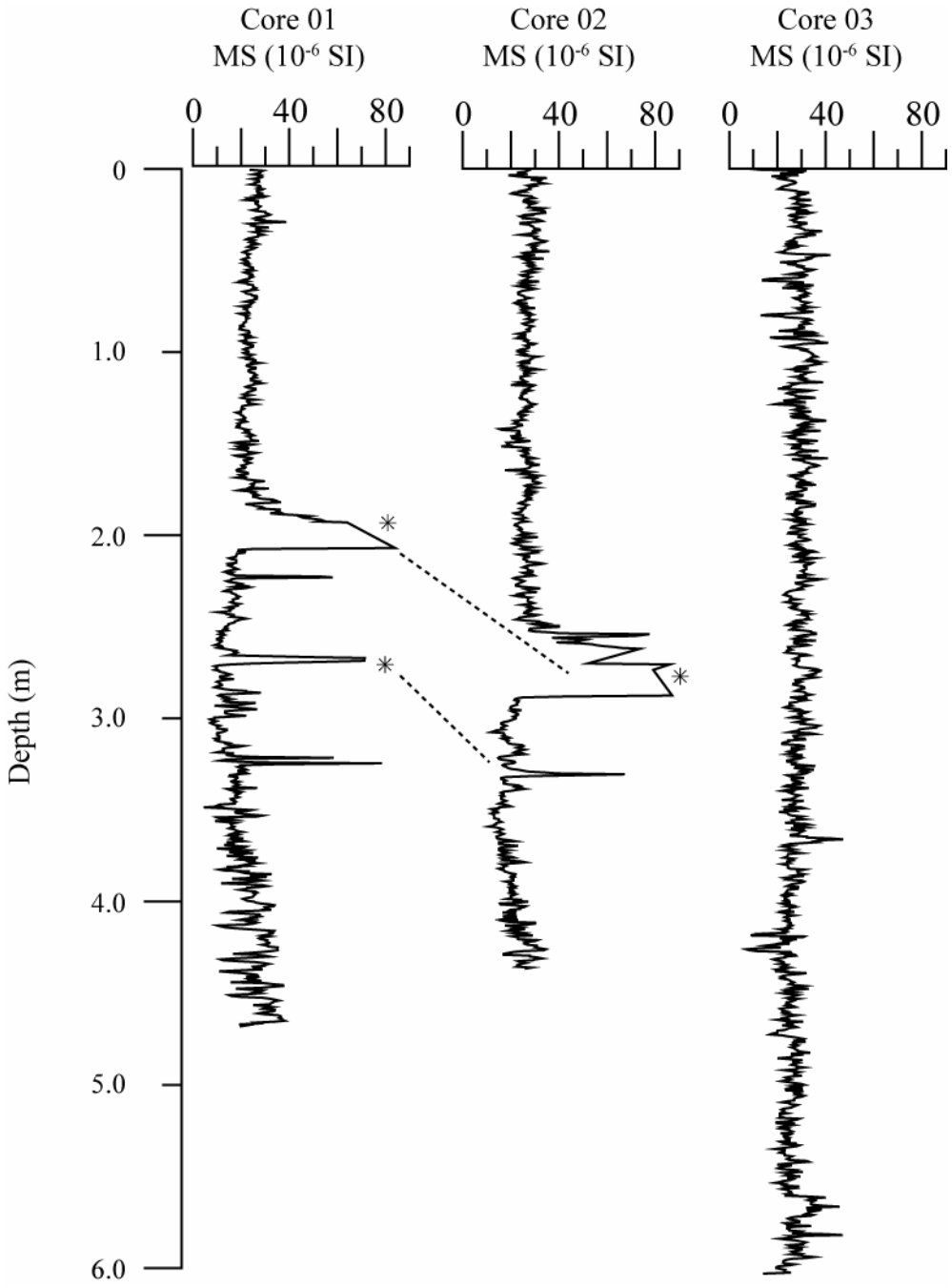

Figure 23: Magnetic susceptibility (MS) profiles for Cores 01, 02 and 03 from Cascade Lake. * indicates MS values that exceed 90 x 10^{-6} SI and dashed lines show correlations between tephras.

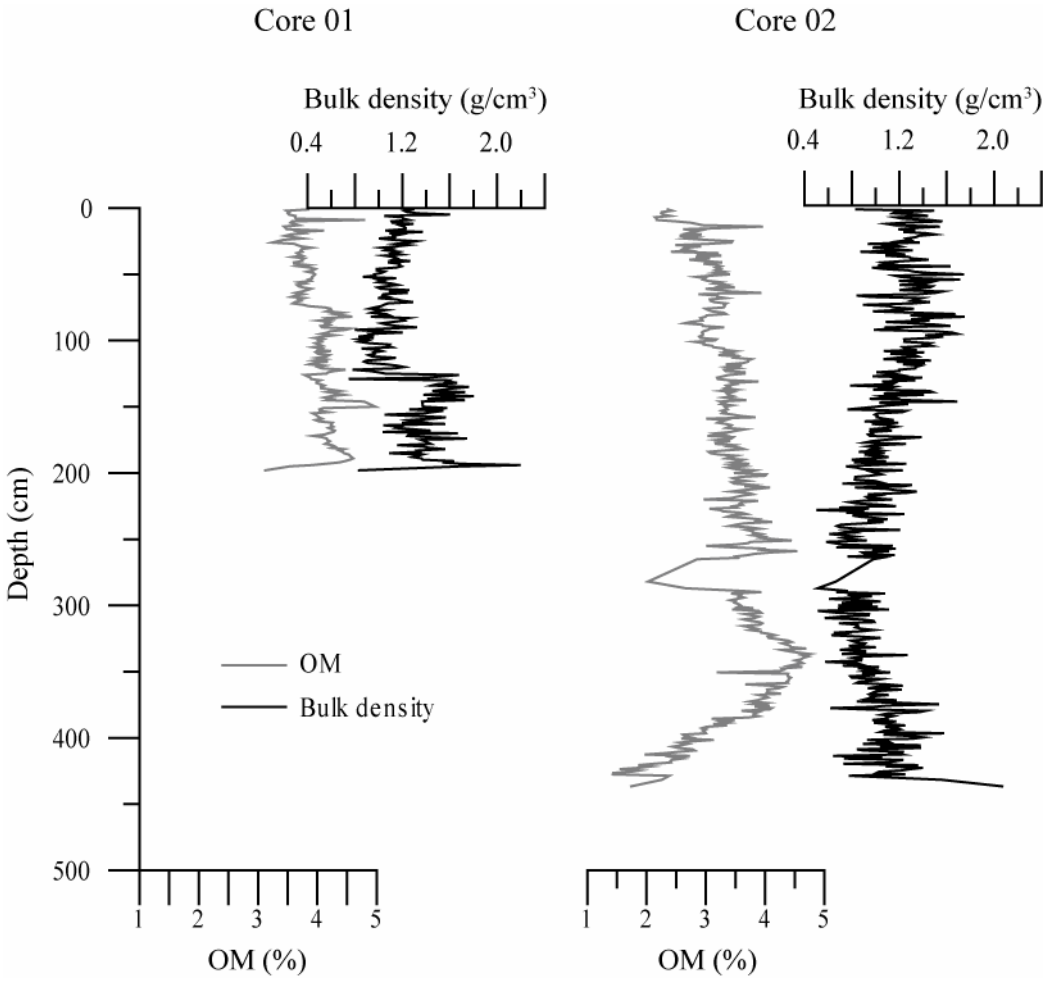

Figure 24: Organic-matter (OM) content and bulk density profiles for the upper 2 m in Core 01 and the entire Core 02.

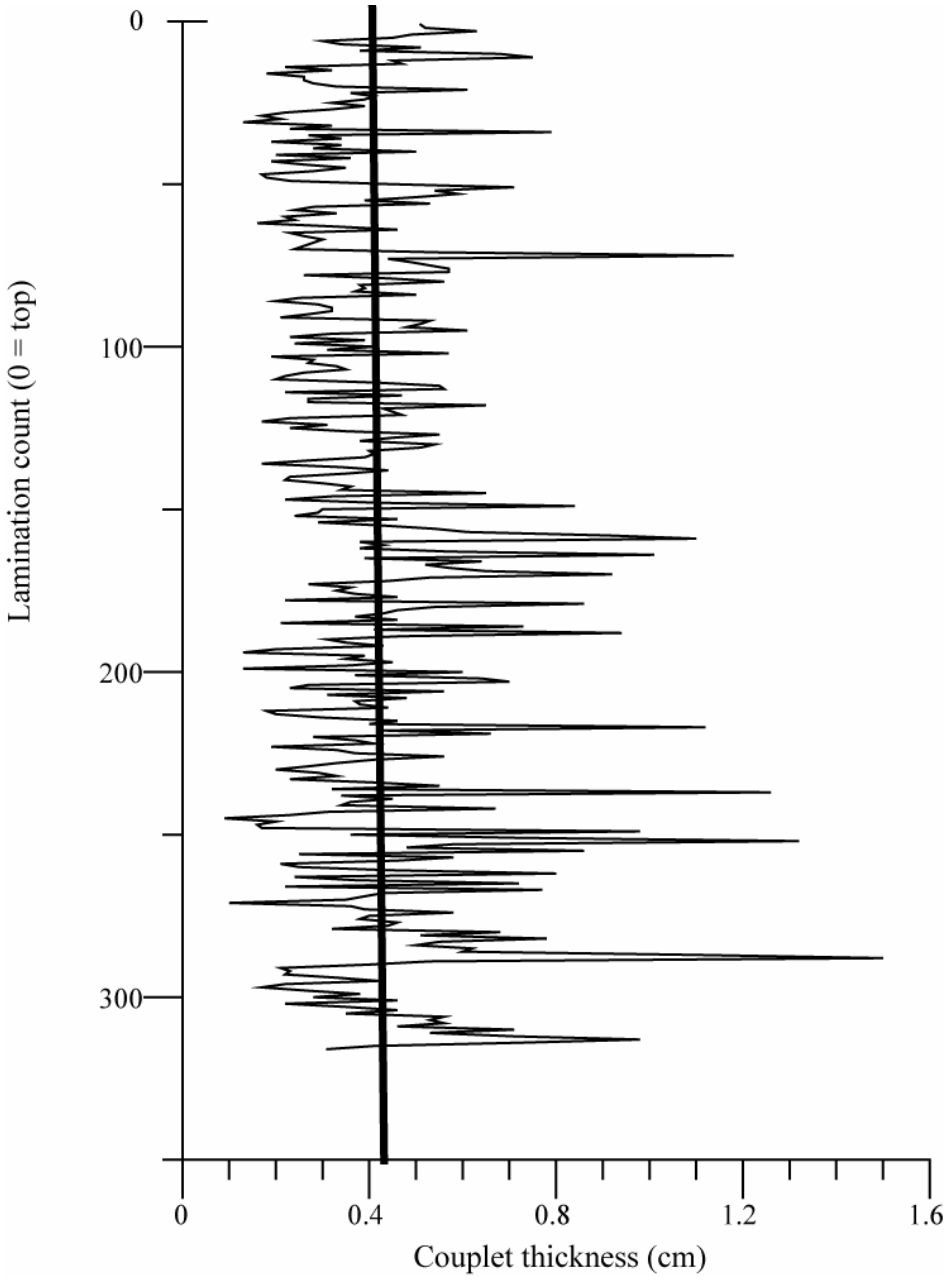

Figure 25: Lamination thickness in the top 1.4 m of Core 02. Of the 316 lamination couplets identified, the average thickness is 0.42 cm (bold line).

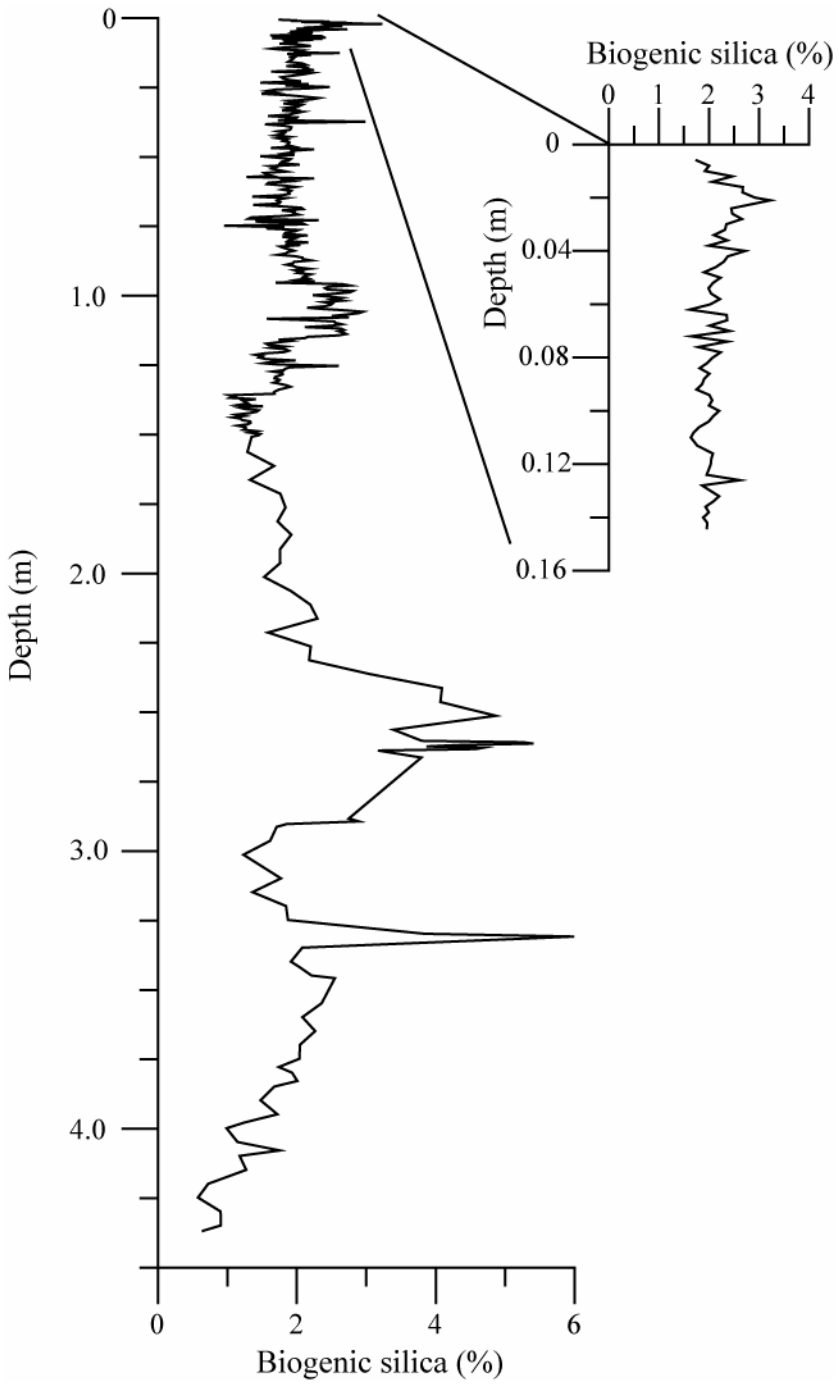

Figure 26: Biogenic silica profiles for Core 02. Inset shows detail of upper 14 cm, the interval sampled at ~3 yr resolution and used to correlate with instrumental climate records.

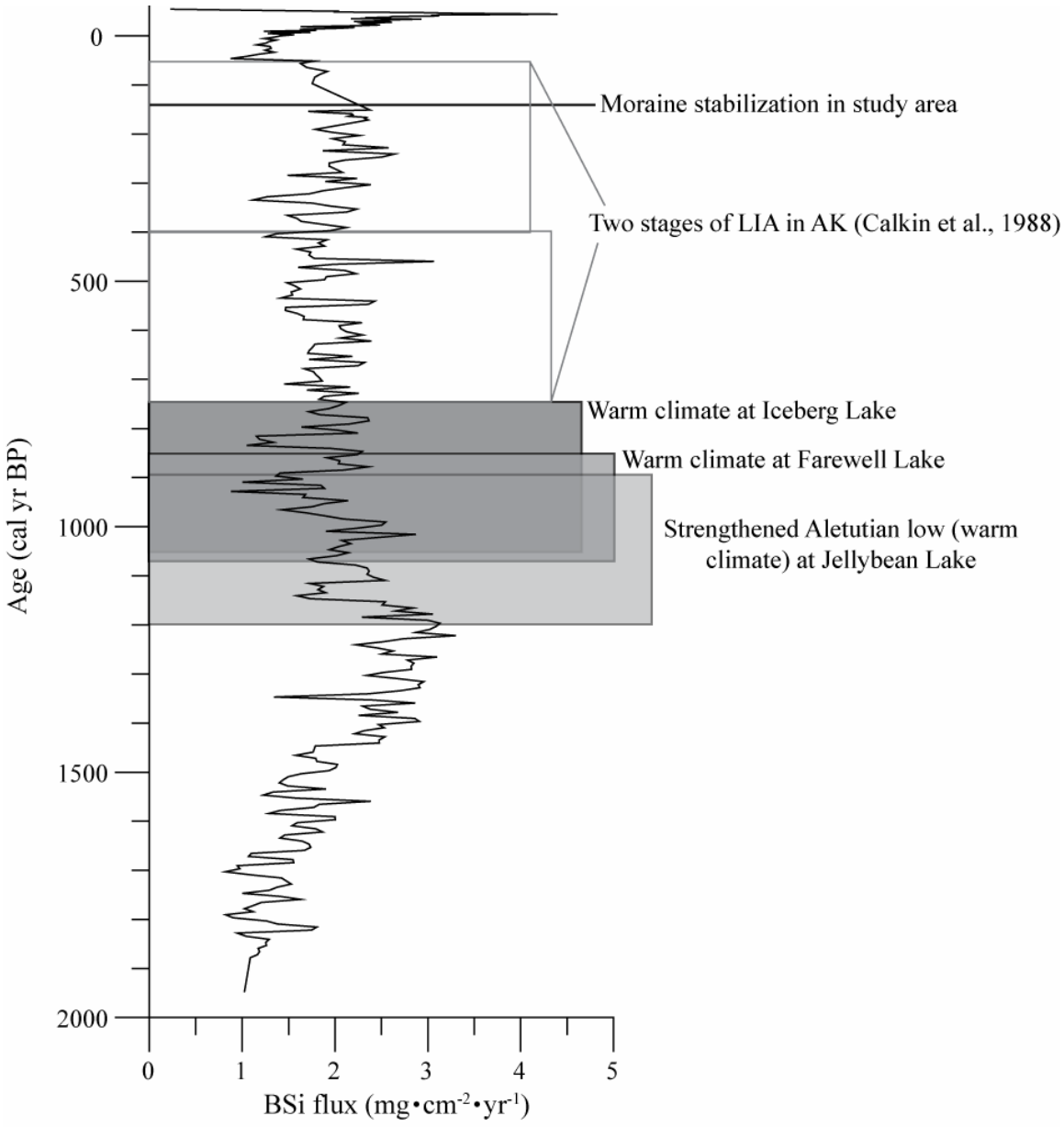

Figure 27: Biogenic silica flux from Core 02 over the last 2200 cal yr BP with periods of recognized warm climate from Iceberg Lake (Loso et al., 2006), Farewell Lake (Hu et al., 2001), and Jellybean Lake (Anderson et al., 2005).

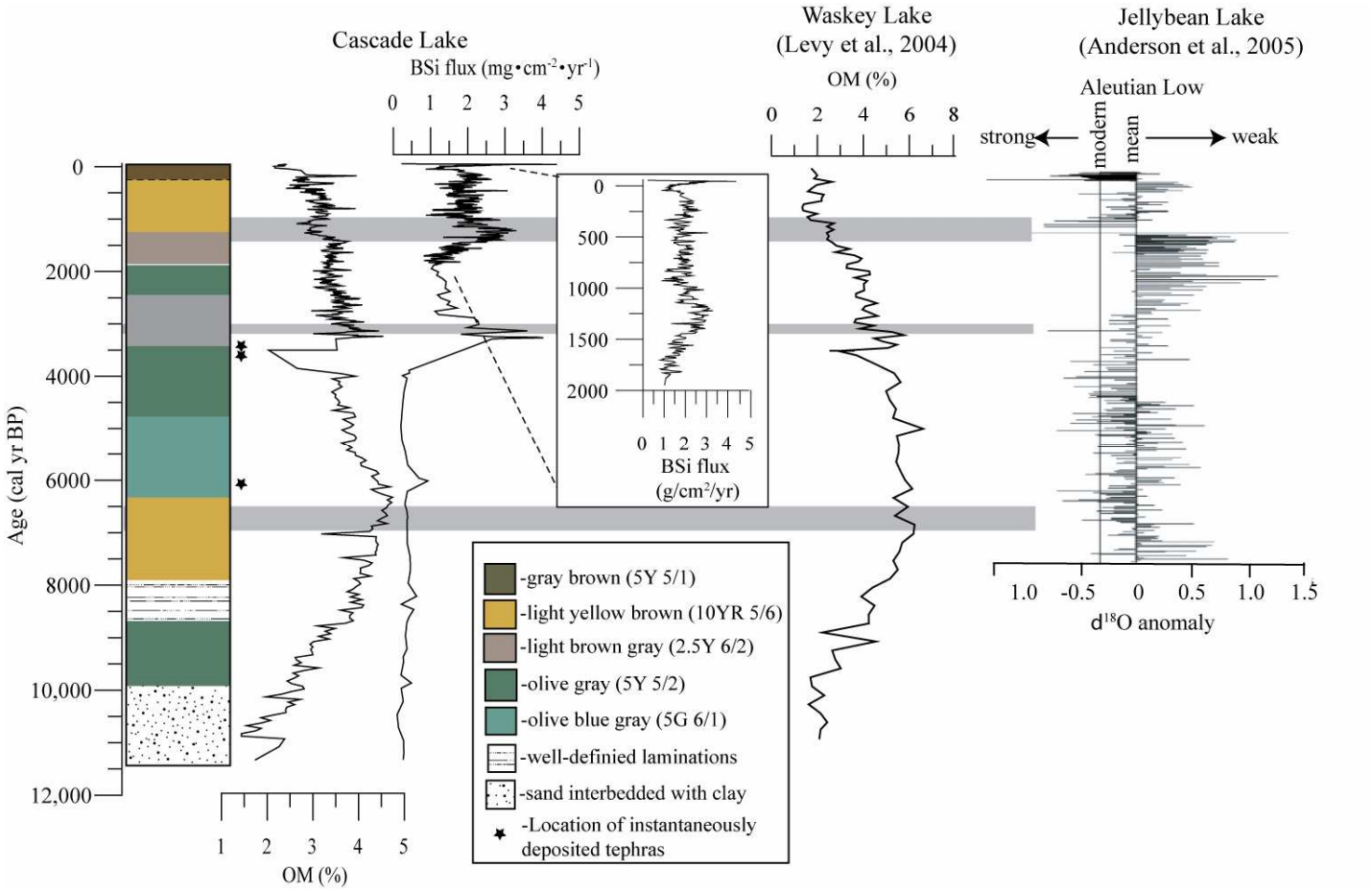

Figure 28: Core 02 proxy data compared to climate events of the Yukon (Jellybean Lake; Anderson et al., 2005) and Waskey Lake (Levy et al., 2004). OM = organic matter; BSi = biogenic silica. Gray bars indicate the Holocene Thermal Maximum (7000 cal yr BP), Neoglaciation onset in the Ahklun Mountains (3000 cal yr BP) and Medieval Warm Period (~1000 cal yr BP).

TABLE A-1. ^{210}Pb AND ^{137}Cs DATA

Depth	Unsupported ^{210}Pb activity		^{137}Cs activity		Age of base
(cm)	(dpm/g)	(± s.d.)	(dpm/g)	(±s.d.)	(years before 2004)
Core 02A					
0.5	9.16	0.53	N.D.		5.48
1.5	3.80	0.37	N.D.		10.95
2.5	4.29	0.26	N.D.		17.58
3.5	3.88	0.23	N.D.		27.31
4.5	1.88	0.17	N.D.		35.90
5.5	1.31	0.19	N.D.		43.22
6.5	0.45	0.16	N.D.		47.38
7.5	0.46	0.16	N.D.		51.13
8.5	0.51	0.15	N.D.		55.88
9.5	1.30	0.24	N.D.		70.45
10.5	0.57	0.17	N.D.		88.45
11.5	0.48	0.14	N.D.		113.58
12.5	0.22	0.14	N.D.		148.35
Core 02					
1.5	7.10	0.78	0.30	0.13	2.86
2.0	8.28	0.57	0.56	0.08	6.74
2.5	6.27	0.69	0.71	0.10	10.04
3.0	6.52	0.54	0.60	0.08	13.80
3.5	5.70	0.81	0.83	0.13	17.53
4.0	3.37	0.78	0.73	0.13	20.01
4.5	3.29	0.57	1.22	0.10	22.51
5.0	3.51	0.58	1.14	0.10	25.59
5.5	2.28	0.78	1.78	0.14	27.71
6.0	2.33	0.59	1.95	0.10	30.21
6.5	2.92	0.73	5.58	0.16	33.43
7.0	3.27	0.70	4.20	0.14	42.11
8.5	1.90	0.59	1.10	0.10	52.51
10.0	2.53	0.53	0.30	0.10	87.27
13.0	1.14	0.51	0.00	0.1	153.57

TABLE A-2. MAJOR ELEMENT GEOCHEMISTRY OF THE 2.85 m TEPHRA IN CORE 02

Point	Na_2O	MgO	Al_2O_3	SiO_2	P_2O_5	K_2O	CaO	TiO_2	MnO	FeO	Total
1	2.397	0.489	15.370	72.958	0.069	2.651	1.706	0.439	0.152	2.392	98.623
2	2.228	0.488	15.429	72.122	0.057	2.415	1.767	0.439	0.094	2.385	97.424
3	3.302	2.605	16.468	59.778	0.784	1.409	5.906	1.306	0.186	6.800	98.545
4	1.290	0.489	15.514	72.879	0.096	2.225	1.797	0.394	0.097	2.357	97.137
5	2.708	3.220	16.466	57.271	0.807	1.131	7.146	1.443	0.194	8.197	98.583
6	1.525	1.323	16.211	64.919	0.538	1.449	3.839	1.093	0.090	3.760	94.748
7	0.997	0.464	15.582	74.064	0.092	1.718	1.820	0.445	0.105	2.434	97.722
8	1.645	2.225	16.145	62.412	0.577	1.508	5.334	1.253	0.142	6.174	97.420
9	1.529	2.784	16.519	58.862	0.754	1.191	6.361	1.409	0.178	7.299	96.888
10	1.089	0.439	15.242	72.922	0.103	1.523	1.767	0465	0.085	2.217	95.853
11	1.665	2.406	16.665	61.372	0.747	1.311	5.706	1.328	0.159	6.429	97.787
12	2.304	2.555	16.635	60.803	0.655	1.229	6.249	1.308	0.223	7.166	99.126
13	1.988	2.920	16.026	56.595	0.658	1.114	6.398	1333	0.213	8.197	95.443
14	1.007	0.479	15.537	73.401	0.137	1.533	1.854	0.435	0.121	2.417	96.923
15	2.141	2.793	16.298	58.920	0.644	1.119	6.287	1.323	0.159	7.402	97.085
16	0.737	0.363	12.259	56.077	0.057	1.075	1.545	0.379	0.090	2.120	74.702
17	0.743	0.406	12.763	61.909	0.050	0.928	1.591	0.395	0.039	2.240	81.064
18	1.851	1.711	16.973	64.354	0.435	1.444	4.587	1.091	0.156	4.729	97.331
19	2.188	0.425	15.680	74.205	0.028	1.957	1.692	0.484	0.110	2.428	99.196
20	1.334	0.428	15.369	73.521	0.147	1.788	1.713	0.470	0.141	2.304	97.214
21	3.169	3.365	16.294	57.525	0.603	0.875	7.251	1.281	0.152	8.807	99.322
22	2.668	2.849	16.595	59.517	0.726	1.024	6.049	1.358	0.199	7.033	98.017
23	3.193	2.899	16.655	58.888	0.758	0.890	6.702	1.433	0.199	7.032	98.650
24	1.587	0.839	15.478	71.489	0.034	1.629	2.695	0.570	0.077	3.061	97.459
25	1.256	0.491	15.828	73.831	0.034	1.636	1.990	0.445	0.114	2.366	97.991
26	2.564	2.577	16.963	60.082	0.625	1.012	5.928	1.528	0.117	6.587	98.042
27	1.349	0.413	15.524	73.514	0.000	1.683	1.880	0.460	0.124	2.556	97.504
28	1.426	0.463	14.704	70.288	0.050	1.432	1.763	0.434	0.119	2.213	92.892
29	1.086	0.446	14.908	71.677	0.069	1.160	1.851	0.439	0.094	2.287	94.017
30	2.796	3.113	16.287	57.436	.736	0.790	6.657	1.311	0.196	7.468	96.789
31	1.277	0.486	15.331	73.576	0080	1.390	1.840	0.429	0.085	2.404	96.898
std.	2.587	5.051	12.431	50.532	0.509	0.729	9.472	3.900	0.198	13.473	98.881

TABLE A-3. MAGNETIC SUSCEPTIBILITY DATA FOR CORE 02

	0	20	40	60	80	100	120	140	160	180	200
0.0		27.6	33.8	27.0	27.0	23.7	27.0	24.6	28.1	27.0	23.5
0.5	27.9	27.8	30.9	26.0	28.0	24.9	26.0	22.8	26.4	28.0	25.3
1.0	26.9	27.2	28.4	24.9	27.8	26.0	28.0	22.2	26.7	26.0	31.2
1.5	26.0	33.4	27.5	31.7	27.7	24.0	26.0	20.2	32.0	26.1	26.9
2.0	23.0	31.5	30.6	26.5	26.5	26.0	25.0	15.3	29.0	24.3	21.7
2.5	23.0	29.7	29.7	24.3	29.4	31.0	26.0	16.4	28.0	23.5	22.5
3.0	27.0	33.9	28.9	26.2	28.2	29.0	25.0	23.5	28.0	24.6	24.4
3.5	19.0	34.2	30.0	28.0	28.7	29.0	24.2	23.6	27.0	26.8	26.2
4.0	22.0	34.3	29.0	23.0	26.4	28.0	24.4	23.6	25.2	26.0	21.8
4.5	26.0	30.5	29.0	25.0	25.0	28.0	24.6	22.7	17.6	26.0	20.6
5.0	35.0	26.7	36.0	28.0	25.7	25.0	23.7	23.8	25.5	26.0	21.5
5.5	29.0	27.9	27.0	30.0	27.3	24.0	23.9	23.9	28.7	24.0	24.3
6.0	28.8	24.0	25.0	28.0	29.0	28.2	26.7	20.3	26.4	25.0	24.2
6.5	32.0	25.0	26.0	25.0	28.0	24.3	26.6	20.5	24.5	24.6	28.7
7.0	31.3	25.0	30.0	24.0	28.0	24.5	27.4	23.6	27.6	24.5	25.6
7.5	31.5	31.0	26.0	23.0	27.0	23.7	27.3	21.7	31.7	23.4	24.5
8.0	33.8	32.0	23.5	23.0	28.0	25.8	28.2	22.9	29.8	21.3	26.4
8.5	29.1	33.0	26.6	23.2	28.0	25.1	30.0	28.1	26.9	22.1	31.2
9.0	27.3	30.0	33.7	24.3	26.0	29.3	29.0	25.1	30.0	25.0	29.7
9.5	29.5	24.0	25.7	25.5	25.0	31.5	27.0	18.2	29.0	25.0	30.6
10.0	27.6	24.0	26.8	25.7	23.0	25.7	28.0	18.5	29.0	25.0	27.4
10.5	27.8	28.0	27.9	27.8	26.0	26.8	26.0	18.9	29.0	26.0	23.3
11.0	28.1	28.2	28.9	26.0	26.0	26.1	27.0	19.8	31.0	23.0	25.1
11.5	26.3	29.3	26.7	26.0	24.0	28.3	26.0	16.0	32.0	24.9	27.6
12.0	24.5	29.5	28.5	23.0	25.0	25.5	25.0	24.0	31.0	24.7	27.5
12.5	25.7	29.7	29.4	23.0	23.0	25.6	27.0	27.0	27.0	26.5	25.4
13.0	20.9	31.9	27.2	22.0	26.0	26.8	24.0	26.0	26.0	23.4	25.2
13.5	20.2	32.0	27.8	27.0	27.0	24.0	23.0	27.0	27.0	23.2	26.1
14.0	22.4	29.0	29.6	23.0	26.0	24.0	23.0	24.3	30.8	21.8	26.8
14.5	24.6	29.0	31.5	24.0	27.0	24.0	26.0	25.6	27.6	21.6	26.7
15.0	28.7	30.0	29.3	26.0	27.0	25.0	25.0	27.0	26.5	22.5	31.5
15.5	28.9	27.0	27.1	25.0	30.0	25.0	24.0	27.3	26.3	23.3	33.3
16.0	29.8	24.1	25.8	30.1	29.2	26.0	24.4	25.7	29.1	24.1	31.2
16.5	26.7	28.3	29.6	25.3	26.3	23.0	24.5	24.5	27.0	24.5	27.0
17.0	25.5	30.5	27.5	24.5	27.5	25.0	25.6	25.0	29.0	23.4	26.0
17.5	25.4	29.6	27.3	25.6	27.6	27.0	21.8	28.5	27.0	24.3	25.0
18.0	29.2	29.8	24.2	26.8	26.8	20.0	22.9	30.0	28.0	24.2	27.0
18.5	27.1	31.4	25.0	25.0	24.3	29.0	22.2	26.4	26.0	25.1	27.0
19.0	29.3	32.5	28.0	28.0	23.4	28.0	21.3	26.3	27.0	27.8	27.0
19.5	27.4	34.6	27.0	29.0	25.6	28.0	24.5	26.6	28.0	24.7	29.0

	220	240	260	280	300	320	340	360	380	400	420
0.0	29.0	30.4	55.5	289.5	22.0	21.2	17.0	15.6	17.0	27.2	23.0
0.5	25.0	28.3	58.4	227.4	21.0	18.4	16.0	16.5	18.0	23.3	23.0
1.0	26.0	27.1	63.2	204.2	20.0	15.5	17.0	15.4	17.0	15.5	31.0
1.5	28.9	27.8	65.7	241.9	19.0	14.7	17.0	15.3	17.0	15.7	30.0
2.0	29.7	25.7	73.6	220.8	17.0	14.9	16.0	14.1	15.0	21.8	26.0
2.5	25.5	25.5	100.4	274.7	16.0	16.2	17.0	16.0	16.1	26.2	26.7
3.0	22.3	27.4	136.3	299.6	16.0	19.4	16.0	17.0	17.3	25.4	25.8
3.5	21.2	31.2	115.1	332.5	17.0	21.5	16.0	16.0	17.4	23.5	26.8
4.0	22.2	29.8	119.8	312.5	18.0	21.7	16.0	15.0	18.6	23.7	30.9
4.5	24.4	25.7	106.7	314.3	17.0	20.9	17.0	14.0	19.8	19.8	30.9
5.0	25.5	23.5	141.5	287.2	16.0	17.3	18.0	14.1	21.9	19.1	30.2
5.5	24.7	23.4	156.3	143.2	16.0	16.6	17.0	14.3	21.7	22.3	32.3
6.0	23.8	22.2	161.2	120.1	17.0	17.0	16.0	16.5	20.5	16.5	34.5
6.5	23.0	25.7	128.1	131.0	14.0	18.3	15.0	19.6	21.3	21.6	33.7
7.0	22.0	31.6	117.3	148.0	13.0	18.7	17.0	21.8	20.2	21.8	24.9
7.5	22.0	32.4	143.4	87.0	11.7	20.0	19.0	15.0	21.0	19.8	21.0
8.0	24.0	34.3	161.6	43.0	16.9	23.0	20.0	15.0	21.0	16.7	19.0
8.5	28.0	29.1	131.8	25.0	17.2	25.0	15.0	15.0	21.0	22.5	17.0
9.0	32.2	31.0	147.0	22.8	17.4	27.0	15.0	18.0	18.0	19.4	17.0
9.5	26.4	40.0	121.0	21.7	16.7	34.0	12.0	23.0	20.0	17.2	28.0
10.0	27.5	40.0	52.0	21.5	18.2	39.2	13.0	20.0	20.4	23.0	28.0
10.5	27.7	33.0	86.0	23.3	19.3	67.4	14.0	16.0	19.5	17.0	31.0
11.0	30.8	28.0	113.0	23.2	16.5	104.5	13.0	15.0	20.6	19.0	33.0
11.5	25.2	27.7	105.7	22.5	17.6	27.7	14.0	15.0	21.7	30.0	30.0
12.0	23.4	27.6	127.6	22.4	18.9	17.9	12.0	19.0	19.9	30.0	29.0
12.5	24.5	29.5	144.5	22.6	18.3	16.0	13.0	15.9	21.2	26.8	23.0
13.0	21.7	36.3	109.3	21.2	18.6	16.0	13.0	16.7	19.4	17.6	24.0
13.5	23.9	40.2	79.2	20.1	19.0	17.0	13.0	18.5	19.5	20.5	26.0
14.0	28.0	77.6	95.0	19.8	20.3	18.0	13.0	16.3	20.7	24.3	24.0
14.5	27.0	114.3	148.8	19.7	24.6	17.0	13.0	15.2	19.9	22.1	23.0
15.0	27.0	71.3	159.6	20.5	25.2	17.0	15.0	16.1	21.0	25.8	23.8
15.5	27.0	48.2	164.4	24.4	24.3	17.0	15.0	20.3	20.0	20.7	22.6
16.0	27.0	37.1	125.1	20.2	22.5	19.0	15.0	21.4	22.0	18.5	28.4
16.5	28.2	46.0	150.0	21.0	23.6	23.0	16.0	16.6	21.0	22.4	26.2
17.0	29.4	51.0	129.0	22.0	25.8	24.0	14.0	17.8	20.0	25.2	
17.5	27.6	49.0	130.0	23.0	24.2	21.9	14.0	17.0	20.1	22.0	
18.0	24.7	47.0	185.0	23.0	22.3	22.7	13.0	24.0	20.3	26.0	
18.5	27.9	39.0	202.0	22.0	21.5	25.5	13.0	26.0	18.5	29.0	
19.0	28.6	48.8	270.8	21.0	24.7	22.3	11.0	22.0	24.7	21.0	
19.5	27.5	53.7	342.7	22.0	25.9	20.1	14.0	16.0	20.8	23.0	

Note: The sums of the column and row headings indicate the depth for the magnetic susceptibility readings. All magnetic susceptibility readings reported in 10^{-6} SI units.

TABLE A-4. PERCENT ORGANIC MATTER DATA FOR CORE 02

	0	40	80	120	160	200	240	280
0		2.97	3.34	3.37	3.33	3.48	3.40	N.D.
1	2.36	3.27	3.01	3.53	3.25	4.02	3.74	N.D.
2	2.43	2.96	2.99	3.31	3.20	4.00	3.90	2.39
3	2.25	3.18	2.91	3.33	3.33	3.59	3.69	N.D.
4	2.25	3.25	2.93	3.65	3.43	3.45	3.79	N.D.
5	2.29	3.17	2.95	3.65	3.40	3.52	3.79	N.D.
6	2.40	3.24	2.74	3.39	3.35	3.69	3.92	N.D.
7	2.15	3.17	2.64	3.29	3.66	3.44	3.80	2.66
8	2.17	3.30	2.94	3.19	3.52	3.48	3.98	N.D.
9	2.17	3.15	2.95	3.20	3.41	3.80	3.92	3.63
10	2.49	3.40	3.31	3.40	3.17	3.65	4.18	3.93
11	2.74	3.08	3.07	3.88	3.28	4.08	4.45	3.43
12	2.84	2.84	3.04	3.45	3.03	3.87	3.76	3.59
13	2.95	2.99	2.96	3.50	3.46	3.62	3.71	3.56
14	3.96	2.95	2.93	3.35	3.43	3.43	3.50	3.64
15	3.36	3.03	2.95	3.39	3.19	3.71	3.01	3.53
16	2.62	3.25	2.95	3.33	3.41	3.79	3.42	3.41
17	2.89	3.15	2.89	3.51	3.16	3.62	3.96	3.50
18	2.78	3.36	2.91	3.27	3.17	3.51	3.92	3.49
19	2.69	3.26	3.18	3.44	3.48	3.43	4.54	3.55
20	2.93	3.49	3.15	3.36	3.39	2.96	4.08	3.59
21	2.56	3.00	2.81	3.38	3.57	3.88	3.82	3.54
22	2.82	3.23	2.97	3.46	3.64	3.61	3.70	3.80
23	2.66	3.41	2.96	3.30	3.32	3.58	3.50	3.44
24	3.00	3.93	3.11	3.45	3.05	3.61	3.53	3.89
25	3.45	2.88	3.12	3.68	3.08	3.47	2.86	N.D.
26	3.43	3.20	3.31	3.25	3.22	3.52	N.D.	N.D.
27	3.04	3.19	3.30	3.31	3.51	3.06	N.D.	N.D.
28	2.49	3.32	3.49	3.26	3.41	3.24	N.D.	N.D.
29	2.92	3.07	3.33	3.44	3.34	3.30	N.D.	N.D.
30	2.64	3.08	3.44	3.32	3.63	3.60	N.D.	N.D.
31	2.61	3.14	3.21	N.D.	3.55	3.68	N.D.	N.D.
32	2.73	3.35	3.53	3.36	3.44	3.43	N.D.	N.D.
33	2.41	3.31	3.49	3.27	3.73	3.36	N.D.	N.D.
34	3.22	3.32	3.77	3.32	3.46	3.70	N.D.	N.D.
35	2.84	3.30	3.71	3.29	3.62	3.90	N.D.	N.D.
36	3.26	3.00	3.71	3.46	3.38	3.86	N.D.	N.D.
37	2.83	3.04	3.63	3.59	3.49	4.12	N.D.	N.D.
38	3.07	3.11	3.34	3.84	3.82	3.65	N.D.	N.D.
39	2.72	3.30	3.61	3.01	3.70	3.51	N.D.	N.D.

	300.0	340.5	380.5	420.5
0.0	N.D.	4.61	3.88	1.86
1.5	N.D.	4.51	3.81	2.07
2.5	N.D.	4.59	3.80	1.87
3.5	N.D.	4.63	3.89	1.55
4.5	N.D.	4.51	3.72	1.87
5.5	3.93	4.41	3.10	1.74
6.5	3.66	4.62	3.48	1.44
7.5	3.78	4.28	3.27	1.43
8.5	3.89	4.31	3.39	2.38
9.5	3.82	4.24	3.12	2.26
10.5	3.64	3.19	3.36	1.74
11.5	3.74	4.39	3.01	
12.5	3.91	4.38	2.94	
13.5	3.95	4.38	3.00	
14.5	3.91	4.43	2.95	
15.5	3.63	4.40	2.99	
16.5	3.75	4.40	3.00	
17.5	3.85	4.37	2.61	
18.5	3.74	4.38	2.64	
19.5	3.93	3.67	2.75	
20.5	3.93	4.12	2.59	
21.5	4.07	4.30	3.13	
22.5	4.16	4.23	2.80	
23.5	4.05	4.04	2.57	
24.5	4.06	4.05	2.69	
25.5	4.23	4.03	2.58	
26.5	4.39	4.27	2.44	
27.5	4.44	3.89	2.54	
28.5	4.29	4.00	2.77	
29.5	4.35	4.04	2.81	
30.5	4.42	3.95	2.54	
31.5	4.44	3.88	2.31	
32.5	4.69	3.75	1.97	
33.5	4.28	4.01	2.73	
34.5	4.39	3.82	2.46	
35.5	4.54	4.07	2.60	
36.5	4.74	3.83	2.42	
37.5	4.63	4.11	2.40	
38.5	4.72	4.07	2.41	
39.5	4.64	3.60	2.12	

Note: The sums of the column and row headings indicate the depth for the loss-on-ignition measurements.

TABLE A-5. BIOGENIC SILICA DATA FOR CORE 02

Depth (cm)	BSi (%)	BSi Flux ($mg \cdot cm^{-2} \cdot yr^{-1}$)
0.60	1.75	0.23
0.80	2.00	0.82
1.00	1.92	1.35
1.20	2.47	2.05
1.40	2.06	1.99
1.60	2.68	2.94
1.80	2.67	3.30
2.00	2.92	4.01
2.10	3.23	4.39
2.40	2.44	3.14
2.60	2.47	3.04
2.80	2.66	3.12
3.00	2.35	2.62
3.20	2.32	2.59
3.40	2.10	2.32
3.60	2.37	2.61
3.80	1.99	2.17
4.00	2.72	2.93
4.20	2.37	2.61
4.40	2.30	2.58
4.60	2.14	2.45
4.80	1.90	2.20
5.00	2.23	2.61
5.20	2.08	2.42
5.40	1.99	2.29
5.60	2.04	2.32
5.80	2.22	2.49
6.00	2.03	2.24
6.20	1.62	1.63
6.40	2.35	2.21
6.60	2.36	2.06
6.80	2.01	1.62
7.00	2.42	1.80
7.20	1.64	1.23
7.40	2.37	1.74
7.60	1.78	1.28
7.80	2.23	1.56
8.00	2.07	1.41
8.20	1.97	1.34
8.40	1.81	1.24
8.60	2.01	1.37
8.80	1.90	1.29
9.00	1.86	1.26
9.20	1.75	1.16
9.40	2.01	1.30
9.60	2.06	1.31
9.80	2.00	1.25
10.00	2.20	1.34
10.20	2.09	1.18
10.40	1.99	1.04
10.60	1.81	0.87
10.80	1.70	1.77
11.00	1.64	1.63
11.30	1.76	1.69
11.60	2.08	1.92
11.80	2.05	1.84
12.00	2.03	1.78
12.40	1.96	1.76
12.60	2.62	2.38
12.80	1.86	1.71
13.00	2.03	1.89
13.20	2.20	2.18
13.40	2.09	2.19
13.60	1.93	2.14
13.80	2.00	2.34
14.00	1.88	2.32
14.20	1.96	2.36
14.40	1.96	2.29
15.75	1.88	1.79
16.25	2.07	1.97
16.75	2.12	2.26
17.25	1.85	1.97
17.75	2.14	2.11
18.25	2.11	2.09
18.75	2.25	2.58
19.25	1.63	1.87
19.75	2.20	2.64
20.25	2.09	2.50
20.75	1.93	2.11
21.25	1.78	1.94
21.75	1.81	1.94
22.25	1.88	2.01
22.75	2.06	2.08
23.25	1.47	1.49
23.75	2.17	2.24
24.25	1.84	1.90
24.75	2.47	2.39
25.25	2.19	2.11
25.75	1.70	1.87
26.25	1.57	1.73
26.75	1.70	1.27
27.25	1.49	1.12
27.75	1.89	1.75
28.25	2.09	1.95
28.75	2.32	2.23
29.25	2.20	2.12
29.75	1.91	1.49
30.25	2.04	1.59
30.75	1.81	1.64
31.25	2.07	1.88
31.75	2.02	2.12
32.25	1.85	1.95
32.75	1.96	1.37
33.25	1.79	1.25
33.75	2.08	1.92
34.25	1.97	1.82
34.75	1.89	1.88
35.25	1.58	1.58
35.75	2.00	1.74
36.25	1.98	1.72
36.75	1.73	1.78
37.25	2.99	3.07
37.75	1.91	1.98
38.25	1.54	1.60
38.75	1.82	2.11
39.25	1.92	2.23
39.75	1.92	1.91
40.25	1.90	1.89
40.75	1.73	1.48
41.25	1.82	1.56
41.75	1.80	1.63
42.25	1.69	1.53
42.75	1.88	1.54
43.25	1.73	1.42
43.75	1.86	2.43
44.25	1.81	2.36
44.75	1.89	1.47
45.25	1.89	1.46
45.75	1.86	1.59
46.25	1.95	1.67
46.75	1.63	1.66
47.25	2.25	2.29
47.75	1.93	2.05

Depth (cm)	BSi (%)	BSi Flux ($mg \cdot cm^{-2} \cdot yr^{-1}$)
48.25	1.95	2.06
48.75	1.82	2.13
49.25	1.96	2.30
49.75	1.47	2.06
50.25	1.71	2.39
50.75	1.91	1.79
51.25	1.88	1.76
51.75	1.78	1.72
52.25	1.76	1.71
52.75	2.04	2.18
53.25	1.61	1.72
53.75	1.69	2.32
54.25	1.64	2.25
54.75	1.74	1.67
55.25	1.85	1.77
55.75	1.53	1.79
56.25	1.56	1.83
56.75	1.64	1.86
57.25	1.28	1.45
57.75	2.25	2.16
58.25	1.76	1.70
58.75	1.91	2.26
59.25	1.59	1.88
59.75	1.57	1.83
60.25	1.81	2.11
60.75	1.98	2.04
61.25	1.88	1.93
61.75	1.79	1.72
62.25	1.91	1.84
62.75	1.88	2.35
63.25	1.89	2.37
63.75	1.79	2.16
64.25	1.36	1.64
64.75	1.85	2.01
65.25	1.74	2.25
65.75	1.71	1.15
66.25	1.76	1.19
66.75	1.74	1.34
67.25	1.37	1.05
67.75	1.76	1.96
68.25	2.06	2.29
68.75	2.09	2.24
69.25	1.78	1.91
69.75	1.96	2.05

Depth (cm)	BSi (%)	BSi Flux ($mg \cdot cm^{-2} \cdot yr^{-1}$)
70.25	1.95	2.04
70.75	2.02	2.36
71.25	1.80	2.10
71.75	1.34	1.41
72.25	1.30	1.36
72.75	2.31	1.65
73.25	1.40	1.00
73.75	2.07	1.85
74.25	2.11	1.89
74.75	0.95	0.88
75.25	1.82	1.68
75.75	1.56	1.65
76.25	2.02	2.14
76.75	1.97	1.88
77.25	1.84	1.75
77.75	1.82	1.42
78.25	2.15	1.69
78.75	1.79	1.90
79.25	1.97	2.09
79.75	1.90	2.55
80.25	1.87	2.51
80.75	2.17	2.24
81.25	1.84	1.90
81.75	2.05	2.87
82.25	1.76	2.47
82.75	1.81	2.07
83.25	1.90	2.17
83.75	1.96	2.04
84.25	1.86	1.94
84.75	1.84	2.14
85.25	1.73	2.01
85.75	1.98	1.72
86.25	2.08	1.81
86.75	2.09	2.22
87.25	2.20	2.35
87.75	1.96	2.37
88.25	1.94	2.35
88.75	1.85	2.42
89.25	1.95	2.54
89.75	2.00	1.73
90.25	2.18	1.88
90.75	1.97	1.82
91.25	2.06	1.90
91.75	2.01	1.59
92.25	2.20	1.74
92.75	2.12	2.54

Depth s(cm)	BSi (%)	BSi Flux ($mg \cdot cm^{-2} \cdot yr^{-1}$)
93.25	2.09	2.51
93.75	2.16	2.84
94.25	2.01	2.65
94.75	2.26	3.05
95.25	1.69	2.29
95.75	2.65	3.00
96.25	2.76	3.13
96.75	2.46	3.09
97.25	2.41	3.02
97.75	2.44	2.87
98.25	2.81	3.30
98.75	2.76	2.74
99.25	2.54	2.52
99.75	2.23	2.22
100.25	2.46	2.45
100.75	2.64	2.63
101.25	2.52	2.51
101.75	2.66	3.10
102.25	2.39	2.78
102.75	2.51	2.85
103.25	2.49	2.82
103.75	2.40	2.83
104.25	2.15	2.53
104.75	2.37	2.34
105.25	2.70	2.66
105.75	2.95	2.96
106.25	2.89	2.90
106.75	2.71	2.92
107.25	2.51	2.70
107.75	2.75	2.36
108.25	1.57	1.34
108.75	2.14	2.41
109.25	2.54	2.86
109.75	2.55	2.30
110.25	2.65	2.38
110.75	2.51	2.68
111.25	2.12	2.25
111.75	2.63	2.86
112.25	2.68	2.91
112.75	2.60	2.47
113.25	2.66	2.53
113.75	2.71	2.31
114.25	2.59	2.21
114.75	2.16	2.54
115.25	2.11	2.47
115.75	1.74	2.48

Depth (cm)	BSi (%)	BSi Flux ($mg \cdot cm^{-2} \cdot yr^{-1}$)
116.25	1.90	1.79
117.25	1.56	1.76
117.75	1.60	1.58
118.25	1.82	1.79
118.75	1.64	1.80
119.25	1.84	2.03
119.75	1.88	2.01
120.25	1.81	1.94
120.75	1.54	1.64
121.25	1.40	1.50
121.75	1.50	1.44
122.25	1.46	1.40
122.75	1.55	1.49
123.25	1.98	1.90
123.75	1.65	1.33
124.25	1.52	1.23
124.75	1.72	1.58
125.25	2.60	2.39
125.75	1.90	1.83
126.25	1.83	1.77
126.75	1.81	1.41
127.25	1.65	1.29
127.75	1.79	2.00
128.25	1.80	2.00
128.75	1.75	1.59
129.25	1.69	1.54
129.75	1.68	1.79
130.25	1.75	1.87
130.75	1.73	1.46
131.25	1.67	1.41
131.75	1.77	1.65
132.25	1.85	1.72
132.75	1.90	1.74
133.25	1.83	1.67
133.75	1.75	1.10
134.25	1.70	1.07
134.75	1.67	1.55
135.25	1.68	1.56
135.75	1.03	0.95
136.25	1.09	0.97
136.75	1.04	0.82
137.25	1.41	1.10
137.75	1.22	1.42
138.75	1.29	1.53
139.25	1.17	1.38
139.75	1.51	1.29
140.25	1.17	1.00
140.75	1.25	1.41
141.25	1.45	1.63
141.75	1.42	1.21
142.25	1.32	1.12
142.75	1.13	1.03
143.25	1.24	1.12
143.75	1.08	0.82
144.25	1.19	0.90
144.75	1.21	1.26
145.25	1.33	1.38
145.75	1.33	1.80
146.25	1.29	1.75
146.75	1.15	0.95
147.25	1.26	1.04
147.75	1.27	1.29
148.25	1.23	1.25
148.75	1.42	1.26
149.25	1.32	1.17
149.75	1.47	1.19
150.25	1.45	1.16
150.75	1.35	1.09
156.25	1.29	1.03
161.25	1.67	1.21
166.25	1.33	1.17
171.25	1.76	1.32
176.25	1.84	1.42
181.25	1.72	1.41
186.00	1.92	1.39
191.25	1.76	1.53
196.25	1.76	1.19
201.25	1.53	1.28
206.25	1.91	1.52
211.25	2.19	1.45
216.25	2.30	1.72
221.25	1.59	1.12
226.25	2.20	1.22
231.25	2.18	2.17
236.25	3.06	2.28
241.25	4.09	2.30
246.25	4.07	1.99
251.25	4.86	3.60
256.25	3.39	1.82
260.25	3.80	2.71
260.75	5.26	3.83
261.25	5.41	3.94
261.75	4.33	4.03
262.25	3.87	3.60
262.75	4.68	2.86
263.25	4.57	2.79
263.75	3.17	2.65
266.25	3.79	N.D.
288.25	2.75	0.42
289.25	2.89	0.44
290.25	1.85	0.25
291.25	1.71	0.37
296.25	1.62	0.29
301.25	1.23	0.25
309.75	1.77	0.20
314.75	1.36	0.23
319.75	1.85	0.32
324.75	1.87	0.39
329.75	3.84	0.69
330.75	6.00	0.93
334.75	2.08	0.38
339.75	1.92	0.31
341.75	2.04	0.36
344.75	2.21	0.39
345.75	2.55	0.37
354.75	2.36	0.38
359.75	2.08	0.45
364.75	2.26	0.46
369.75	2.05	0.40
374.75	2.04	0.63
377.75	1.74	0.22
379.75	1.93	0.55
382.75	2.01	0.42
384.75	1.67	0.37
389.75	1.48	0.33
394.75	1.72	0.37
397.75	1.24	0.27
399.75	0.99	0.28
404.75	1.15	0.21
407.75	1.75	0.48
409.75	1.18	0.21
414.75	1.27	0.27
419.75	0.72	0.11
424.75	0.58	0.14
429.75	0.90	0.28
434.75	0.91	0.28
436.75	0.65	0.27